NTNU
Norwegian University of
Science and Technology

Numerical modelling and simulations for lowering of an offshore wind turbine tripod

Dapeng Xu

Marine Technology
Submission date: June 2016
Supervisor: Zhen Gao, IMT

Norwegian University of Science and Technology
Department of Marine Technology

NTNU – Trondheim
Norwegian University of
Science and Technology

Numerical Modelling and Simulations for Lowering of an Offshore Wind Turbine Tripod

Dapeng Xu

June 26, 2016

PROJECT / Master Thesis

Department of Marine Technology

Norwegian University of Science and Technology

Abstract

Offshore wind industry is developing very fast. Transport and installation are important aspects for reducing the life-cycle cost of offshore wind farms. In shallow waters (10-30 m of water depths), monopile foundations have been widely used, while in deep waters (water depths > 50 m), it is beneficial to use jacket foundations which are transparent to the wave loads. For the water depths in between, the tripod foundation might be considered due to its simplicity as well as high stiffness.

This thesis addresses the modelling and dynamic analysis one installation phase for tripods: the lowering into the sea. Due to non-stationarity, current numerical methods used for steady-state conditions are not applicable for simulating the lowering phase. In this thesis, time-domain simulations were performed to account for the responses of the coupled vessel-tripod system.

A systematic methodology to assess the operational limits based on the installation procedure, numerical models and safety criteria was introduced. For the tripod lowering process, the allowable sea states were also established by using the methodology.

These numerical models, methods and dynamic analysis form the basis for assessing the operational limits for the tripod lowering operation. The operational limits are necessary during the planning phase of the operation. The allowable sea states together with weather forecasts provide the basis for the decision making during the execution of the operation.

Acknowledgement

This thesis work was highly supported by my supervisor, Prof. Zhen Gao. I appreciate his insightful comments and the useful information he has provided. I would like to express my deepest thanks for his guidance and supervision. I gained a lot from Zhen's deep knowledge, experience and great enthusiasm and discipline in scientific research.

Moreover, I also would like to thank PhD candidates Lin Li and Xiaopeng Wu for their help and suggestions. I am grateful for their generous support and discussions on every detail in my work. It was a great pleasure and experience to work with them.

Dapeng Xu

June 2010

Trondheim, Norway

Preface

This thesis is submitted to the Norwegian University of Science and Technology(NTNU) for partial fulfilment of the requirements for the degree of master. The thesis work has been performed at Department of Marine Technology, NTNU, Trondheim, with Prof. Zhen Gao.

The topic of this thesis is the numerical modelling and Simulations for lowering of an offshore wind turbine tripod. The work was initiated the previous semester, autumn 2015, in terms of a project work that covered a literature study on marine operations related to installation of offshore wind turbines. Some of the information gained through the project work is applied in this report.

Contents

List of Figures

List of Tables

Chapter 1

Introduction

1.1 Background and motivation

Offshore wind industry is developing very fast. Offshore wind power counts for about 1 percent of the total wind power installed all over the world (Twidell and Gaudiosi (2009)). Development has mainly taken place in countries in the north of Europe, round the North Sea and the Baltic Sea. Due to the growing interest in wind turbine energy, several new projects have been initiated and the number of operators is increasing.

New challenges arise when installing and accessing far shore wind farms and a throughout planning of the relating marine operations are necessary. Also the amount of wind turbines at site is highly relevant for the evaluation of the planning of installation. A marine operation as installation of offshore wind turbines is complex and the operation is composed of a number of sub operations. Cost which is directly linked to time consumption of the operation is a challenging parameter. Since the installation of offshore wind turbine farms consist of repetitive installation operations, small improvements and time savings will greatly improve the grand scheme of operation. As the industry develops more extensive knowledge, improvements are to be made to better adapt to the challenges offshore. In addition, better and more cost efficient solutions can be developed for the wind energy concepts to be more competitive in the energy market.

Installation is an important aspect for reducing the life-cycle cost of offshore wind farms. In shallow waters (10-30 m of water depths), monopile foundations have been widely used, while in deep waters (water depths > 50 m), it is beneficial to use jacket foundations which are transparent to the wave loads. For the water depths in between, the tripod foundation might be considered due to its simplicity as well as high stiffness. In Phase III of OC3, the water depth

was increased to 45 m and the monopile used in Phases I and II was replaced with a tripod substructure, which is one of the space-frame concepts proposed for offshore installations in water of intermediate depth. The rotor-nacelle assembly of the NREL 5-MW turbine including the aerodynamic, structural, and control system properties—remained the same as in Jonkman et al. (2009), but the support structure (tower and substructure) was changed.

1.2 Foundation Installation Methods

The method of installation of foundations plays an important role for wind turbines, which influences the staging port layout, size, and location to the offshore wind farmsite. For different foundations, different methods are fulfilled. Therefore ,it is significant for manufacturers and contractors to learn types of foundations of wind turbines. Typically, types of foundations are distinguished by different water depths. Table 1.1 shows the the estimated depths of foundation types of offshore wind farm.

Table 1.1: Foundation types

Water Depth(m)	Foundation Type	Rated Power
0-30(30+)	Monopiles,Gravity-Based,Tripod	2-3 MW(3MW+)
30-70	Jacket	3-6 MW
>50-100	Floating	5-7MW

1.2.1 Monoplies Foundation Installation

A typical monopile is a long tube with a diameter of 4 to 5 meters. The monopile typically weighs around 500 tons, making it one of the lighter support structures. On deeper sites like Walney 2, the monopiles weigh up to 810 tons and are up to 69 meters long in a water depth of 30 meters. The monopiles are normally driven into sea bed by hydraulic hammers. The constant pounding with the hammer leads to the steel becoming brittle and unsuitable for large load bearing. Therefore, the solution is to place a transition piece with a slightly different diameter on top of the monopile. The transition piece is pre-assembled onshore with a connecting flange for the tower, an access platform, ladders, tubes for cables and other secondary structural members. The piece is connected with the monopile with an overlap length of around 1.5 times of the monopile diameter Wind (2005). The annulus between the pile and the transition piece is grouted with high-density concrete and the transition piece is adjusted to true vertically.

The installation of monopile in general includes two main steps: upending and driving/drill operations. After arrival on site, the pile is upended and lowered through water so that it is sitting vertically on the sea bed. A hydraulic hammer is placed on top of the pile and it is driven into the seabed to a predetermined depth. A rocky subsurface may prevent driving operations, in which case a drill will be inserted into the pile to drill through the substrate.

After the monopile is secured in the seabed, a transition piece is lifted and grouted onto the pile. In some cases the transition piece may be bolted. The transition piece is typically installed immediately after piling by the same vessel that drove the pile, but if two vessels are employed in installation, a separate vessel may follow behind the foundation installation and install the transition piece.

1.2.2 Gravity-Based Foundation Installation

Gravity-based structures (GBS) are large concrete (or steel) foundations which secure the turbine to the seabed through their weight These foundations, which weight over 2500 tons, are very common in industry.

GBS are best suited to relatively shallow water locations and sites where pile driving is difficult. GBS were the first type of foundations to be used in the offshore wind industry. Eleven of them were installed at the Vindeby wind farm off Lolland, Denmark in 1991. Since then, they have only been used at five other locations till 2010 Archer et al. (2014). In shallow waters less than 15 meters they are cheaper than monopile foundations, and cost savings are significant when used on a large project like the 72 turbine Nysted wind farm off Denmark, built in 2003. However, GBS are also applied in deeper waters. The deepest gravity foundations in operation are in Thornton Bank with a water depth up to 28 meters Peire et al. (2009). The largest of the structures is 44 meters high and weighs 3000 tons.

The gravity based structure is typically constructed out of steel reinforced concrete. Steel gravity base is affordable in very shallow waters. However, in above 10 meters depth it generally is not competitive with other types of structures. The cost of the steel structure is in general proportional with the depth squared. Large concrete gravity bases have been widely used in the oil and gas industry and in bridge construction. They are also far less affected by fluctuations in the cost of steel than other foundation types and require minimal lifetime maintenance.

1.2.3 Jackets and Tripods Foundation Installation

A jacket foundation is a lattice structure. A square cross section with the structural members is fitted to four corner tubes to create a light and strong construction that will withstand large forces at light weight. Jacket foundation has a small cross-section area in the splash zone since it is make from small diameter steel tubes. Hence, the forces created from the waves are less compared to the gravity-based foundation, the monopile and the tripod. While the jacket is strong and lightly built, the nodes where the tubes are welded together are extremely difficult to manufacture, and the cast high-tensile steel nodes are very expensive. Furthermore, all the welding on a jacket are handmade, which increases the cost of a jacket.

A tripod has a relatively small cross section in the splash zone-due to only having one large tube compared to the jacket. It has several small tubes protruding from the splash zone.

Both jackets and tripods use a number of anchor piles fitted through the base of the foundation. The legs of the jackets and tripods transmit environmental and topsides loads into the piles and subsequently into the sea bed. Jacket foundations has been used in offshore wind farms

The installations of a jacket foundation and a tripod are similar. Jackets and tripods are transported onboard of a barge or an installation vessel to the offshore site. Jackets and tripods for offshore wind turbines can range from 400-1000 tons and from a height of 30-90m in water depth of app 20-70m. In general, the size of these jackets and tripods are smaller and lighter than those used in oil and gas industry in deeper waters. Some available offshore installation vessels have the lift capacity to place these foundations.

The jackets can be transported either in the upright position or in the horizontal position depending on the size of the foundations and the available transportation barges. The first offshore wind project using jacket foundations, the Beatrice Demonstrator Project involved two 5 MW turbines situated in 45 m water depth with around 62 meters tall and 750 ton (including transition piece, pile sleeves substructure and mud mats). The jacket support structure was transported to the offshore location on a barge in the horizontal position. There, the heavy lifting vessel Rambiz equipped with two cranes lifted the structure off the barge and tilted it until it was in an upright position. At Alpha Ventus wind farm, three jackets were transported in the upright position on one barge and towed to the offshore site. Being around 50 meters tall and weighing between 500 and 800 ton, not every barge and crane can install the jacket. Once on site, the semi-submersible crane vessel Thialf was used to lift and install the foundation on the sea bed.

The piles used to secure jackets and tripods to the seafloor are significantly smaller in diameter and length than monopile foundations, and operations are similar to the offshore oil and gas industry. Piles could be app from 50-200 tons with diameters ranging from 1.8-2.5m and lengths from 20-70m. Pile design is directly related to the soil characteristics. The installation of piles could be carried out either after positioning the jackets (post-piling) or before jackets installation (pre-piling).

Table 1.2: Installation methods for three types of bottom-fixed foundations

Type of foundations	Installation methods
Monopiles	Upending and lowering
	Upending and lowering (smaller crane)
Gravity-based	Lowering (large crane)
	Ballasting and lowering (smaller crane)
Jacket and Tripod	Lowering; pre- or post-piling
	Upending and lowering; pre or post-piling

1.3 Outline of thesis

Background and motivation is made known in chapter 1. Then chapter 2 gives an introduction to the thesis and provides general information about the installation vessel and the tripod foundation for an offshore wind turbine. Moreover, the operational restrictions are introduced. Environmental data with emphasis on waves is presented in chapter 3. Chapter 4 presents the how to establish the numerical models for the coupled system and the corresponding methods. A description of the software SIMO, the theory which applies to SIMO is covered by this chapter. Also eigenvalue analysis is performed.

Chapter 5 provides information concerning the time domain method. After modifying the models in dynamic analysis, the responses of the coupled system are obtained. In order to study those results further, the effects from winch speed and tripod draft are discussed respectively. Chapter 6 gives the method to assess the operational limits. Then the weather window analysis is performed. An overall conclusion and a proposal for further work are included in chapter 7.

Chapter 2

Theory Background

In order to analyze the tripod lowering process theoretically, the related theories are essential be introduced before performing numerical simulations. In this chapter, the theory backgrounds are presented, including numerical modelling of the coupled system of heavy lift vessel and tripod foundation, numerical methods for each step in dynamic simulations, and the simulation program SIMO(SImulation of complex Marine Operation).

2.1 JONSWAP Spectrum

First of all, the environmental conditions of the installation site should be considered. The recommended wave spectrum in the thesis is the JONSWAP spectrum given by the International Ship Structures Congress. The JONSWAP spectrum is commonly used spectrum for North Sea applications and is considered as a rational model for wind generated sea. The formula of the JONSWAP spectrum is given by Veritas (2010a):

$$S(f) = \frac{\alpha g^2}{(2\pi)^4} f^{-5} \exp(-\frac{5}{4}(\frac{f}{f_p})^{-4}) \gamma^{\exp(-0.5(\frac{f-f_p}{\sigma f_p})^2)} \tag{2.1}$$

where

f	=	wave frequency
T	=	wave period
α	=	generalised Phillips' constant
g	=	acceleration of gravity
f_p	=	spectral peak frequency
T_p	=	peak period
σ	=	spectral width parameter
γ	=	peak-enhancement factor

The generalised Phillips, constant can be obtained as follows:

$$\alpha = 5(\frac{H_s^2 f_p^4}{g^2})(1-0.287 ln\gamma)\pi^4 \tag{2.2}$$

σ will equal to 0.07 for $f \leq f_p$ and 0.09 for $f \geq f_p$ respectively, and

$$\gamma = \begin{cases} 5 & for \quad \frac{T_p}{\sqrt{H_s}} \leq 3.6 \\ \exp(5.75 - 1.15\frac{T_p}{\sqrt{H_s}}) & for \quad 3.6 \leq \frac{T_p}{\sqrt{H_s}} \leq 5 \\ 1 & for \quad 5 < \frac{T_p}{\sqrt{H_s}} \end{cases} \tag{2.3}$$

2.2 Morsion Element

In order to establish the numerical model for the tripod foundation, the Morison element was introduced. The Morison model is used to calculate hydrodynamic loads based on Morison equation. In addition to representing the complete or parts of the structure the Morison model is used to include external forces from mooring lines and tethers in a hydro model. The Morison model is put together from a set of slender elements(Morison elements) by strip theory. The slender elements are based on 2 node beam elements and single nodes in a first level super-element. The slender elements are actually defined by assigning hydrodynamic properties to nodes and beam elements.

2.2.1 Long Wave Approximation

For slender element it is better to use Morison equation to calculate wave forces, however, as the precondition, long-wave approximation must be fulfilled. The excitation loads have a particular form in the case of long-wave approximation, or small-volume structure approximation, which is of practical relevance in many circumstances. The figure below confirms that the long-wave approximation is good for $\lambda > 5D$, the incident waves tend to be unaffected by the structure, which means the induced loads are partially connected with the acceleration(mass loads) and partially with the velocity(viscous loads) of the incident waves at the center of the body, as the body was not there. For $\lambda < 5D$ wave diffraction important.

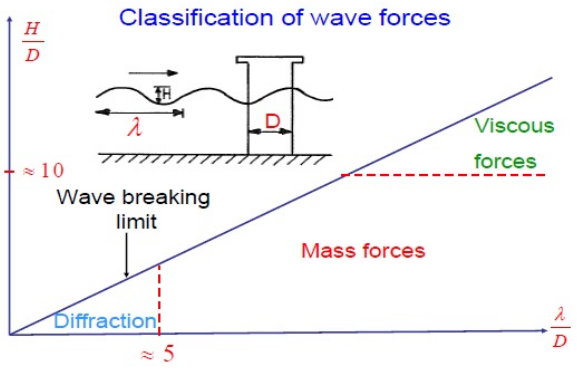

Figure 2.1: Long Wave Approximation

2.2.2 Coefficients of Morison Equation

The wave force $f_{W,s}$ per unit length on each strip of a moving circular cylinder normal to the member can be determined by Morison equation(Faltinsen (1993)).

$$f_{W,s} = \rho_w C_M \frac{\pi D^2}{4} \ddot{\xi}_s - \rho_w C_A \frac{\pi D^2}{4} \ddot{x}_s + \frac{1}{2} \rho_w C_q D \left| \dot{\xi}_s - \dot{x}_s \right| \left(\dot{\xi}_s - \dot{x}_s \right) \tag{2.4}$$

In this equation, the positive force direction is the wave propagation direction. The first term in the equation is the wave excitation force including diffraction and Froude-Kriloff force;

The second term is the inertial force and the last term is the quadratic drag term, where

$\ddot{\xi}_s$	=	fluid particle acceleration at the center of the strip
$\dot{\xi}_s$	=	fluid particle velocity at the center of the strip
$\ddot{x}_s$	=	acceleration at the center of the strip due to the body motions
$\dot{x}_s$	=	velocity at the center of the strip due to the body motions
D	=	outer diameter of the member
C_M	=	mass coefficient
C_A	=	added mass coefficient
C_q	=	quadratic drag force coefficient

C_M and C_q rely on several parameters, say the Reynolds number(Re), the Kaulegan-Carpenter number(KC) and the surface roughness ratio(Δ)(Veritas (2010a)).

2.3 Lift Wire Coupling

Like monopile lowering activities, the internal lifting tool is also used for tripod installation, and it is connected with the hook through slings. The slings were assumed to very stiff in the current model. Moreover, the connection between hook and tripod foundation was assumed to be rigid, and for simplicity it was modelled as one body. Thus, both lowering systems included two rigid bodies which were coupled through the lift wire. The couplings between the vessel and the tripod include hydrodynamic interaction and mechanical coupling during the lowering process.

Coupling points are defined as points on a body where coupling forces can be attached. Specific properties such as a winch can be added to a coupling point and by this allowing the user to hoist in or out wire. This is of interest for installation of the transition piece as the structural parts will be lifted up from the vessel and also lowered down at the desired location.

The simple wire coupling is modelled as a linear spring based on:

$$\Delta l = \frac{T}{k} \tag{2.5}$$

where

Δl	=	change in elongation of line
T	=	wire tension
k	=	effective axial stiffness

The effective axial stiffness is given by:

$$\frac{1}{k} = \frac{l}{EA} + \frac{1}{k_0} \tag{2.6}$$

where

E	=	modulus of elasticity
A	=	cross-section area
l	=	unstretched wire length(may be variable with respect to time)
$\frac{1}{k_0}$	=	connection flexibility(crane flexibility)

2.4 Methods of Analysis

2.4.1 Coupled Equations of Motions

After the numerical modelling for the coupled system of the heavy lift vessel and the tripod foundation, the numerical simulations should be performed based on the coupled equation of motions. The two-body coupled lifting system has 12 degrees of freedom(DOFs) of rigid body motions, the equation of motion may be written as follows Clough and Penzien (1993):

$$[m + A(\omega)]\ddot{x} + C\dot{x} + D_1\dot{x} + D_2 f(\dot{x}) + K(x)x = q(t, x, \dot{x}) \tag{2.7}$$

where

m	=	body mass matrix
$A(\omega)$	=	frequency-dependent added mass
C	=	frequency-dependent potential damping matrix
$D_1(\omega)$	=	linear damping matrix
D_2	=	quadratic damping matrix
f	=	vector function where each element is given by $f_i = \dot{x}_i \lvert\dot{x}_i\rvert$
$K(x)$	=	(position-dependent) hydrostatic stiffness matrix
x	=	position vector
q	=	exciting force vector

The exciting forces, $q(t, x, \dot{x})$, can furthermore be expressed as follows

$$q(t, x, \dot{x}) = q_{W1} + q^1_{WA} + q^2_{WA} + q_{CU} + q_{EXT} \tag{2.8}$$

where

q_{W1}	=	wind drag force
q^1_{WA}	=	1^{st} order wave excitation force
q^2_{WA}	=	2^{nd} order wave excitation force
q_{CU}	=	current drag force
q_{EXT}	=	other forces as wave drift damping, specified forces and forces from station-keeping and coupling elements

2.4.2 Time-domain Method

In SIMO can the equation of motion(equation 2.7) either be solved by convolution integral or separation of motions. Separation of motions is an alternative to solving the whole differential equation (equation 2.7) in time domain by use of the retardation function. Instead the motions are separated in a high-frequency part and a low frequency part. The high-frequency

motions are solved in frequency domain. This requires the motions to be linear responses to waves. The low-frequency motions, however, are solved in time domain.

The method of convolution integral is the method that will be used in this report. By making use of convolution integral is the frequency-dependent equation of motion expressed as a dynamic equilibrium where the frequency dependent parts are sat equal to a force that varies sinusoidally at one single frequency, ω. Furthermore, the inverse Fourier transform is used to transform the frequency-dependent equation into a function of time.

The time-dependent equation of motion can be written as follow:

$$[m + A_\infty]\ddot{x} + D_1\dot{x} + D_2 f(\dot{x}) + Kx + \int_0^t \mathrm{h(t-\tau)\dot{x}(\tau)d\tau} = q(t, x, \dot{x}) \tag{2.9}$$

$$h(\tau) = \frac{2}{\pi}\int_\infty^0 c\cos(\omega\tau)d\omega = -\frac{2}{\pi}\int_\infty^0 \omega a \sin(\omega\tau)d\omega \tag{2.10}$$

where $\int_0^t \mathrm{h(t-\tau)\dot{x}(\tau)d\tau}$ is the convolution integral which is forces due to frequency-dependent added-mass and damping. Moreover, $h(\tau)$ is the retardation function and may be expressed, for $\tau > 0$, as in equation 2.10. In SIMO is the retardation function computed by a transform of the frequency-dependent damping. In addition, a value of the added mass is required. The other parameters included in equation 2.9 are the same as those outlined in the explanation of equation 2.7.

2.4.3 Numerical Integration

In SIMO, there are three methods capable for application of numerical integration, Modified Euler method, 3^{rd}-order Runge-Kutta-lie method and Newmark-β predictor-corrector method (Ormberg (2009)). In this thesis, the last method, Newmark-β was introduced as numerical integration method. The following shortened notation is used:

$$\begin{aligned} x_k &= x(t_k) \\ \dot{x}_k &= \dot{x}(t_k) \\ \xi_k &= \xi(t_k) \\ f_k &= \ddot{x}_k = f(x_k, \dot{x}_k, \xi_k) \end{aligned} \tag{2.11}$$

where ξ is a vector of inputs not depending on x or $\dot{x}$. When the body is coupled to other bodies, ξ will include the positions or velocities of these bodies as well.

Predictor:

$$\begin{aligned} \dot{x}_{k+1}^{(0)} &= \dot{x}_k + T f_k \\ x_{k+1}^{(0)} &= x_k + T \dot{x}_{k+1}^{(0)} \end{aligned} \tag{2.12}$$

Corrector:

$$\begin{aligned} f_{k+1}^{(i)} &= f(x_{k+1}^{(i)}, \dot{x}_{k+1}^{(i)}, \xi_{k+1}) \\ \dot{x}_{k+1}^{(i+1)} &= \dot{x}_k + T[(1-\gamma) f_k + \gamma f_{k+1}^{(i)}] \\ x_{k+1}^{(i+1)} &= x_k + T\dot{x}_k + (\tfrac{1}{2} - \beta) T^2 f_k + \beta T^2 f_{k+1}^{(i)} \end{aligned} \tag{2.13}$$

Steps in the equation above are repeated a predefined number of times, and as a future extension until

$$\begin{aligned} \left| x_{k+1}^{(i+1)} - x_{k+1}^{(1)} \right| &< \varepsilon \\ \left| \dot{x}_{k+1}^{(i+1)} - \dot{x}_{k+1}^{(1)} \right| &< \varepsilon / T \end{aligned} \tag{2.14}$$

where ε is vector of specified numbers.

The parameter γ governs the damping in the numerical integration:

- $\gamma > \frac{1}{2}$ gives positive damping
- $\gamma = \frac{1}{2}$ gives no damping
- $\gamma < \frac{1}{2}$ gives negative damping

The parameter in the last step of equation 2.13 should be chosen in the interval [0,0.5]. With $\gamma = \frac{1}{2}$, the folowing known integration methods can be obtained:

- $\beta = 0$ Second central difference
- $\beta = \frac{1}{12}$ Fox-Goodwins method
- $\beta = \frac{1}{6}$ Linear acceleration
- $\beta = \frac{1}{4}$ Constant average acceleration(trapez method), unconditionally stable

2.4.4 Frequency-domain Method

If we can assume a steady state condition then the linear dynamic motions and loads on the structure are harmonically oscillating with the same frequency as the wave loads that excite the structure. Steady state means that there are no transient effects present due to initial conditions.

Rigid body motion in linear sea-keeping means that all points which is a member of the body is exclusively defined by the motions given at the origin in the coordinate system. Thus,

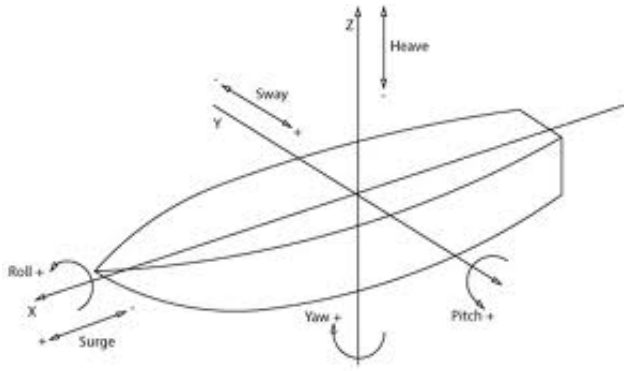

Figure 2.2: 6-degree of freedom system

when considering a system that is experiencing rigid body motion, the motion of any point on the body can be described by equation below:

$$\mathbf{S} = (\eta_1 + z\eta_5 - y\eta_6)\mathbf{i} + (\eta_2 - z\eta_4 + x\eta_6)\mathbf{j} + (\eta_3 + y\eta_4 - x\eta_5)\mathbf{k} \tag{2.15}$$

Each of the displacements mentioned,

$$\eta_i = \eta_{i,a} \exp(i\varphi) \tag{2.16}$$

where

η_i	=	displacement in the i-th degree of freedom
$\eta_{i,a}$	=	amplitude in the i-th degree of freedom
φ	=	phase angle

The transfer function is the response amplitude per unit wave amplitude. The function describes the relation between harmonic excitation and its linear response.

$$H(\omega, \beta) = \frac{\eta_{i,a}}{\varsigma_a} \tag{2.17}$$

With other symbols and rearranged can the expression be written as in equation

$$Y(\omega) = H(\omega) * X(\omega) \tag{2.18}$$

where $Y(\omega)$ is the response motion, $H(\omega)$ is the transfer function and $X(\omega)$ is the wave ele-

vation. Each value of the frequency represents a point on the transfer function. To find the resulting response motion in irregular sea must the contributions from each frequency component be added together either by summation or by integration. It is necessary to find the transfer function on a continuous frequency interval if the transfer function is to be combined with a wave spectrum.

By considering the related spectra in frequency domain can the following expression be obtained

$$S_{yy}(\omega) = |H(\omega)|^2 * S_{xx}(\omega) \tag{2.19}$$

where $S_{yy}(\omega)$ is the response spectrum, $|H(\omega)|$ is the absolute value of the transfer function, i.e. the Response Amplitude Operator (RAO), and $S_{xx}(\omega)$ is the wave spectrum. The RAO, Response Amplitude Operator, is the transfer function of the body motions. It is the response amplitude per unit wave amplitude and is essential in the evaluation of stability of a marine unit.

2.4.5 Eigenvalues of Coupled System

Considering a crane vessel with a load hanging in the crane, 2 bodies connected by a wire, there are altogether 12 DOFs. The system considered is illustrated as below. The load may hang in air or water but is handled as a point mass. For the vessel it is assumed that y=0 is a plane of symmetry. Motions of the vessel is referred to an earth fixed coordinate system (x,y,z) which is in origin of vessel at rest. The motions of the load are referred to the center of the load.

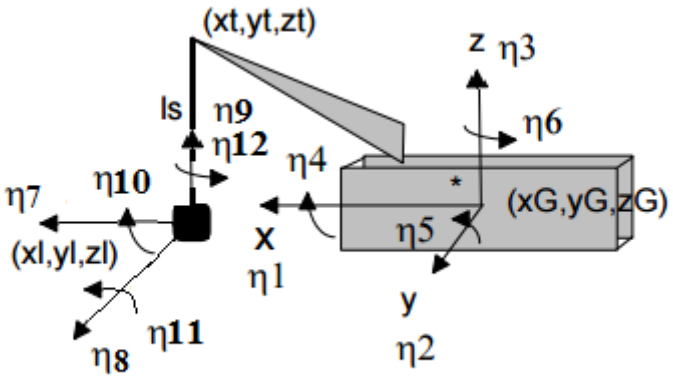

Figure 2.3: Model of crane vessel with load. For the vessel y=0 is a plane of symmetry

The undamped eigenfrequencies and eigenmodes of the coupled system can be obtained from:

$$(-{\omega_0}^2\mathbf{M} + \mathbf{C})\mathbf{x} = \mathbf{0} \tag{2.20}$$

where

ω_0	=	eigenfrequency
M	=	mass matrix of the vessel and load(12*12) including the added mass
C	=	stiffness matrix including hydrostatic effects, mooring effects and coupling between vessel and load(12*12)
x	=	motion matrix, $(\eta_1, \eta_2, \eta_3, \eta_4, \eta_5, \eta_6, \eta_7, \eta_8, \eta_9, \eta_{10}, \eta_{11}, \eta_{12})^T$

Then the eigenvalues and eigenmodes of the system is given from:

$$\lambda \mathbf{x} = \mathbf{M}^{-1}\mathbf{C}\mathbf{x} \tag{2.21}$$

To each eigenvalue, $\lambda_i = {\omega_0}_i^2$, corresponds an eigenvector ξ_i. ξ_i defines the contribution from each of the different degrees of freedom to this specific resonant mode of motion. Differe t from a rigid body, there are not pure eigenmodes for a system with coupling effects. The eigenmodes have contributions from several of standard degrees of freedom(Nielsen (2007)).

2.5 Weather Window

After numerical simulations, the results of dynamic analysis can be obtained. Based on the data, the weather window analysis can be performed to give acceptable working time periods.

In order to account for uncertainty in weather forecast, the weather limit for execution of a marine operation must be reduced compared to the design weather condition. This is done by introducing the α-factor.

$$OP_{WF} = \alpha * OP_{LIM} \tag{2.22}$$

where

- **Operational Criterion**: Maximum weather condition for execution of the marine operation – determined during the planning process and controlled by weather forecast. Notation OP_{WF}.
- **Design Criterion**: Weather condition used for calculation of design load effects (weather forces and load effects like vessel motions and accelerations etc.). Notation OP_{LIM}.

The definition of weather window is the period of time which is sufficient in length to safely carry out a marine operation. Weather forecasted environmental conditions shall remain below the operational criterion (OP_{WF}) for the whole length of the period.

The duration of marine operations shall be defined by an operation reference period, T_R (Gudmestad and Skjerpe (2012)):

$$T_R = T_{POP} + T_C \tag{2.23}$$

where

T_R	=	Operation reference period
T_{POP}	=	Planned operation period
T_C	=	Estimated maximum contingency time.

Marine operations with a reference period (T_R) less than 96 hours and a planned operation time (T_{POP}) less than 72 hours may normally be defined as weather restricted. The planned operation period start point for a weather restricted operation shall normally be defined at the issuance of the last weather forecast.

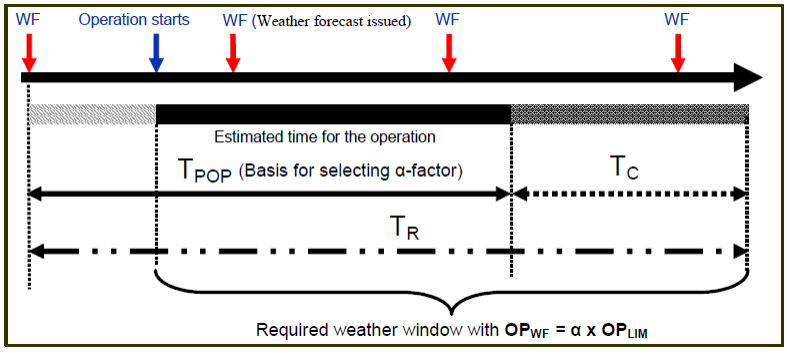

Figure 2.4: Operation Periods (Gudmestad and Skjerpe (2012))

2.6 Introduction of SIMO

The simulation program SIMO(SImulation of complex Marine Operations) developed by MARINTEK. The numerical models in the thesis were established by using the SIMO program. SIMO is capable of solving the non-linear equations of motions in the time domain for coupled marine systems exposed in wind, wave and current, such as lifting operations, launching and

offshore mating operations.

There are 6 modules communicating by a file system in SIMO. According to Reinholdtsen and Falkenberg (2001), how these modules function are thoroughly described.

- **INPMOD** - manipulation of input data
- **STAMOD** - initial condition and static equilibrium
- **DYNMOD** - dynamic response calculation
- **OUTMOD** - output module
- **S2XMOD** - export of time series to various file formats
- **PLOMOD** - plotting module (common with the Riflex program system)

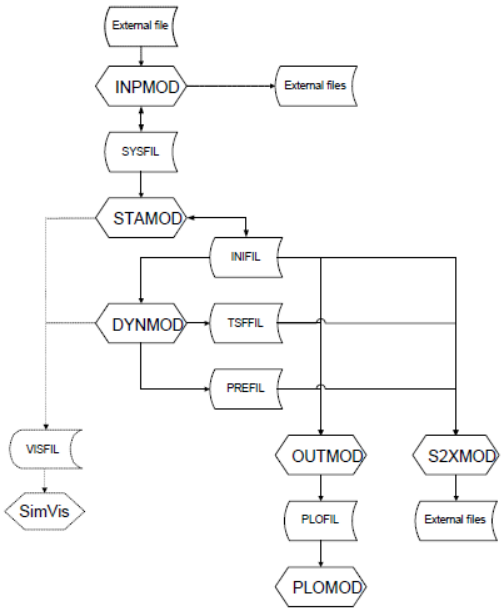

Figure 2.5: Layout of the SIMO program system and file communication between modules

The purpose of the INPMOD module is to provide interfaces to external input data sources, for example hydrodynamic programs, and to modify the system description file, SYSFIL.

In order to define the initial conditions for the dynamic simulation, the STAMOD module is necessary. The description of the system to be simulated comes from a file, SYSFIL. Moreover, it is possible to make a selection between the environmental conditions. Calculation of static equilibrium position with or without average environmental forces applied may be performed as well as calculation of natural periods and oscillation modes of the system. The written file

INIFIL then contains information about the environment, body- and position data. In addition to produce an initial condition file, INIFIL, for use by DYNMOD.

The purpose of the DYNMOD module is to perform time domain calculations of the response. The input has already been given in the file INIFIL from STAMOD. Before starting time integration of the equation of motion, the various simulation parameters must be initialized. can be executed.

The OUTMOD mo0dule is used to read time series files generated in the DYNMOD module. Further on, this module generates print and plot of time series and statistical parameters as well. The results are written to the plot file PLOFIL.

The S2XMOD module exports results obtained from dynamic analysis, i.e. time series to various file formats as for example MATLAB, i.e. time series to variuos file formats. In present verion export to MATLAB ("m"-file), export to ASCII-file and export to DIRECT ACCESS file are available.. Further on, this module also provides simple statistics and plots of time series.

The purpose of the PLOMOD module is to plot results generated by OUTMOD.

Chapter 3

Description of Installation Conditions

3.1 Installation System

There are several sub-operations constituting the installation of the tripod foundation. Among them, the lowering process analysis is very necessary, since the forces and motions of tripod are more complex than other steps. Although the knowledge from oil and gas technology can be applied as the practical experience for offshore marine operations, when performing the installation of wind turbine components the operators will be facing new challenges due to the uncertainty of different sea state. One challenge is the limited experience and therefore not yet extensive knowledge about effective and optimal installation methods. Moreover, large lift heights and assembly precision (vessel motions) are other challenges which again can be connected to the limitation of capacity and the impact by environmental conditions. The lift wire tension related to installation of the tripod foundation and corresponding motions of the coupled system are what will be considered in the thesis.

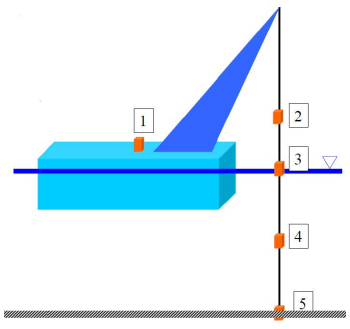

Figure 3.1: Five phases of a lift

Table 3.1: Five phases of a lift operation

Number	Phase
1	Lift-off from deck.
2	Object hanging in air.
3	Crossing of splash zone.
4	Object submerged, water depth variation
5	Landing on seabed.

Since the operation duration for installing an offshore wind turbine foundation is limited, which means the operation will only be started when it can be guaranteed that acceptable

weather conditions are to persist throughout the operation. Based on the data available can the feasibility be calculated for the entire year, within the seasons or on monthly basis. The response amplitude operator, RAO, for the installation vessel, and the eigenvalues of the coupled system, in addition to information about the operational criteria are necessary in the evaluation of an installation operation.

With increasing physical insight in addition to the expansion of operational software more parameters have been introduced to predict the feasibility of marine operations. Practical experience is an important factor in planning and execution of marine operations, but it is still essential with further numerical analysis. Hence, as the operations are becoming more complex the need for consistent methods for calculating loads and motions is increasing. Both the programming environment MATLAB and the simulation tool SIMO will be used for evaluation of the lowering process of an offshore wind turbine tripod foundation.

3.1.1 Installation Vessel

The vessel was a mono-hull heavy lift vessel. The crane was capable of performing lifts of up to 5000 tons at an outreach of 32 m in fully revolving mode. The main hook featured a clear height to the main deck of the vessel of maximum 100m. The vessel had been designed with a combination dynamic positioning system and eight catenary mooring line system. The positioning system allowed the operations of the vessel in shallow water and in close proximity to other structures. Therefore, the lifting capacity and the positioning system of the floating vessel made it capable of performing the installation of monopiles or jackets in shallow-water sites.

Table 3.2: Characteristics of installation vessel 1

Item	Value
Length overall [m]	183.0
Length between perpendiculars [m]	171.6
Breadth moulded [m]	37.8/47.0
Draught at side [m]	18.2
Operational draught(crane lifting mode) [m]	13.5
Displacement [tons]	5.12E4

The crane is capable of performing lifts of up to 5,000[t] at an out reach of 32[m] in fully revolving mode. This capacity is available while for allowing for sideleads of up to 2°. When allowing for sideleads of up 3°, a maximum capacity of 4,500[t] is available. The main hook further features a clear height to the main deck of the vessel of maximum 100[m]. This com-

bination of clearances and allowable sideleads make the crane, apart from being one of the highest capacity cranes available, also suitable for large and odd-sized loads.

In addition to the main hook, two auxiliary hooks of 800 and 200[t] capacity and a whip hoist of 110[t] are available. However, only the main hook was taken into account in the numerical simulation.

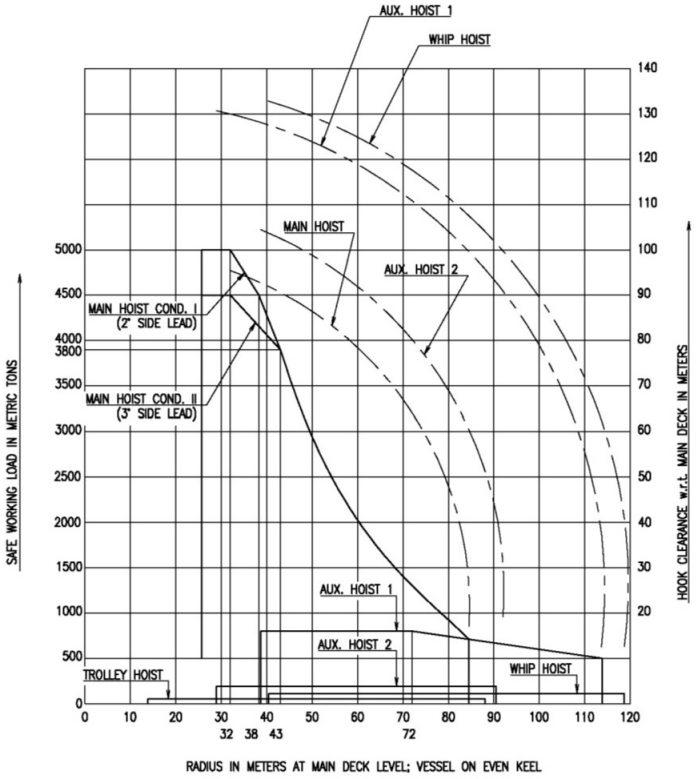

Figure 3.2: Load-radius chart of main crane

Mooring system now is a necessary equipment for installation vessels. The mooring system of the installation vessel 1 consists of 8 mooring lines with the same mechanical properties, they are arranged at stem and bow equally. By the constraints of mooring lines, the vessel horizontal motion can be reduced a lot during the installation operation.

Table 3.3: Property of mooring line

Component	Available Length	MBL	Weight	EA
76mm wire rope	2000	381.22	0.020772	32400

3.1.2 Tripod Foundation

As the water depth was increased to 45 m, the monopile used in shallow water was replaced with a tripod substructure, which is one of the space-frame concepts proposed for offshore installations in water of intermediate depth. The rotor-nacelle assembly of the NREL 5-MW turbine including the aerodynamic, structural, and control system properties—remained the same, but the support structure (tower and substructure) was changed. The tripod support structure is shown below. The detailed geometric parameters of tripod foundation can seen in the Appendix A.

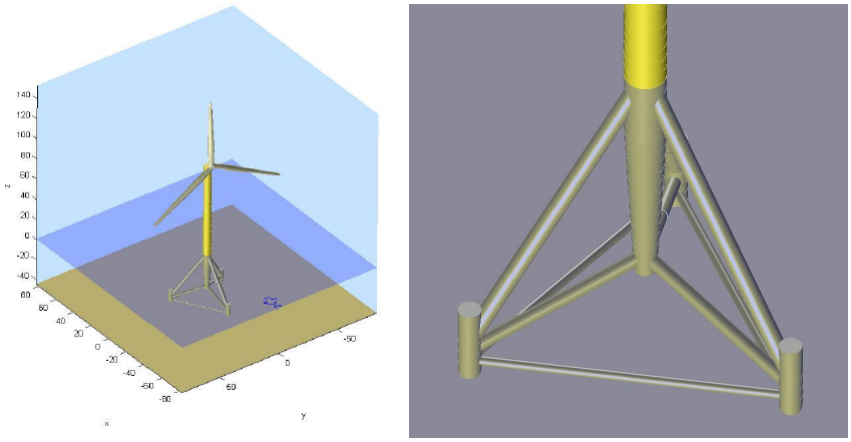

Figure 3.3: Tripod support structure

Table 3.4: Main parameters of the tripod foundation

Item	Value
Total height [m]	63
TP position∗ [m]	(0,0,45)
Center column out diameter [m]	5.7
Brace outer diameter [m]	1.2-3.15
Tripod mass [tons]	885
∗ refer to the center point of the tripod bottom	

The tripod structure presents new challenges in wind turbine modeling. For instance, it is not a tree-like structure and has to support dynamic loads through axial forces rather than bending moments. The tripod is also a good test for the offshore structure modeling capabilities of codes because it incorporates a number of features not present in conventional monopile support structures (Jonkman and Musial (2010)):

- No overall axial symmetry; there is asymmetry between forward and backward and between fore-aft motion and side-side motion.

- Different numbers of members connect at various nodes.
- The central member is significantly tapered.
- Members are at varying angles to the vertical.

3.1.3 Operational Requirements

In order to perform installation operation successfully, the operational requirements of environmental condition must be specified at the early stage of the operation plan. In consideration of the lowering process, the influence of waves will be emphasized. Since the maximum operating condition of installation vessel 1 requires the significant wave height less than 2.5m, the criterion for the operation can be set as $Hs < 2.5m$.

Besides significant wave height, the lift wire tension limit is an important criterion as well. Actually, the lift wire tension is highly related to the sea state, not merely based on the significant wave height. The factors of wave peak period, wave direction and others all can have an impact on the lift wire tension. Hence, this is a criterion for the lowering operation. In the following work, five lift wire tension limits, 11MN, 10.5MN, 10MN, 9.5MN and 9MN, will be introduced to perform the weather window analysis.

3.2 Environmental Conditions

Marine operations are highly dependent on environmental conditions and a prediction of the operational weather window is critical. Especially the impact from waves, wind and current are of interest, but also other environmental parameters as ice, the impact of tides and marine growth may be considered. Waves are of special interest as they directly influence the motions of an installation vessel.

In design of offshore structures weather statistics plays an important role. In particular the extreme value statistics is important. In the long term approach, the statistics of individual waves heights or responses over several years are considered, i.e. each three hour stationary sea states is considered independent of all previous and coming sea states. A practical way of obtaining long term extreme values is, however, by computing the extreme value statistics for all combinations of wave heights Hs and spectral peak periods Tp as obtained from a scatter diagram. The long term statistics are obtained by a weighted summation of the responses. The weight factor is the probability of occurrence of each of the sea states(Nielsen (2007)).

3.2.1 Installation Site

The site for the operation is located at Site NO.15 with water depth around 45m. For the North sea center which is very far from shore, the water depth is still very small. However, the water depth in the Atlantic area does vary. The sites with shallow water depth are suitable for bottom-fixed concepts(Li et al. (2015)).

Figure 3.4: Location of 18 potential European offshore sites

3.2.2 Wave Conditions

Since the Site NO.15 has been selected, the statistics of significant wave height and peak period at this site are essential for simulating the sea state. Statistics of wave heights and wave periods are presented in scatter diagrams. They are based on either short term or long term periods. Short term statistics in hindcast are based on one hour duration of a stationary sea state, which means a stationary condition with constant parameters. Thus, the wave spectrum, the mean wind velocity and the current are constant. However, the long term statistics depend on data for individual wave heights or responses over several years. Information can be provided by available scatter diagrams. Sources for marine wind and wave data are observations and numerical models.

The environmental limitations mentioned before are related to the significant wave height, so the data for significant wave height in hindcast will be considered only. Actually, nevertheless the wave direction impacts the wave significant wave a lot, as a simplification, the influence of wave direction was neglected and all values for significant wave height have been considered as omnidirectional in the analysis.

Based on the 10-year hindcast data between May and Seotember, the sea states can be illustrated in the $Hs-Tp$ diagram. It should be mentioned that the variation of the spectral peak period is discontinuous, so it is indeed necessary to randomize the original hindcast periods

such that some of the events are shifted to empty columns.

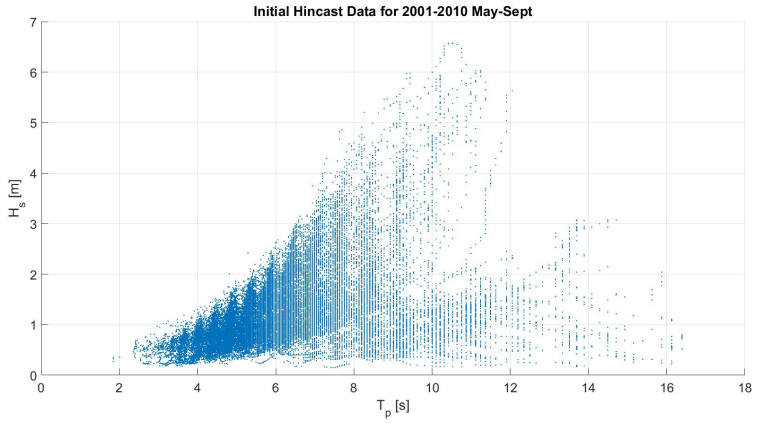

Figure 3.5: Initial Hincast Data for 2001-2010 May-SeptInitial Hincast Data for 2001-2010 May-Sept

First, peak period number i is defined by:

$$i = ROUND\left\{1 + \frac{\ln(\frac{T_p^*}{3.244})}{0.09525}\right\} \tag{3.1}$$

where T_p^* is the original peak period.

Then, the modified peak period, Tp, is given as:

$$T_p = 3.244 * \exp[0.09525 * ()i - 0.5 - rnd] \tag{3.2}$$

where rnd is uniformly distributed in the range 0 - 1.

The modified hindcast data can be seen as below:

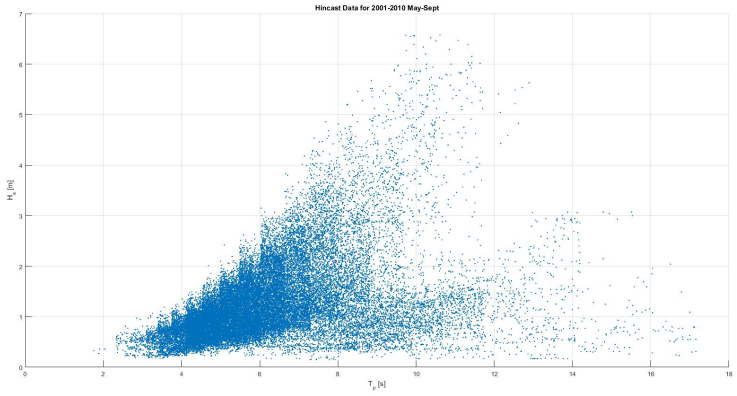

Figure 3.6: Modified Hincast Data for 2001-2010 May-SeptInitial Hincast Data for 2001-2010 May-Sept

However, the significant wave height varies with the seasons. Generally, the environmental conditions in summer are more calm than others, this why most marine operations take place during summer time. Therefore, the values for significant wave height in summer should be focused on.

Hs(m)	PDF	CDF
0,5	0,04582	0,04582
1,0	0,253491	0,299311
1,5	0,248186	0,547497
2,0	0,164967	0,712463
2,5	0,105262	0,817725
3,0	0,066356	0,884082
3,5	0,042151	0,926273
4,0	0,030052	0,956325
4,5	0,017582	0,973907
5,0	0,011831	0,985738
5,5	0,006446	0,992185
6,0	0,003815	0,99600
6,5	0,001517	0,997547
7,0	0,000936	0,998483
7,5	0,00073	0,999213
8,0	0,000548	0,99976
8,5	0,000183	0,999943
9,0	2,28E-05	0,999966
9,5	3,42E-05	1

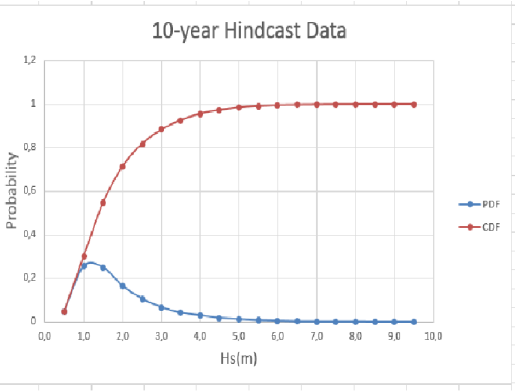

Figure 3.7: 10-year statistical distribution of Hs

Hs(m)	PDF	CDF
0,5	0,073883	0,073883
1,0	0,371977	0,445861
1,5	0,275517	0,721378
2,0	0,138126	0,859504
2,5	0,068056	0,92756
3,0	0,035212	0,962772
3,5	0,016885	0,979657
4,0	0,008606	0,988263
4,5	0,004711	0,992974
5,0	0,003159	0,996133
5,5	0,001825	0,997958
6,0	0,001471	0,999428
6,5	0,000408	0,999837
7,0	0,000163	1

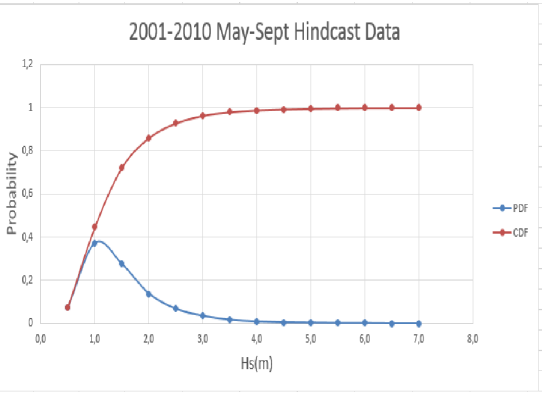

Figure 3.8: 2001-2010 May-Sept statistical distribution of Hs

By comparison between both figures above, it can be concluded that if the limitation of the significant wave height less than $2.5m$ is the only requirement for marine operations, the installtaion can be carried out most of the time between May and September. This means that operators will have more freedom to perform installation since there is no much restriction from the environmental conditions. But, instead of significant wave height, the lift wire tension was introduces as the main limitation for the operation, therefore more analysis based on environmental conditions should be performed.

The figures above are made up of data points updated one hour. However, as an installation operation will last longer than one hour also wave statistics for a longer perspective are of interest. For the needs of the installation operation sufficiently calm weather over an adequate

period of time is required for the execution of the operation. It is desired that the operation can be executed without disturbances so the need for stopping and starting up again is at the minimum. This can be done when the desired conditions are fulfilled within a period with sufficient duration.

In a whole, the duration of installation and the lift wire tension related to significant wave height and spectral peak period are significant when establishing the weather window for marine operation in the following analysis.

3.2.3 Typical Sea States

In order to analyze the lowering process further, it is necessary to do 3-hour stationary simulations for the coupling system of vessel and tripod with several submergence of the tripod, therefore the typical sea states for examination should be decided before doing simulations. Different sea states affect the system a lot and thus several significant wave height and spectral peak period are of interest.

Scatter diagram for Hs and Tp from 2001-2010 May-Sept hindcast data (Site No. 15)

Tp / Hs [m]	1.0-2.0	2.0-3.0	3.0-4.0	4.0-5.0	5.0-6.0	6.0-7.0	7.0-8.0	8.0-9.0	9.0-10.0	10.0-11.0	11.0-12.0	12.0-13.0	13.0-14.0	14.0-15.0	15.0-16.0	16.0-17.0	17.0-18.0	Marginal for Hs
0.0-0.5	3	68	649	967	272	149	153	173	98	82	33	17	23	13	11	2	0	2713
0.5-1.0	0	83	1152	4866	3610	1863	513	543	484	311	75	38	62	31	6	22	0	13659
1.0-1.5	0	0	37	1818	3327	2281	1142	587	307	351	170	62	19	8	4	4	0	10117
1.5-2.0	0	0	0	89	1753	1702	747	466	115	66	64	38	22	5	5	0	0	5072
2.0-2.5	0	0	0	1	220	1263	563	285	80	26	14	13	31	2	1	0	0	2499
2.5-3.0	0	0	0	0	5	422	479	249	83	15	6	0	32	2	0	0	0	1293
3.0-3.5	0	0	0	0	0	34	310	134	110	17	7	0	4	4	0	0	0	620
3.5-4.0	0	0	0	0	0	1	100	86	105	17	7	0	0	0	0	0	0	316
4.0-4.5	0	0	0	0	0	0	29	54	60	23	7	0	0	0	0	0	0	173
4.5-5.0	0	0	0	0	0	0	6	25	38	42	5	0	0	0	0	0	0	116
5.0-5.5	0	0	0	0	0	0	0	8	17	32	10	0	0	0	0	0	0	67
5.5-6.0	0	0	0	0	0	0	0	0	13	31	9	1	0	0	0	0	0	54
6.0-6.5	0	0	0	0	0	0	0	0	0	12	3	0	0	0	0	0	0	15
6.5-7.0	0	0	0	0	0	0	0	0	0	6	0	0	0	0	0	0	0	6
Marginal for Tp	3	151	1838	7741	9187	7715	4042	2610	1510	1031	410	169	193	65	27	28	0	36720

Figure 3.9: Scatter diagram for Hs and Tp from 2001-2010 May-Sept hindcast data (Site No. 15)

Based on the scatter diagram above, the frequency of occurrence of spectral peak period can be obtained.

Tp / Hs [m]	1,5	2,5	3,5	4,5	5,5	6,5	7,5	8,5	9,5	10,5	11,5	12,5	13,5	14,5	15,5	16,5	17,5
0.0-0.5	0,00110579	0,0250645	0,23921858	0,35643199	0,10025802	0,05492075	0,05639513	0,06376705	0,03612237	0,03022484	0,01216366	0,00626613	0,0084777	0,00479174	0,00405455	0,00073719	0
0.5-1.0	0	0,00607658	0,08434	0,35624863	0,2642946	0,13639359	0,03755765	0,03975401	0,03543451	0,02276887	0,00549089	0,00278205	0,00453913	0,00226957	0,00043927	0,00161066	0
1.0-1.5	0	0	0,00365721	0,17969754	0,32885243	0,22546209	0,11287931	0,05802115	0,03034496	0,03469408	0,0168034	0,0061283	0,00187803	0,00079075	0,00039537	0,00039537	0
1.5-2.0	0	0	0	0,01754732	0,34562303	0,33556782	0,14727918	0,09187697	0,0226735	0,01301262	0,0126183	0,00749211	0,00433754	0,0009858	0,0009858	0	0
2.0-2.5	0	0	0	0,00040016	0,08803521	0,50540216	0,22529012	0,11404562	0,03201281	0,01040416	0,00560224	0,00520208	0,01240496	0,00080032	0,00040016	0	0
2.5-3.0	0	0	0	0	0,00386698	0,32637278	0,3704563	0,19257541	0,0641918	0,01160093	0,00464037	0	0,02474865	0,00154679	0	0	0
3.0-3.5	0	0	0	0	0	0,05483871	0,5	0,21612903	0,17741935	0,02741935	0,01129032	0	0,00645161	0,00645161	0	0	0
3.5-4.0	0	0	0	0	0	0,00316456	0,3164557	0,2721519	0,33227848	0,05379747	0,0221519	0	0	0	0	0	0
4.0-4.5	0	0	0	0	0	0	0,16763006	0,31213873	0,34682081	0,13294798	0,04046243	0	0	0	0	0	0
4.5-5.0	0	0	0	0	0	0	0,05172414	0,21551724	0,32758621	0,36206897	0,04310345	0	0	0	0	0	0
5.0-5.5	0	0	0	0	0	0	0	0,11940299	0,25373134	0,47761194	0,14925373	0	0	0	0	0	0
5.5-6.0	0	0	0	0	0	0	0	0	0,24074074	0,57407407	0,16666667	0,01851852	0	0	0	0	0
6.0-6.5	0	0	0	0	0	0	0	0	0	0,8	0,2	0	0	0	0	0	0
6.5-7.0	0	0	0	0	0	0	0	0	0	1	0	0	0	0	0	0	0
Marginal for Tp	0,00110579	0,03114108	0,32721578	0,91032564	1,13093027	1,64212246	1,98566759	1,69538009	1,89935689	3,55062528	0,69024735	0,04638919	0,06283762	0,01763659	0,00627516	0,00274323	0

Figure 3.10: Scatter diagram showing frequency of occurrence of spectral peak period, Tp, and significant wave height, Hs

Then the mean peak period should be calculated . The mean value of the peak period for each value of the significant wave height has been found by using the formula below.

$$\overline{T_p} = \frac{\sum (T_i * P_i)}{\sum P_i} \tag{3.3}$$

where T is the period and P is the probability of occurrence. The values for significant wave height and the related values for the mean value of the peak period that will be used in the response analysis are presented below.

Table 3.5: Typical Sea States

Sea State	Hs(m)	Mean Value Tp(s)
1	0,25	5,52
2	0,75	5,67
3	1,25	6,41
4	1,75	6,73
5	2,25	7,16
6	2,75	7,70
7	3,25	8,23
8	3,75	8,68
9	4,25	9,07
10	4,75	9,63
11	5,25	10,16
12	5,75	10,46
13	6,25	10,70
14	6,75	10,50

Chapter 4

Numerical Modelling and Analysis

Accurate and realistic modelling is required to quantify the dynamic response of different installation systems, allowing for better planning of the operations. Tripod lowering process is a typical lifting operation activity. Based on the data for floating vessel and tripod foundation, proper theories should be selected when establishing the corresponding models.

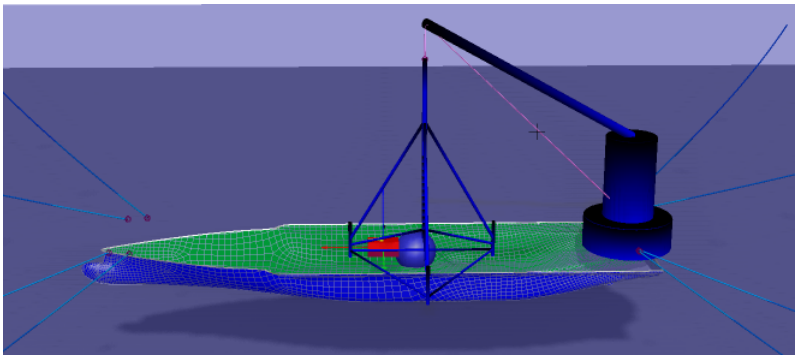

Figure 4.1: Numerical Model in SIMO

In order to get the probability of being able to work in a specific time period, in this chapter, numerical simulations have been performed to investigate the heavy lift operations considering the responses of lift wire tension and some motions of significance during the lowering process.

4.1 Modelling of Heavy Lift Vessel

4.1.1 Characteristics of Vessel Numerical Model

According to the data for heavy lift vessel mentioned before, the potential added mass and damping coefficients, the hydrostatic stiffness and the first order wave excitation force transfer

functions of the vessel were calculated in WADAM based on the panel method(Veritas (2010b)), and then the retardation functions and the first order excitation force were obtained. In the current vessel model, waves were considered as main factor, and wind and current forces can be neglected.

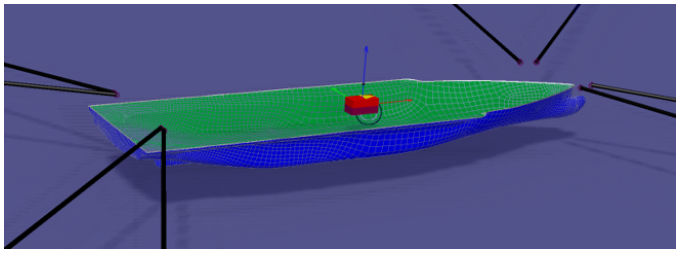

Figure 4.2: Numerical Model for Heavy Lift Vessel

The dynamic responses of a floating crane and a heavy load with a flexible boom were studied in Park et al. (2011) by modelling the crane boom using finite element method (FEM). In their study, the maximum lifting capacity of the crane was 3600 tons and the load considered was above 1300 tons, more than 30% of the crane capacity, which can be considered as an elastic boom. However, the load from tripod is just around 880 tons, only 18% of the crane capacity, much lower than 30%, therefore, the connection between vessel and crane boom can be considered as rigid.

4.1.2 Response Amplification Factor(RAO)

By calculating related hydrodynamic coefficients with fixed water depth, this model was introduced into SIMA as the installation vessel for tripod. Since only head sea is taken account in simulations, the vessel heave and pitch motions are dominated.

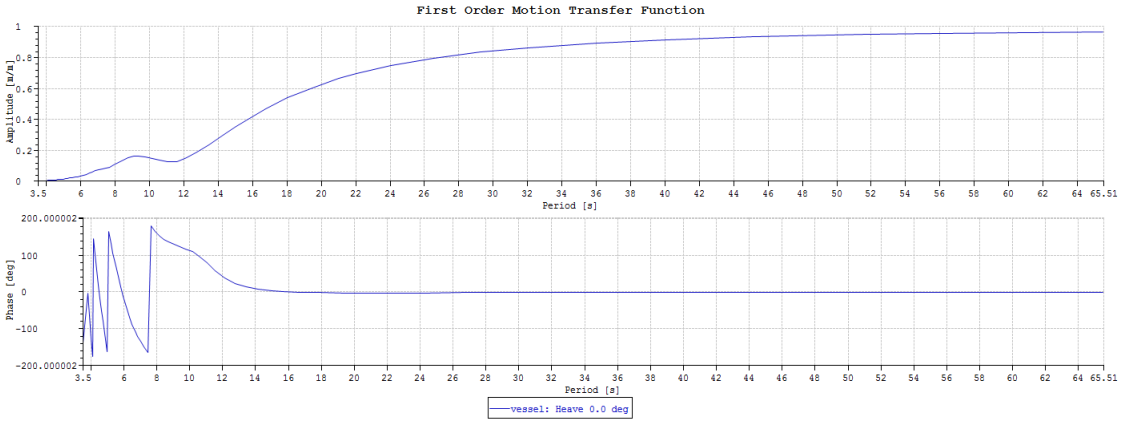

Figure 4.3: Response amplitude operator of Heave with head sea

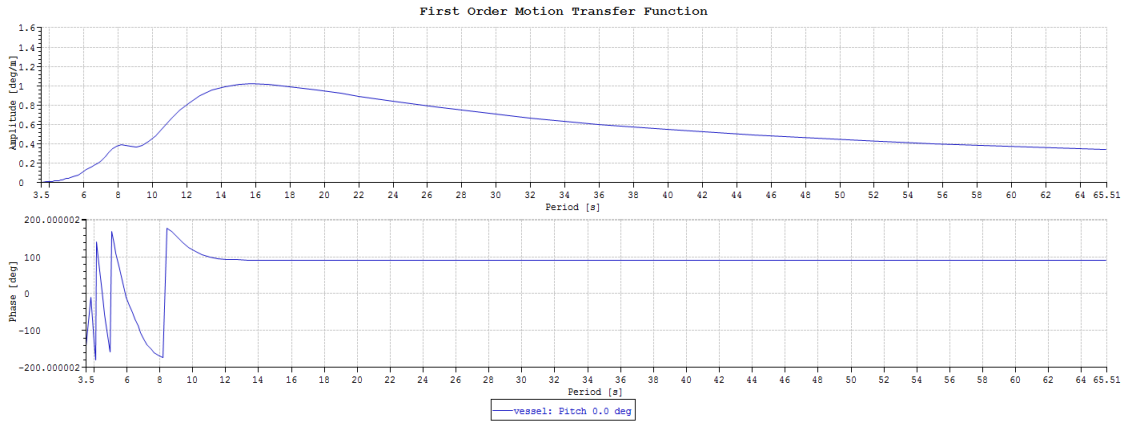

Figure 4.4: Response amplitude operator of Pitch with head sea

4.1.3 Coordinate System on Vessel

The global coordinate system was a right-handed coordinate system with the following orientation: the X-axis pointed towards the bow, the Y-axis pointed towards the port side, and the Z-axis pointed upwards. The origin was located at mid-ship section, center line and still-water line when the vessel was at rest. The positions of the crane tip and the tripod were chosen based on practical operations.

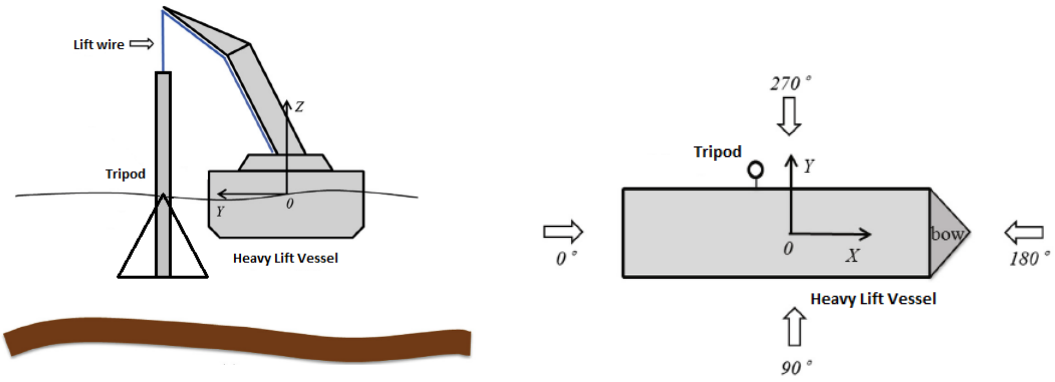

Figure 4.5: Definitions of global coordinate system

4.1.4 Ballast Water

Since the vessel numerical model was obtained without considering tripod, in order to balance the weight of tripod at the beginning of the lowering process(roll angle is largest), the ballast water is necessary. In SIMO, the time dependent mass allows the user to model the effects of a mass that can vary both in magnitude and in position, so the time dependent mass was

introduced as the ballast water. Generally, during the lowering process, operators will adjust the ballast water for different submergence of tripod, however, because all tripod members are hollow, the buoyancy of tripod is relatively small, which means the variation of ballast water is not obvious, therefore, the weight of ballast water was fixed for simplicity.

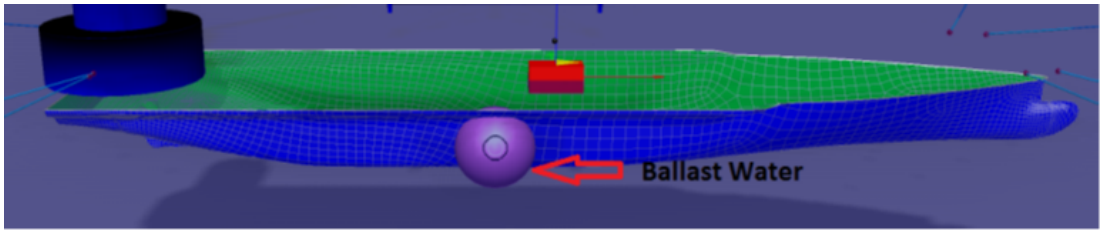

Figure 4.6: Position of Ballast Water

Table 4.1: Weight and Position for Ballast Water

Weight	X-position	Y-position	Z-position
1500tons	-11.2m	-18.0m	-8.0m

4.2 Modelling of Tripod Foundation

The external forces on the tripod consist of the gravity force, the buoyancy force and the hydrodynamic wave forces. In order to obtain more accurate responses for motion and forces, the tripod model should be established reasonably.

4.2.1 Applicability Check for Slender Element

Since the water depth at site no. 15 is limited(45m), for simplicity, the linear potential theory with limited water depth is valid. The relationship between wave length λ and wave period T can be described by the following equation(Faltinsen (1993)).

$$\lambda = \frac{g}{2\pi} T^2 \tanh \frac{2\pi}{\lambda} h \tag{4.1}$$

Based on the data from hindcast, the main range of wave period is from 4s to 15s. By using the equation above, the corresponding wave lengths can be calculated.

Table 4.2: Results from linear regular wave theory with 45m water depth

Wave Period T(s)	3,58	4,38	5,66	8,03	10,03	12,01	14,05	16,15
Wave Length $\lambda(m)$	20	30	50	100	150	200	250	300

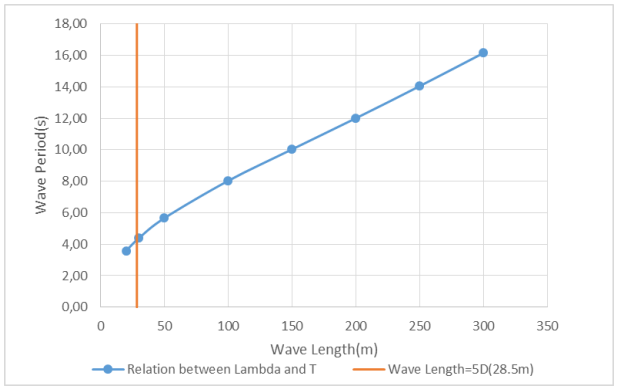

Figure 4.7: Relationship between wave length λ and wave period T

For the given tripod foundation, the upper part of central column has the largest diameter 5.7m. If this value satisfy the long-wave approximation, other braces of the tripod fulfill the requirement automatically. From the figure above, it is obvious to see that most sea states with relatively longer wave length located in the main range of wave period, therefore, one can say using slender element(Morison element) as numerical model is reasonable.

4.2.2 Selection of C_M, C_A and C_q

Since the outer surface of the tripod was assumed to be smooth, and Reynold number had a magnitude of 10^6 to 10^7. Moreover, KC number in the operational sea states was in the range of 1-3. According to Park et al. (2011), the quadratic drag coefficient for all the tripod members was selected as $C_q = 1.0$, which takes into account the flow separation of the water outside of the tripod.

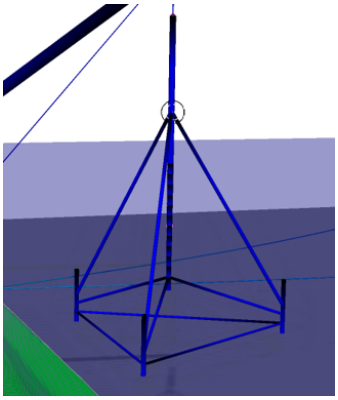

Figure 4.8: Tripod Numerical Model in SIMO

Since all the tripod members are hollow, during the lowering process of tripod, both central column and braces are filled with water. According to Li et al. (2014), the inertia and added

mass coefficients were used for tripod members, $C_M = C_A = 2$. However, it is difficult to build hollow cylinder by using slender elements in SIMO. In order to introduce the current values of C_M and C_A into the numerical model, therefore, the valid slender elements were used to replace the real physical model, which leads that the diameters of numerical model in SIMO are much smaller than realistic tripod.

Moreover, it should be mentioned that the slamming forces on the tripod and the variation of buoyancy due to filling water are neglected in the time-domain simulations.

4.3 Tripod Lowering System

The typical lowering system for tripod foundation can be seen as following. The water depth for installation is 45m.

Figure 4.9: Lifting arrangement for tripod installation

4.3.1 Modelling of Crane System

From the load-radius chart of main crane(Figure 2.3), the boom length of the crane can be set as 90m. Since the weight of tripod(885tons) in the range of save working load for main crane, there should be no problems with the capacity. In the system description file, the origin of the coordinate system is set to be midship (91.5 m from stern) and at still water level. According to the layout of heavy lift vessel(see Appendix A), the x-position of the crane is 79m behind the origin and the z-position of the boom lower end is 36.6m above the water surface. Assume the minimum installation distance between tripod and vessel side is 40m, in addition the height of crane tip is 80m. By using the following equation, the position of crane tip can be found.

$$Boomlength = \sqrt{x^2 + y^2 + z^2} \tag{4.2}$$

Table 4.3: Boom Position

	X	Y	Z
Boom lower end	-79	0	36.6
Crane tip	-11.2	40	80

4.3.2 Lift Wire Coupling

Knowing the position of each line end, the elongation and thereby the tension of the lift wire may be determined. The material damping in the wire was included in the model.

Table 4.4: Parameters for Simple Coupling

Wire Length(m)	Connection Flexibility(N/m)	Material Damping(Ns)	Cross-section Stiffness(N)
115.4	2.0e-09	1.582e+08	7.91e+09

It should be mentioned that the initial length 115.4m was used to make sure the center of tripod 50m above the water line, which means the tripod in air at the beginning of lowering process, with air gap of 5m.

Table 4.5: Statically calculated positions(difference from modelled)

Body	X	Y	Z	Rx	Ry	Rz
vessel	0.117 (0.12)	-0.241 (-0.24)	-0.373 (-0.37)	-2.21 (-2.2)	-0.0846 (-0.085)	0.00 (0.00)
tripod	-11.2 (0.00)	42.8 (2.8)	49.9 (-2.1)	0.00 (0.00)	0.00 (0.00)	30.0 (0.00)

Because of the tripod's gravity, the lift wire was stretched by 2.1m. The vessel position was also influenced, however, the effect was limited and satisfied the safe working requirement.

4.4 Frequency-domain Simulations

From a hydrodynamical point of view is it sufficient to analyse a structure in incident sinusoidal waves of small steepness, since it is possible to obtain results in irregular seas by linearly superposing results from regular wave components.

For the tripod lowering process, the draft of the tripod varies with time changing. In order to study every steps of the lowering process further, it is essential to perform simulations with different tripod drafts. Since the tripod drafts are dependent on the length of lift wire, the wire length was set as variable to replace the tripod draft in the following simulations. But different from simulations of lowering process, the simulation with fixed tripod draft is a stationary process. When assuming linear and steady-state conditions can the response be calculated based

on analysis in frequency domain.

4.4.1 Eigenvalue Analysis

The natural modes of the coupled vessel-tripod lowering system include 12 DOFs. During the lowering process, the properties rely on the tripod position. Thus, the selected tripod positions(presented by lift wire lengths) can be seen as below:

Table 4.6: Selected tripod position for eigenvalue analysis

Lift Wire Length(m)	**Draft of Tripod(m)**
115,4	-5,0(in air)
120	-0,3(in air)
125	4,5
130	9,4
135	14,2
140	19,2
145	24,1
150	29,1
157,5	36,5
165	43,9

Based on the numerical model built before, the corresponding eigenvalues of the coupled system can be calculated by running static simulations in SIMO. It should be mentioned that all the modes are coupled.

4.4.2 Response Analysis

Since the position of the tripod foundation is fixed, the coupled system is affected by the wave elevation only. In order to simulate such a stationary process, 3-hour simulations are recommended, which means the simulation length should be 10800s. Similar as the eigenvalue analysis, the range of the tripod position is also from air to water, the corresponding lift wire lengths can be seen as below. Moreover, each condition contains 20 wave seeds as well.

Table 4.7: Wire Lengths

Condition	1	2	3	4	5	6	7	8	9	10
Wire Length(m)	120	125	130	135	140	145	150	155	160	165

In **Chapter 3**, the typical Sea States have been already obtained. For simplicity, three typical sea states were considered in simulations.

Table 4.8: Selected Sea States

Sea State	Hs(m)	Mean Value Tp(s)	ω_p(rad/s)
1	1,25	6,41	0,98
2	1,75	6,73	0,93
3	2,25	7,16	0,88

4.5 Time-domain Simulations

The lowering process of tripod foundation should be considered as a non-linear system, in order to study the dynamic responses of this operation, time-domain simulations are recommended. Then the principle of superposition is omitted. Instead a random time realization of the spectrum is considered for a given sea state and the system motions are estimated in time domain by using for example potential theory as in SIMO. In the thesis work, the equations of motions were solved by Newmark-β numerical integration with a time step of 1 second. Moreover, the environmental input was based on stochastic irregular waves , and the time series of the wave kinematics were obtained using the Fast Fourier Transformation(FFT) algorithm from JONSWAP wave spectrum of given significant wave height, Hs and spectral peak period, Tp.

4.6 Modifications for Time-domain Simulations

Before running the dynamic analysis, different from steady-state conditions, some model parameters should be modified in order to calculate correct responses successfully. The following part talks about these important parameters in time-domain simulations.

4.6.1 Simulation Length

The length of simulation should include the whole lowering process, which means the bottom of tripod foundation moves from 5m above the water surface to 2m above the seafloor. Since the water depth is 45m, the drop height is 48m. Considering the winch speed is 0.05m/s, the lowering process should last for 960s.

However, the result can be unstable if only the lowering process was simulated, so it is necessary to simulate the process before and after the lowering operation. Before lowering, 600s was added to simulation the process of tripod foundation in the air; When the foundation arrives above the seafloor, it will be hanged there for 440s. Therefore, the whole simulation length is 2000s. If the winch speed was changed, for convenience, the start time of lowering is still fixed at 600s and the simulation lengths after lowering are flexible.

4.6.2 Winch Speed

Winch speed means the lowering velocity of lift wire, which is highly related to the slamming impact velocity of tripod foundation. Since the impact load with high pressure peaks always appears in the impact process between objects and water, it is necessary to avoid such a strong slamming force appearing during the installation operation. The simple and effective method is to control the winch speed, however, this does not means the lower winch speed the better, because a too slow speed may increase the lift wire tension and the tripod motions when the tripod foundation goes through the splash zone. In this case, the winch speed is set as 0.05m/s initially. This effect of different winch speeds will be discussed in detail in the following part.

4.6.3 Catenary Line

In order to find the probability of installation in different sea states, some extreme sea states should be taken into consideration. In those worse sea states, the motion of vessel can be amplified. In this situation, the mooring lines should have a higher maximum tension limit to keep the vessel with a stable motion. Otherwise, it is hard for dynamic simulation to find a equilibrium and this can lead to an incomplete result of the probability of being able to work. Therefore, the tension limit of mooring lines should be large enough. In this case the tension limit was set as 2e+07N.

4.6.4 Wave Spectrum

The irregular wave is used to simulate the real sea state, the JONSWAP spectrum is recommended because of the installation location during operation. In the time-domain simulation will irregular waves be considered. However, in order to simplify the simulation process, the wave theory for each frequency component is the the linear wave theory, and only wave is taken into consideration and the influences of swell, wind and current are neglected. The spectrum modeled is a simple JONSWAP spectrum in SIMO dependent on the spectral peak period T_p and the significant wave height H_s. The waves are modeled as long crested waves and the average wave propagation direction is zero degree(head sea).

Table 4.9: Selection of T_p and H_s in Time-Domain Simulations

Spectral Peak Period T_p (s)														
1	2	3	4	5	6	7	8	9	10	11	12	13	14	15

Significant Wave Height H_s (m)										
1	1,5	2	2,5	3	3,5	4	4,5	5	5,5	

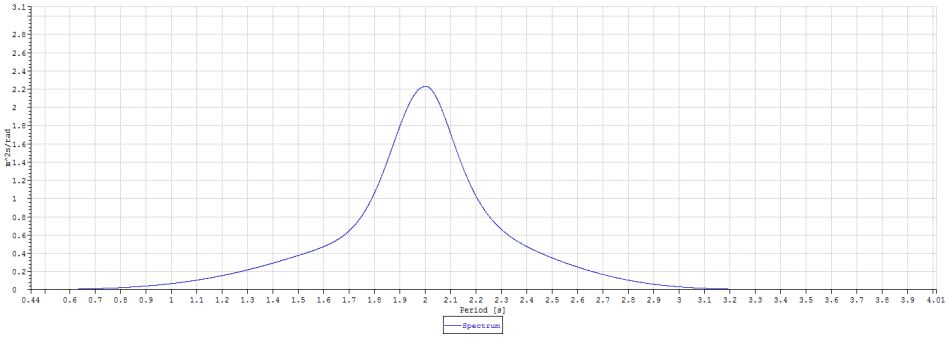

Figure 4.10: JONSWAP spectrum for Hs=6m, Tp=2s

4.6.5 Wave Seeds

The number and length of simulations were chosen in order to account for the variability of stochastic waves and to provide a reasonable statistical basis for comparison. First of all, the number of wave seeds should be defined, then the method of ensemble average was introduced.

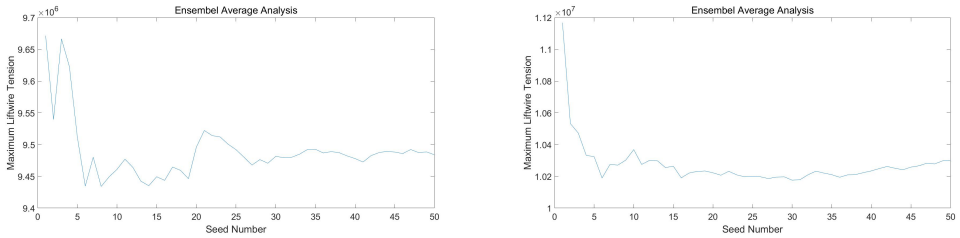

Figure 4.11: Ensemble average analysis for given sea states(Hs=3m,Tp=5s) and (Hs=3m,Tp=6s)

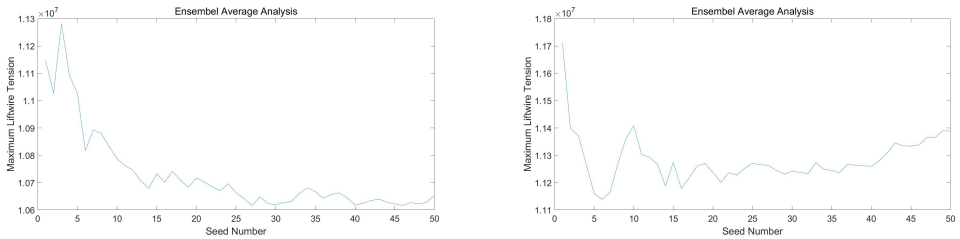

Figure 4.12: Ensemble average analysis for given sea states(Hs=4m,Tp=5s) and (Hs=4m,Tp=6s)

From the figures above, the curves of the four selected conditions become stable when seed number from 20 to 30. Actually, a large number of wave seeds is better for simulating a stochastic process. However, with the limit of computing power and time, a reasonable seed number of 20 is suggested. 20 realizations of irregular waves were generated at each environmental condition using different seeds(960s for each seed) for tripod lowering process. 20 repetitions of the simulation corresponded to an operation with a duration of approximately five hours.

Chapter 5

Results of Numerical Simulations

After performing the numerical simulations for the coupled vessel-tripod system, some results are obtained. In this chapter, these results will be shown and some derivative conclusions will be discussed as well.

5.1 Results of Frequency-domain Analysis

5.1.1 Eigenvalues of Coupled System

Before studying the eigenvalues of the coupled system, the eigenvalues of the heavy lift vessel should be introduced firstly in order to make a comparison with the coupled system. From the table below, it is expected that the vessel motions will play an significant role in the response of the tripod when the wave tripod are approximately from 8s to 16s.

Table 5.1: Eigenvalues of crane vessel with 45m water depth

Mode	Excursion	8,56	9,87	15,69	24,54	38,16	47,41
SURGE	**1.00(m)**	-0,23	-0,06	0	0	0	**1**
SWAY	**1.00(m)**	0	0	0,12	-0,03	**1**	0
HEAVE	**1.00(m)**	-0,12	**1**	0	0	0	0
ROLL	**1.00(deg)**	0	0	**1**	0,09	-0,03	0
PITCH	**1.00(deg)**	**1**	0,1	0	0	0	0
YAW	**1.00(deg)**	0	0	-0,03	**1**	0,01	0

By running static simulations in SIMO, the eigenvaluses of the coupled system can be obtained. Since the draft of tripod is changing during the lowering process, the properties of the system vary with time. Therefore, the eigenmodes and eigenperiods rely on the position of tripod. However, in the operation, the change of tripod's draft is due to the variation of lift wire

length, so in the subsequent analysis, the wire length was set as the main variable. The length of lift wire is chosen as 130m(draft is about 9.4m) in the table. The eigenvalues shown in the table for each body refer to its own body-fixed coordinates.

Table 5.2: Eigenvalues of the coupled system with wire length=130m

Body	**Mode**	**Excursion**	**0,92**	**4,15**	**4,94**	**8,69**	**9,29**	**9,89**
vessel	**SURGE**	**1.00(m)**	0	0	0	-0,1	0	-0,06
vessel	**SWAY**	**1.00(m)**	-0,02	0,01	0	0	0,06	-0,09
vessel	**HEAVE**	**1.00(m)**	-0,01	0	0	-0,05	0	**1**
vessel	**ROLL**	**1.00(deg)**	-0,16	0,15	0	-0,03	0,47	-0,08
vessel	**PITCH**	**1.00(deg)**	0	0	-0,01	0,42	0	0,11
vessel	**YAW**	**1.00(deg)**	0	0	0	0,02	-0,01	0,02
Tripod	**SURGE**	**1.00(m)**	-0,01	0,37	**0,68**	**0,62**	-0,44	0,21
Tripod	**SWAY**	**1.00(m)**	0	**0,69**	-0,37	-0,24	**-0,8**	0,12
Tripod	**HEAVE**	**1.00(m)**	**1**	0,14	0	0,04	0,44	**0,97**
Tripod	**ROLL**	**1.00(deg)**	0	**-1**	**0,55**	0,39	**1**	-0,21
Tripod	**PITCH**	**1.00(deg)**	-0,02	**0,54**	**1**	**1**	**-0,53**	0,35
Tripod	**YAW**	**1.00(deg)**	0	0	0	0	0	0

Body	**Mode**	**Excursion**	**24,13**	**28,51**	**33,27**	**38,56**	**49,64**	*********
vessel	**SURGE**	**1.00(m)**	-0,03	0	0,13	0,02	**0,78**	0
vessel	**SWAY**	**1.00(m)**	-0,05	-0,04	-0,02	**1**	0	0
vessel	**HEAVE**	**1.00(m)**	0	0	0	0,03	0	0
vessel	**ROLL**	**1.00(deg)**	0,01	0,09	-0,01	0,15	0	0
vessel	**PITCH**	**1.00(deg)**	-0,01	0	-0,01	0	0,01	0
vessel	**YAW**	**1.00(deg)**	**0,72**	-0,03	0,08	0,03	-0,02	0
Tripod	**SURGE**	**1.00(m)**	-0,02	0,16	**-0,57**	0,36	**1**	0
Tripod	**SWAY**	**1.00(m)**	0	0,22	0,36	**0,78**	**-0,59**	0
Tripod	**HEAVE**	**1.00(m)**	0,01	0,08	0	0,14	0	0
Tripod	**ROLL**	**1.00(deg)**	-0,16	**1**	**0,63**	**0,83**	-0,29	0
Tripod	**PITCH**	**1.00(deg)**	**-1**	**-0,58**	**1**	-0,31	-0,49	0
Tripod	**YAW**	**1.00(deg)**	0	0	0	0	0	**1**

When the eigenperiod = 0.92s, 4.15s, 4.94s, 28.51s and 33.27s, these conditions are dominated by tripod motions when vessel is nearly still, where condition of 0.92s is heave motion of the tripod, the other 4 conditions are relatively more complex, the dominating motions are made of horizontal motions(surge and sway) and rotational motions(roll and pitch).

Combining with the eigenvalues of vessel, the condition of 8.69s is corresponded to the natural period of vessel pitch. In this situation, the violent pitch motion of the vessel excites the pitch motion of the tripod, and there is an obvious motion of the tripod in surge at the same time. Different from condition of 8.69s, when the eigenvalue equals to 9.29s, the roll motion of vessel and tripod is dominated. However, there is no corresponding value in the eigenvalues of vessel to prove this situation is excited by the vessel roll motion, therefore the difference

between them should be produced by the coupling of tripod. The sway motion of the tripod is also obvious. For the condition of 9.89s, the coupled system is dominated by heave motion. In the coupled system, the vessel also has an obvious yaw motion around 24s, and there is an important pitch motion of the tripod simultaneously. For the conditions of 38.56s and 49.64s, the horizontal motions are significant, both vessel and tripod.

It should be mentioned that the eigenperiod of tripod yaw motion could not be calculated in SIMO since the value is too large. Moreover, it is secondary in the study.

During the installation, the position of tripod changes with the running winch, and increasing length of the lift wire changes the total restoring stiffness. Further on, the added mass increases due to the increasing submergence. Therefore, it is essential to analyze the relationship between eigenvalues and positions of tripod. Considering the wave period range in the study is below 20s, so for simplicity, only eigenvalues in this range were taken into account.

Table 5.3: Eigenvalues of the coupled system motions with varying tripod positions in the wave period range(mode 1: tripod heave; mode 2: tripod roll 1; mode 3: tripod pitch 1; mode 4: tripod roll 2; mode 5: tripod pitch 2; mode 6: vessel heave)

Lift Wire Length(m)	**Draft of Tripod(m)**	**Eigen Mode NO.**					
		1	**2**	**3**	**4**	**5**	**6**
115,4	**-5,0(in air)**	0,81	2,61	3,25	5,81	8,82	9,89
120	**-0,3(in air)**	0,89	3,16	3,86	7	8,73	9,89
125	**4,5**	0,9	3,69	4,45	8,16	8,7	9,89
130	**9,4**	0,92	4,15	4,94	9,29	8,69	9,89
135	**14,2**	0,94	4,62	5,43	10,4	8,68	9,89
140	**19,2**	0,95	5,01	5,81	11,4	8,67	9,89
145	**24,1**	0,96	5,46	6,27	12,49	8,67	9,89
150	**29,1**	0,98	6,28	7,2	14	8,71	9,89
157,5	**36,5**	1	7,15	8,02	15,86	8,85	9,89
165	**43,9**	1,02	8,52	8,52	19,02	9,01	9,9

From data in the table, the heave , roll and pitch motions of the coupled system are dominated in the range of wave period. It should be mentioned that only the most dominating modes were included in this table, however, there were also other obvious motions accompanying with the dominating mode. For instance, when the large vessel heave motion happens, the tripod heave and pitch motions are also significant, the main reason of the large tripod pitch motion at this situation is the x-position of tripod is not at origin , which leads to the pitch moment on the tripod when the vessel has an obvious heave motion.

Actually, in the coupled system of the vessel and the tripod, it is difficult to interpret the 12 eigenmodes because of the coupling effects, however, some general results still can be obtained. According to Figure 5.1, it is obvious to see that there is no change with the eigenperiods

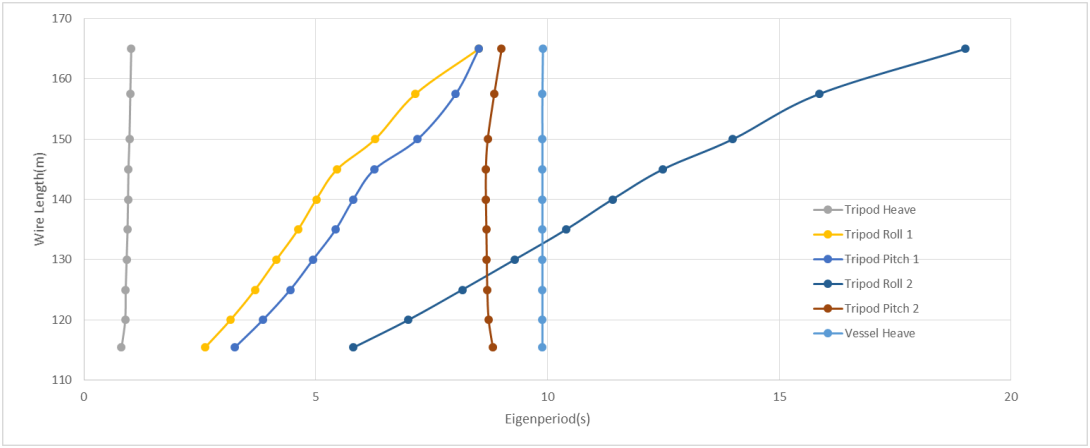

Figure 5.1: Eigenvalues of the coupled system motions with varying tripod positions in the wave period range

of mode 1, 5 and 6. Generally, since the eigenvalue of mode 1 is too small compared with the range of wave period(from 2s to 15s), such a mode can be neglected. On the other hand, mode 5 and 6 should be paid attention to, especially when the wave period around 9s, the operator should take some measures to avoid these dangerous motions. The other three modes all increase dramatically due to changes in the restoring forces and significant contributions from the added mass, especially for mode 4.

5.1.2 Spectrum Analysis

The spectrum analysis is necessary to study the effect from different tripod positions further. Based on the times series of the coupled system motion, the corresponding spectra can be gain. However, the incident wave affects the tripod rotational motion a lot and other motions of the coupled system are relatively stable. Therefore, the spectra for the tripod rotational motions will be discussed mainly. In the following figures, the curve no. (1,11,21,...,91) is corresponded to the condition from 1 to 10.

Figures from 5.2 to 5.4 show the response spectra of tripod roll motion for the three sea states respectively. In Figures 5.2 and 5.3, when the lift wire length reaches 145m, the tripod roll motion gets more fierce compared with other positions. In this case, it is obvious to see that the excitation from the incident wave to the tripod roll motion. For Figure 5.4, this peak moves to condition 5 with 140m lift wire length. As a whole, at different positions, the tripod roll motions are basically caused by the incident wave. Further on, such an influence focuses on conditions with wire length from 125m to 145m, which corresponds to the main part of the tripod crossing the splash zone.

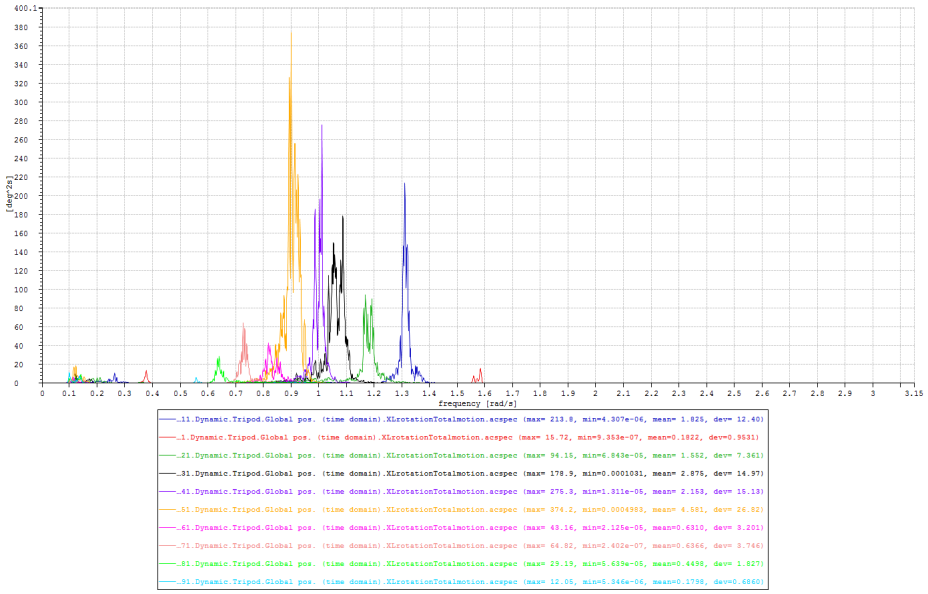

Figure 5.2: Response spectra of tripod roll motion with 10 different tripod drafts for $Hs = 2.25m$ and $Tp = 7.16s$

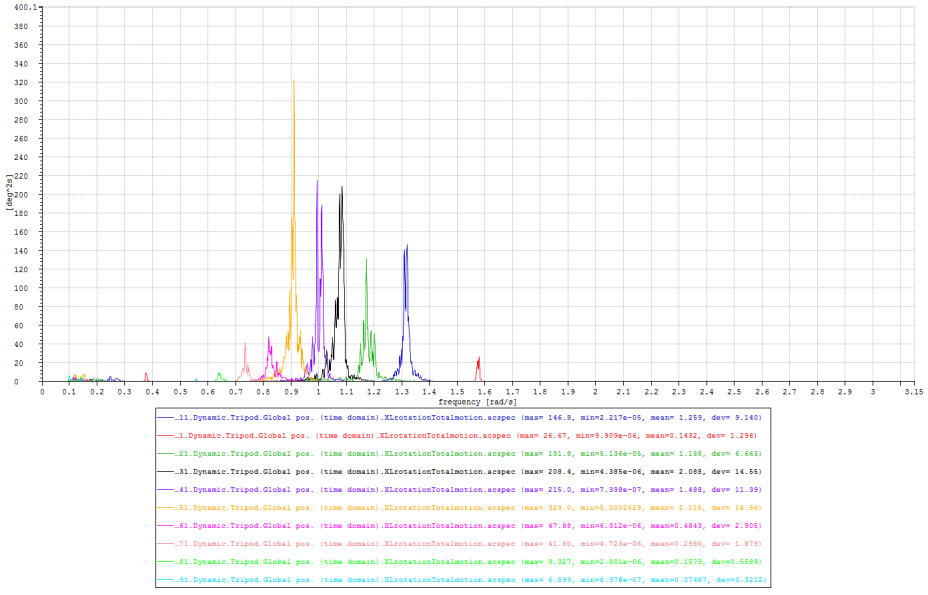

Figure 5.3: Response spectra of tripod roll motion with 10 different tripod drafts for $Hs = 1.75m$ and $Tp = 6.73s$

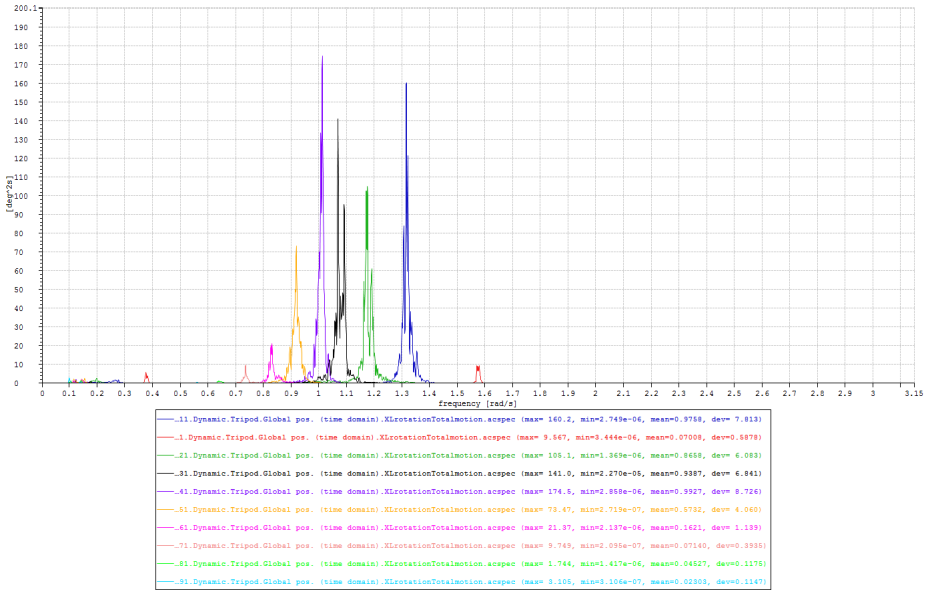

Figure 5.4: Response spectra of tripod roll motion with 10 different tripod drafts for $Hs = 1.25m$ and $Tp = 6.41s$

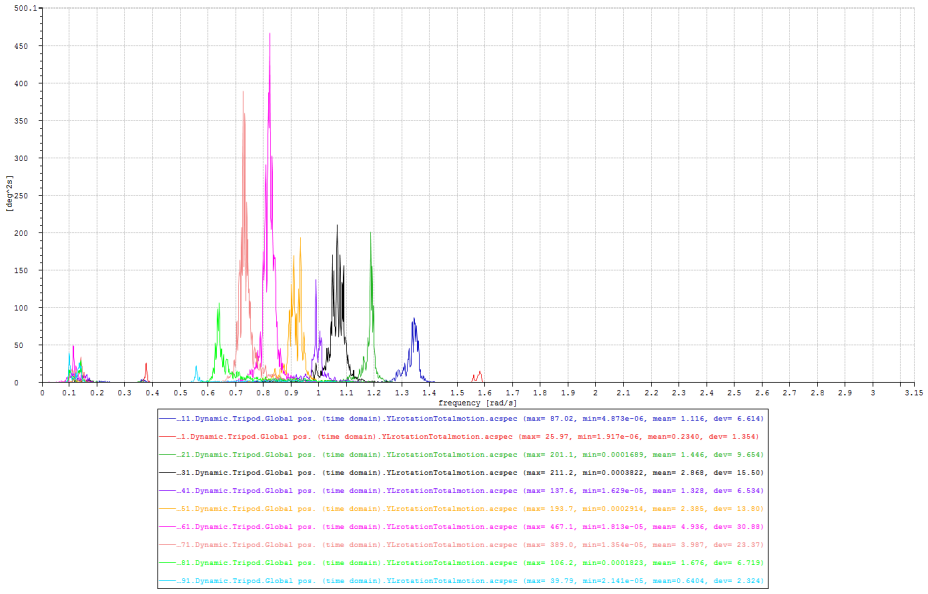

Figure 5.5: Response spectra of tripod pitch motion with 10 different tripod drafts for $Hs = 2.25m$ and $Tp = 7.16s$

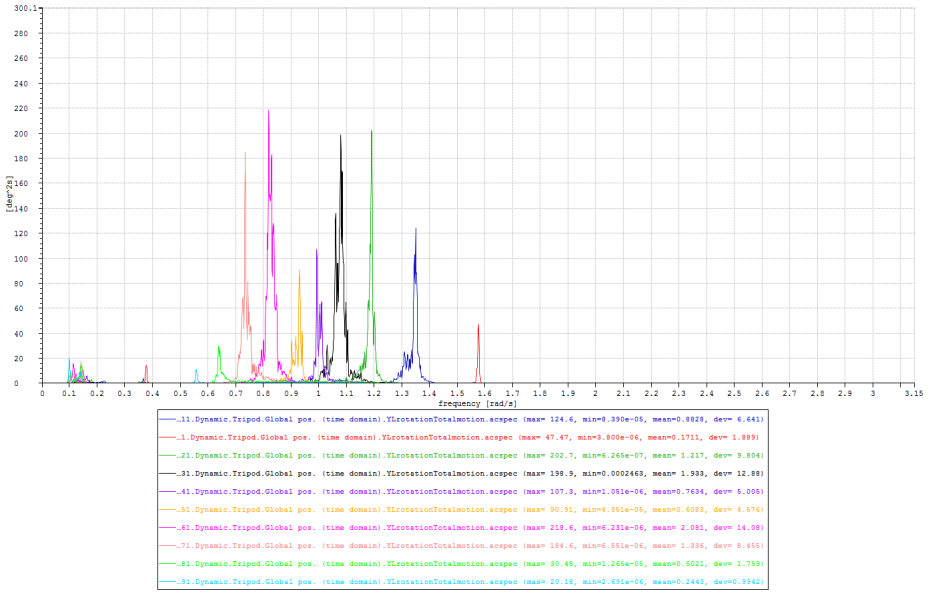

Figure 5.6: Response spectra of tripod pitch motion with 10 different tripod drafts for $Hs = 1.75m$ and $Tp = 6.73s$

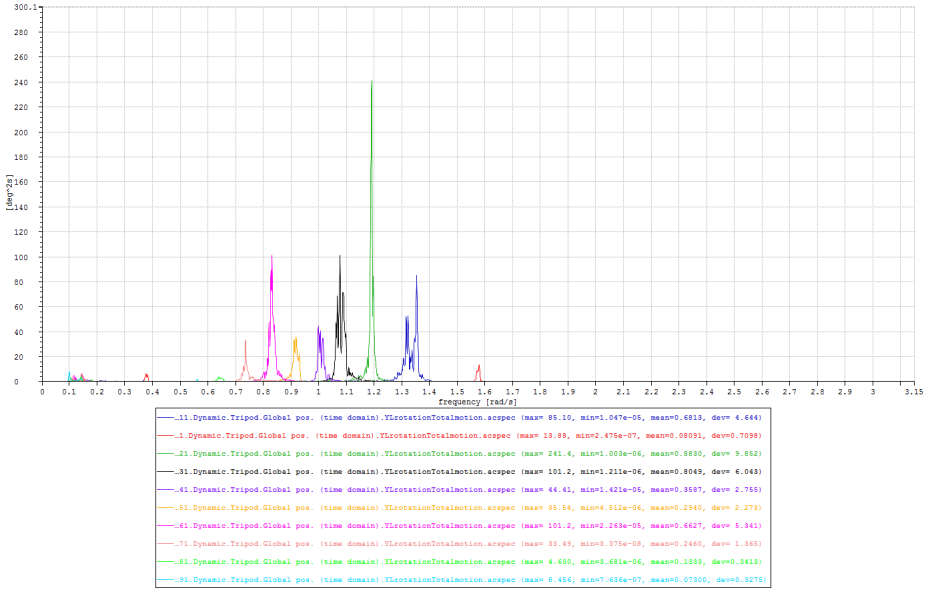

Figure 5.7: Response spectra of tripod pitch motion with 10 different tripod drafts for $Hs = 1.25m$ and $Tp = 6.41s$

Figures from 5.5 to 5.7 show the response spectra of tripod pitch motion for the sea states above respectively. When the wire length is around 150m, the tripod pitch motion becomes more sensitive to the incident wave from Figure 5.5. With the sea state getting calm, most responses of the tripod pitch motion become decreased excluding the condition with 130m wire length.

Based on the discussion above, combined with the results of eigenvalue analysis, the range of spectral peak period in the case is from 6.41s to 7.16s, which corresponds to the period of tripod rotational motions(roll and pitch) dominating in Figure 5.1. On the other hand, the spectrum analysis also reflects responses of such two motions with more concentrated energy relatively.

5.1.3 Statistical Analysis

In order to describe the effect from different tripod position more directly, the statistics for the lift wire tension are listed below.

Table 5.4: Statistics of the lift wire tension with different wire lengths for $Hs = 2.25m$ and $Tp = 7.16s$

Lift Wire Length(m)	Lift Wire Tension(N)			
	Max	Min	Mean	STD
120	9,0438E+06	8,4178E+06	8,6790E+06	5,6610E+04
125	1,0448E+07	7,1414E+06	8,5416E+06	3,1070E+05
130	1,0351E+07	7,1258E+06	8,3927E+06	3,0245E+05
135	1,1307E+07	6,1142E+06	8,2209E+06	4,2958E+05
140	9,6952E+06	6,8369E+06	8,1320E+06	2,7075E+05
145	1,0094E+07	6,5808E+06	8,0527E+06	3,3721E+05
150	9,2208E+06	6,8724E+06	7,9620E+06	2,3798E+05
155	8,8340E+06	6,9847E+06	7,8744E+06	1,7711E+05
160	8,5609E+06	7,0933E+06	7,7771E+06	1,4380E+05
165	8,2009E+06	7,2614E+06	7,6841E+06	1,1406E+05

Based on Figure 5.8, 5.9 and 5.10, a general trend can be seen that the lift wire tension is significant when the lift wire length between 125m and 145m, which is agreed with the conclusion in spectrum analysis. Besides, during this period, the oscillation of the lift wire tension is also notable. Then the lift wire tension decreases with the position of the tripod foundation getting deeper in water. The main reason is that the buoyancy of tripod gets larger when more parts get into water.

When talking about the lift wire tension, those related motions such as heave and pitch motions should be observed. However, as mentioned before, the response of heave motion is

Table 5.5: Statistics of the lift wire tension with different wire lengths for $Hs = 1.75m$ and $Tp = 6.73s$

Lift Wire Length(m)	Liftwire Tension(N)			
	Max	Min	Mean	STD
120	8,8847E+06	8,4793E+06	8,6793E+06	4,5019E+04
125	1,0245E+07	7,3334E+06	8,5333E+06	2,7543E+05
130	9,9313E+06	7,2604E+06	8,3747E+06	2,6805E+05
135	1,0065E+07	6,8080E+06	8,2114E+06	3,2151E+05
140	9,1080E+06	7,2124E+06	8,1275E+06	1,8780E+05
145	8,9910E+06	7,3075E+06	8,0465E+06	1,5833E+05
150	8,5816E+06	7,3321E+06	7,9579E+06	1,2765E+05
155	8,3470E+06	7,4262E+06	7,8701E+06	9,0782E+04
160	8,2279E+06	7,3919E+06	7,7751E+06	8,3458E+04
165	7,9789E+06	7,4244E+06	7,6835E+06	6,9435E+04

Table 5.6: Statistics of the lift wire tension with different wire lengths for $Hs = 1.25m$ and $Tp = 6.41s$

Lift Wire Length(m)	Liftwire Tension(N)			
	Max	Min	Mean	STD
120	8,8101E+06	8,5555E+06	8,6790E+06	2,8366E+04
125	9,7553E+06	7,5688E+06	8,5216E+06	2,1234E+05
130	9,6461E+06	7,3535E+06	8,3560E+06	1,9727E+05
135	9,1211E+06	7,3443E+06	8,2025E+06	1,7857E+05
140	8,6618E+06	7,5267E+06	8,1243E+06	1,1094E+05
145	8,4023E+06	7,7117E+06	8,0426E+06	6,6116E+04
150	8,2313E+06	7,6767E+06	7,9557E+06	5,9216E+04
155	8,0522E+06	7,6782E+06	7,8677E+06	4,3236E+04
160	7,9907E+06	7,5704E+06	7,7746E+06	4,6303E+04
165	7,8382E+06	7,5370E+06	7,6833E+06	3,8304E+04

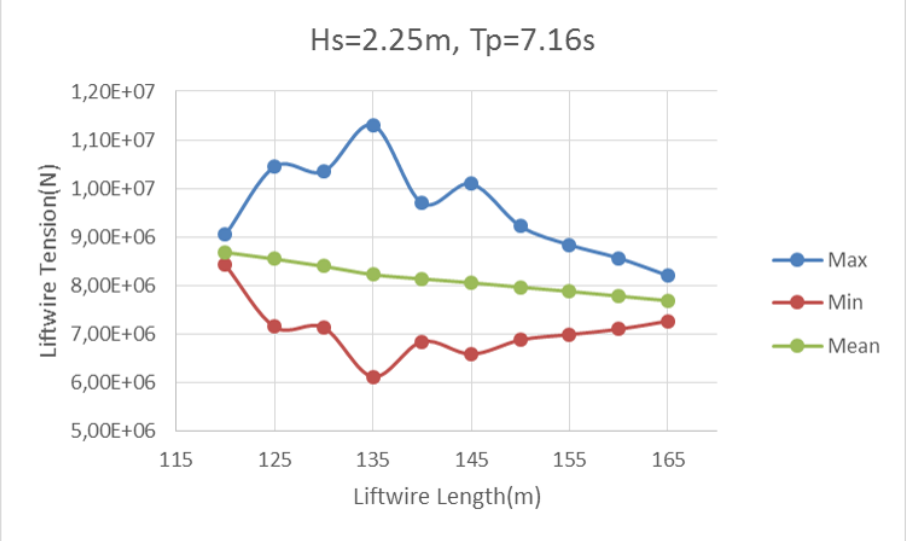

Figure 5.8: The statistical characteristics of the lift wire tension varying with different wire lengths for $Hs = 2.25m$ and $Tp = 7.16s$

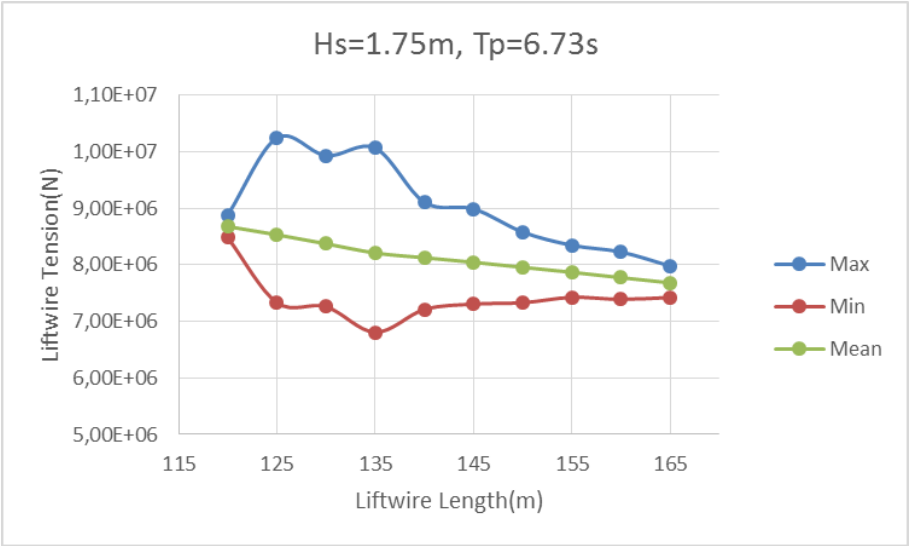

Figure 5.9: The statistical characteristics of the lift wire tension varying with different wire lengths for $Hs = 1.75m$ and $Tp = 6.73s$

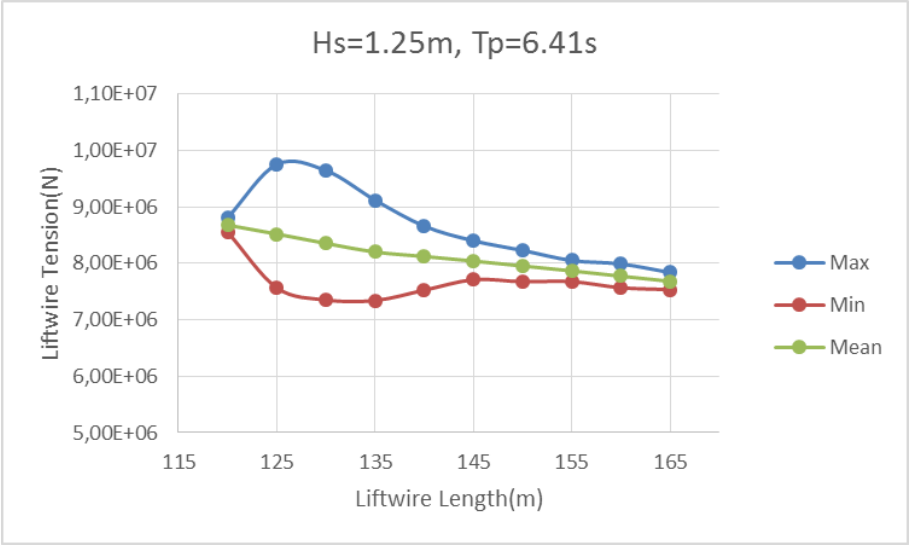

Figure 5.10: The statistical characteristics of the lift wire tension varying with different wire lengths for $Hs = 1.25m$ and $Tp = 6.41s$

not obvious, thus, only pitch motion will be discussed.

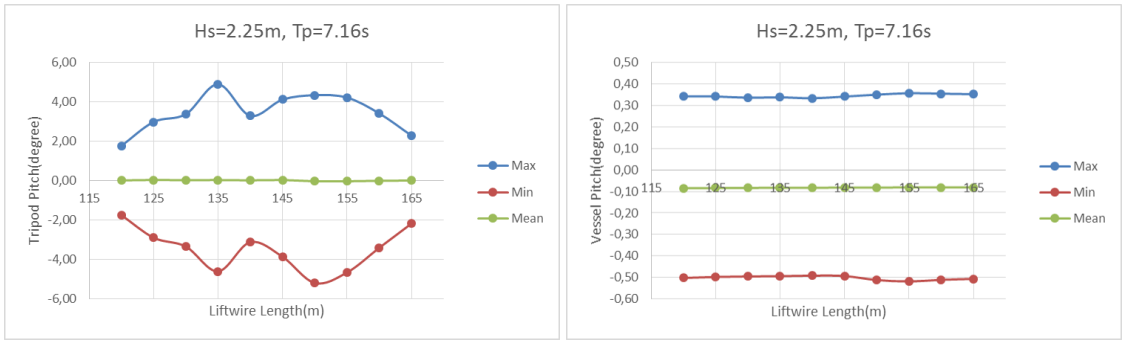

Figure 5.11: The statistical characteristics of the pitch motion varying with different wire lengths for $Hs = 2.25m$ and $Tp = 7.16s$ (left:tripod pitch; right:vessel pitch)

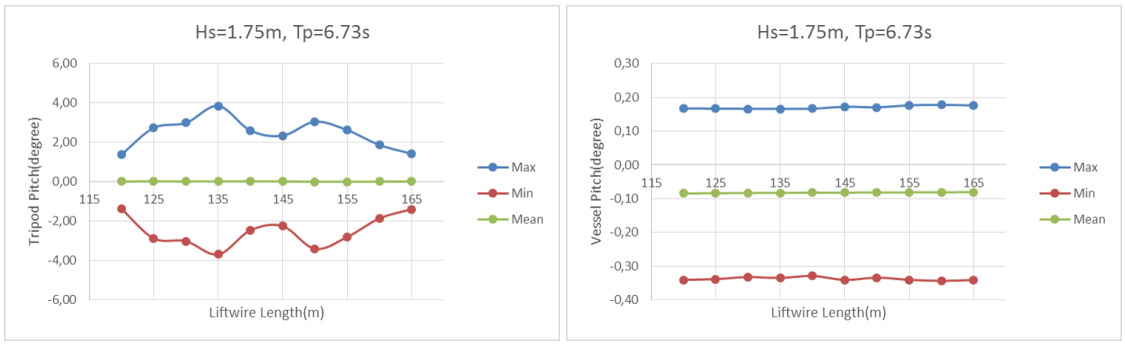

Figure 5.12: The statistical characteristics of the pitch motion varying with different wire lengths for $Hs = 1.75m$ and $Tp = 6.73s$ (left:tripod pitch; right:vessel pitch)

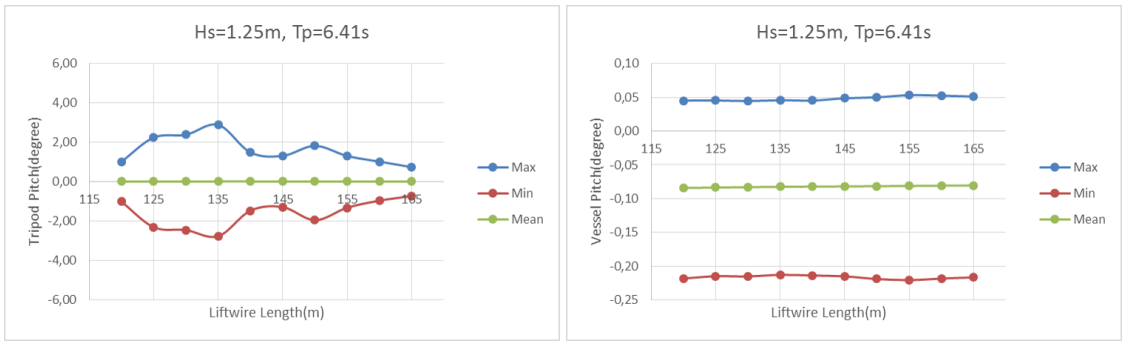

Figure 5.13: The statistical characteristics of the pitch motion varying with different wire lengths for $Hs = 1.25m$ and $Tp = 6.41s$ (left:tripod pitch; right:vessel pitch)

In figures above, the trends of the tripod pitch motion at different sea states are similar. However, the variation of the tripod position has little effect on the vessel pitch motion, so the relative pitch angle between tripod and vessel should have the same trend as the tripod pitch motion. Similar as the response of the lift wire tension, when the lower part of the tripod crossing the splash zone, there are significant pitch motions of the tripod foundation. To certain

degree, the large relative motion between tripod and vessel is possible to cause relatively large wire tension. The difference between the trends of pitch motion and wire tension is also clear, with the tripod foundation getting deeper in water, the response of the tripod pitch motion does not decrease like the lift wire tension. This illustrates that the pitch motion is not sensitive to the change of tripod buoyancy.

5.2 Time Series of Responses for One Case

After simulating the lift operation based on the initial settings, some results related to time series will be discussed firstly. In order to explain this process easily, the condition of $T_p = 8s$, $H_s = 6m$ and wave seed=8 was chosen as an example.

5.2.1 Lift Wire Tension

The figure below shows the changing process of the lift wire tension over time.

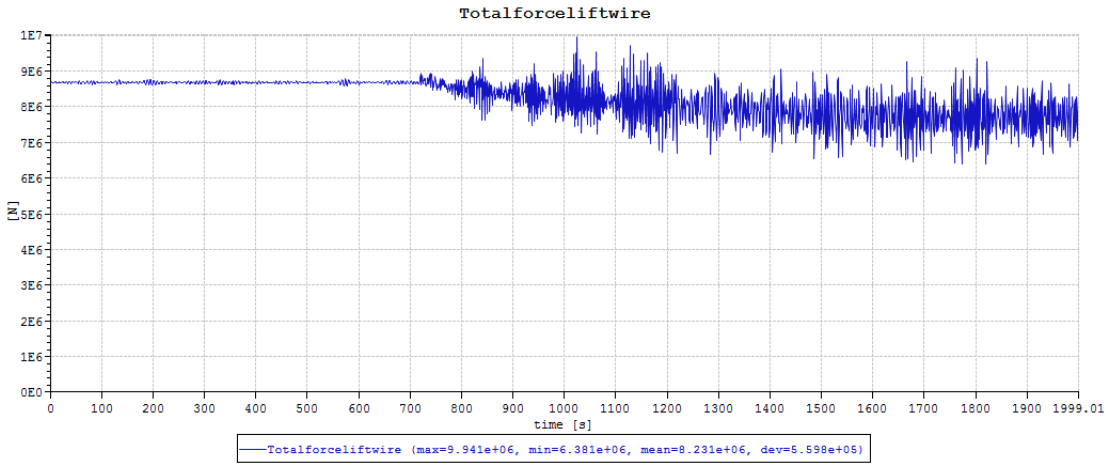

Figure 5.14: Time series of the liftwire tension

During the first 700s, the tripod foundation is hanged in air and the tension keeps around 8.7e+06N which is almost equal to the tripod gravity. So the vessel motion does not affect the tripod motion when the tripod hanging in air. At 720s the tripod begins to go crossing the splash zone, the lowering process lasts to about 1560s. In this phase, the maximum tension force 9.94e+06N appears around 1020s, and there are two relatively intensive oscillation periods, from 950s to 1080s and from 1100s to 1210s respectively. Actually, for different conditions, the locations of these oscillations of lift wire tension are highly different from each other, however, when the main structure of tripod crossing the splash zone the oscillation often appears.

Combined with Figure 5.8, 5.9 and 5.10, the most significant responses in stationary condition also appear at the position of the tripod foundation crossing the splash zone , which corresponds to the time series of the lift wire tension obtained here.

What need to be noticed is that this process is not realistic, since the forces acting on the tripod crossing splash zone are more complex. All the force components can be seen as below.

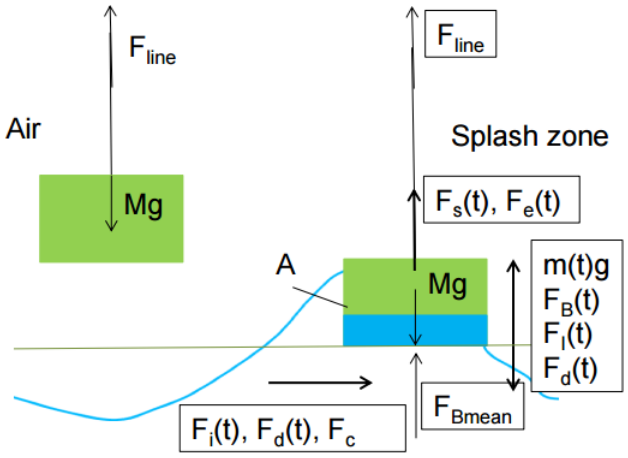

Figure 5.15: Overview of forces acting on tripod in splash zone

Where weight in air, Mg and mean buoyancy, F_{Bmean} are fixed values; $m(t)g$ is the time dependent mass and varies slowing with the water filling; $F_B(t)$ is the time dependent buoyancy; A is the added mass due to the tripod motion; the slamming force, $F_s(t)$ due to entry into water and exit impulse force, $F_e(t)$ due to wave exit; the wave excitation forces includes inertia force F_i and drag force F_d; F_c is the steady, horizontal current force when submerged.

Since the wave excitation forces and slamming forces were neglected, the force equilibrium was simplified as figure above. It is obvious to see there is a significant variation for the lift wire tension, F_{line} in the period between 'water contact' and 'fully water filled'. Further on, such a variation is also related to the water entry velocity(the winch speed). If the winch speed is slow enough that the force condition will be steady, it is possible to obtain the result in Figure 5.14.

5.2.2 Vertical Position of the Tripod CoG

By comparison between lift wire tension and tripod vertical position, the general trends are similar, however, the vertical motion of tripod foundation is not so sensitive to the wave elevation, the changing process is very smooth and clear.

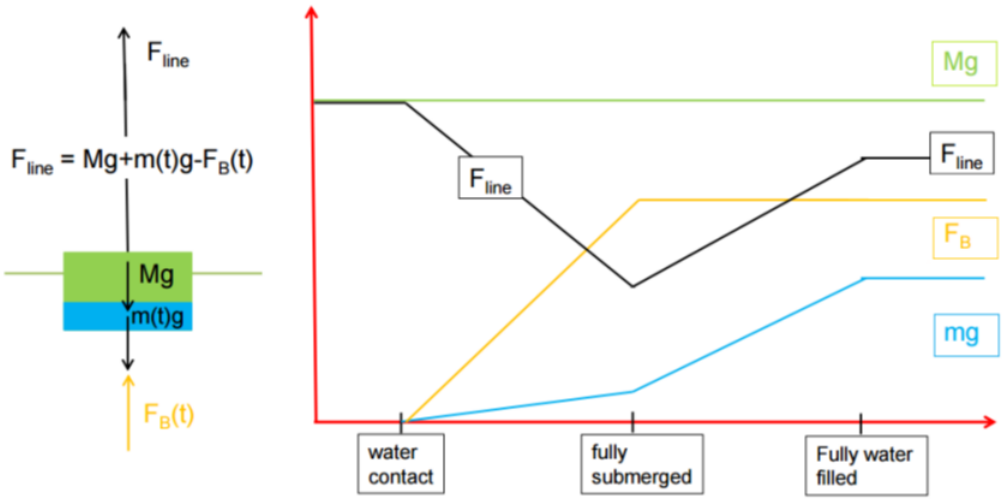

Figure 5.16: Forces acting on tripod in steady condition

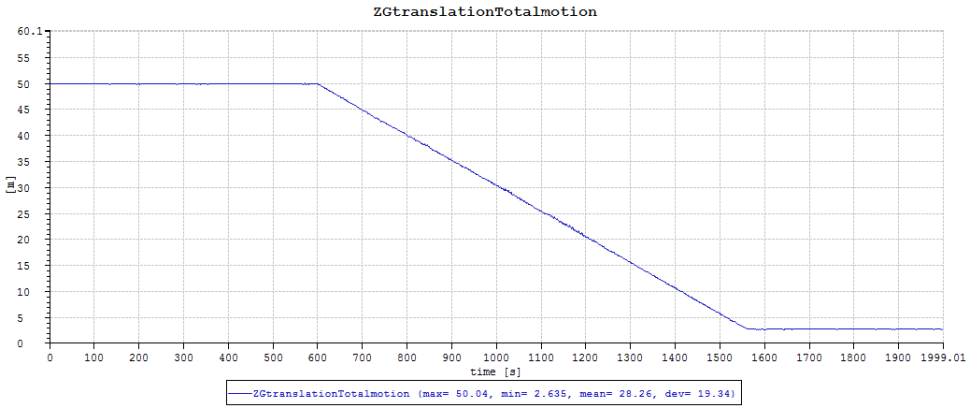

Figure 5.17: Time series of the vertical position of the Tripod CoG

5.2.3 Horizontal Rotation of the Tripod CoG

Regarding to the tripod rotation about z-axis, the initial rotation starts from 30 degree since this position is better to install(the reason was talked about in Modelling). Around 700s the tripod foundation begins to get into the water, then the tripod rotates in the opposite direction and this trend stops after 750s. With more structures into water, the tripod starts to spin counterclockwise with a relatively high angle speed. The period from 750s to 1250s is correspond to the lower part crossing the splash zone. After this period, the rotation motion is not so obvious and gets to a steady situation before landing. As a whole, the rotation of tripod stops when the tripod dives to a certain water depth, and this phenomenon will be talked more in the later part.

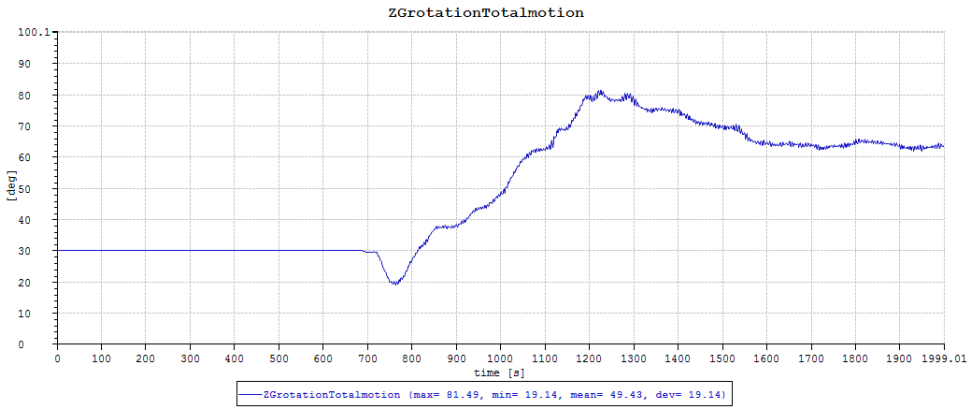

Figure 5.18: Time series of the horizontal rotation of the Tripod CoG

5.3 Response of the Coupled System

In this section, all the results were obtained from the dynamic analysis of 3000 realizations. From the simulation of 3000 realizations, in each time series, there are corresponding statistical characters such as maximum values, mean values and standard deviations(STD). There are 150 sea states(15 spectral periods and 10 significant wave heights) and every sea state is corresponded to 20 wave seeds. Firstly, in one sea state, for instance 20 maximum values are gain from 20 realizations. Then the mean value of these 20 maximum values is considered as the maximum value of this sea state. Using the same way, the mean value and STD of each sea state can be obtained.

As the main operational limitation, the lift wire tension is the focus of the simulation. However, in order to study further the variations of the lift wire tension in different conditions, the

related motions of the coupled system will be also observed.

5.3.1 Response of the Lift Wire Tension

By exporting the results of the lift wire tension from SIMO, the following cloud pictures were obtained.

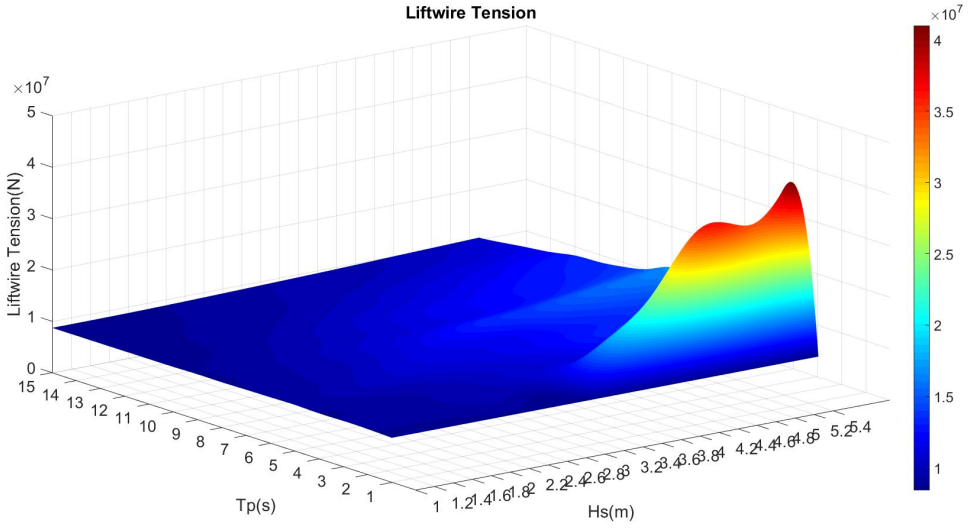

Figure 5.19: 3D Hs-Tp contour of extreme lift wire tension during lowering

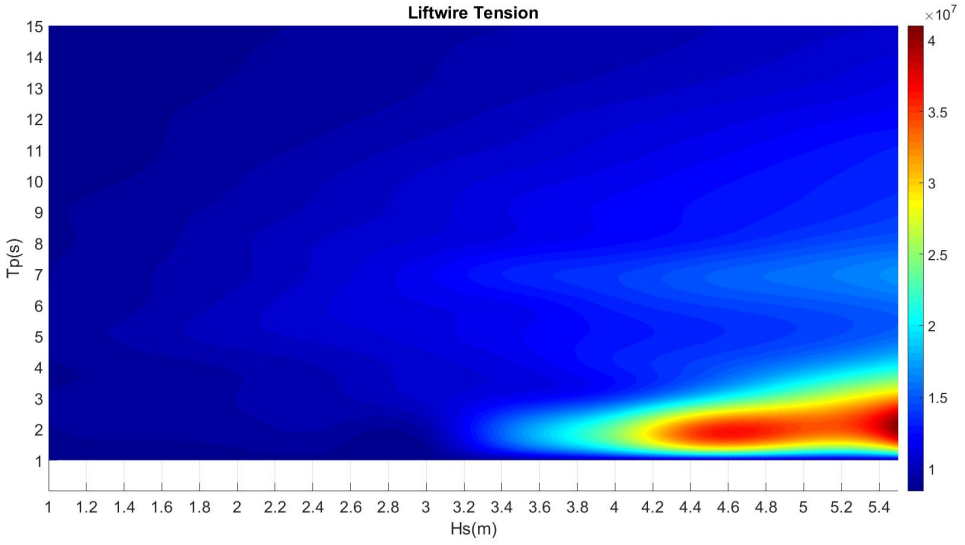

Figure 5.20: Hs-Tp contour of extreme lift wire tension during lowering

From Figure 5.19 and 5.20, the general trend of extreme lift wire tension is obvious. For a given spectral peak period, with the increasing significant wave height, the extreme lift wire

tension also increases. However, with a given significant wave height, the variation of extreme lift wire tension is complex. The dark red region represents the largest values among these extreme values of lift wire tension. In Figure 5.19 and 5.20, the dark red region located at the bottom right corner, which means the largest tension will appear around $Tp = 2s$.

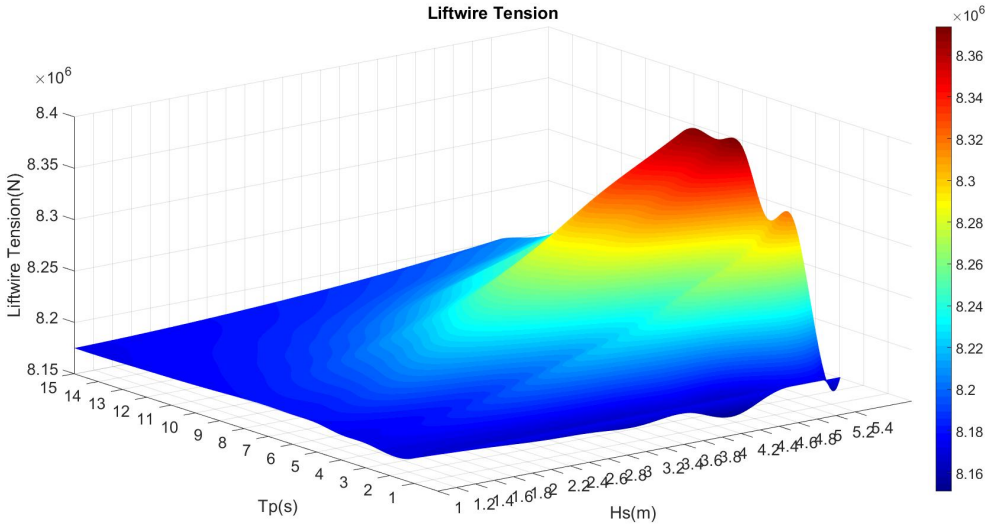

Figure 5.21: 3D Hs-Tp contour of mean lift wire tension

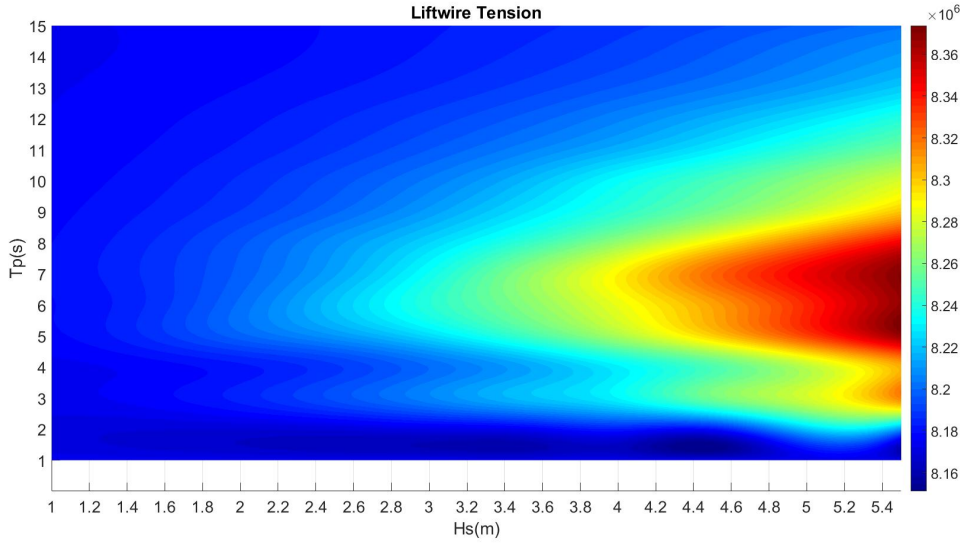

Figure 5.22: Hs-Tp contour of mean lift wire tension

In order to study this phenomenon further, the analysis of mean value and STD is essential to be performed. From Figure 5.23 and 5.24, one can say the values of the dark red region in Figure 5.19 and 5.20 are extremely unstable.

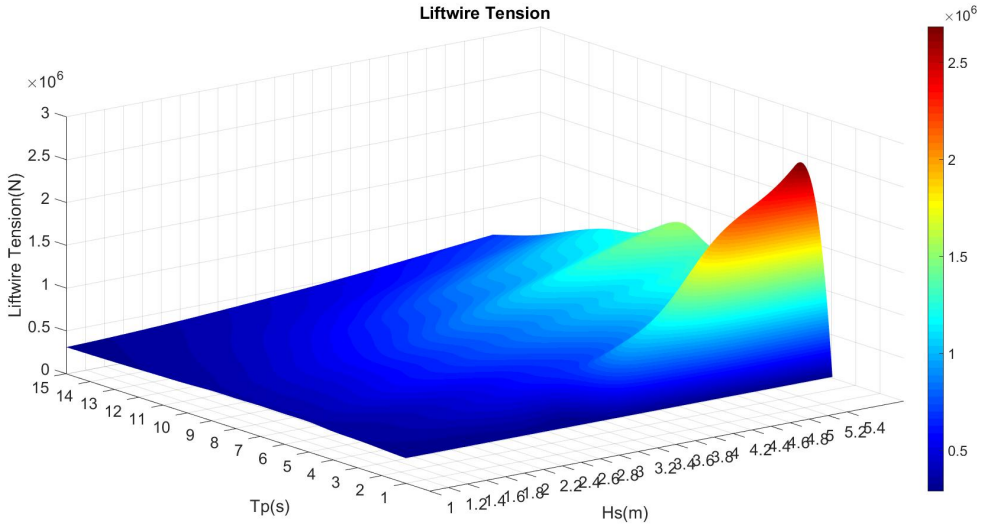

Figure 5.23: 3D Hs-Tp contour of lift wire tension STD

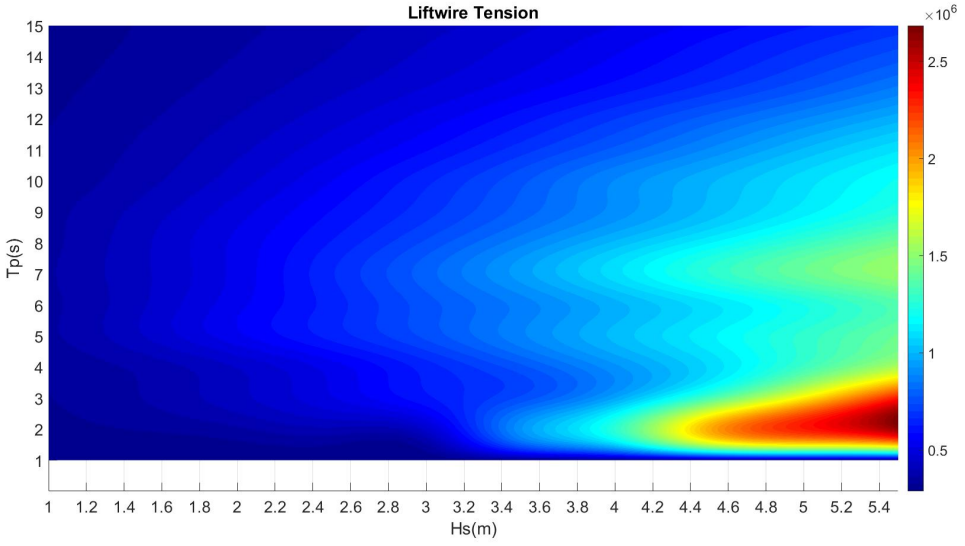

Figure 5.24: Hs-Tp contour of lift wire tension STD

To explain the contour of high Hs, low Tp is not reliable, the time series of extreme lift wire tension with high Hs and low Tp should be checked.

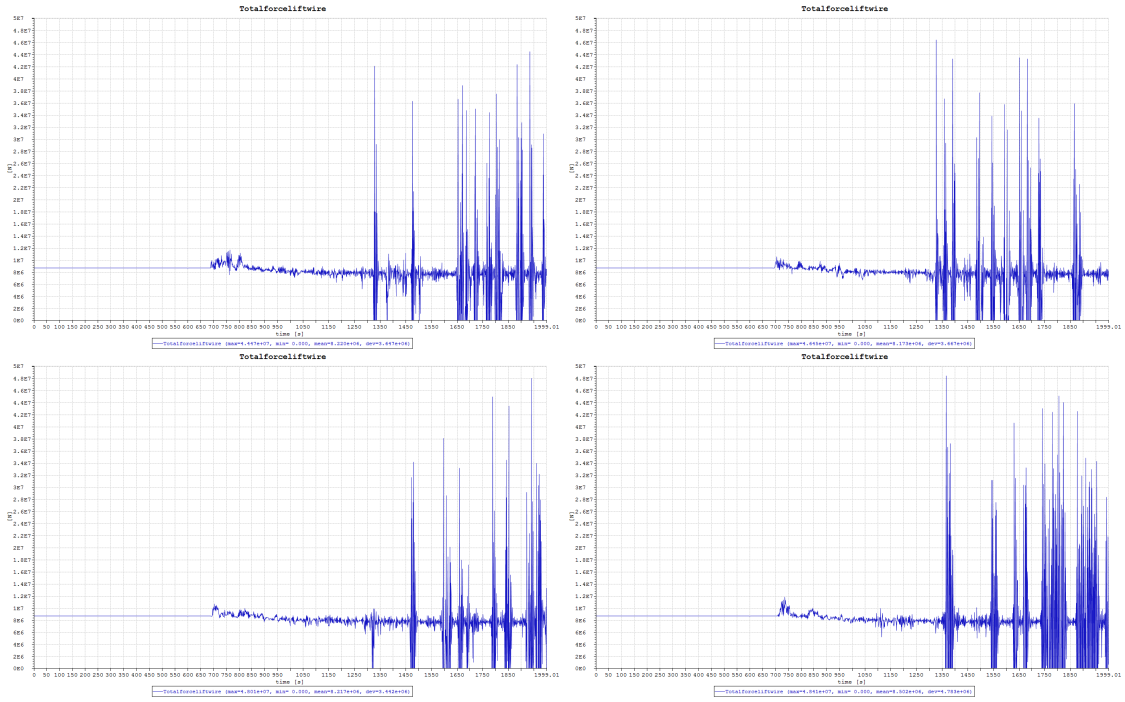

Figure 5.25: Time series of extreme lift wire tension with sea state $Hs = 5.5m$, $Tp = 2s$

In Figure 5.25, those unstable time series happened around 1350s, which illustrates the unreliability of results at this sea state. Actually, the high Hs and low Tp will bring a large wave steepness(the ratio between wave height H and wave length λ). When the steepness is larger than or equals 1/7, the wave becomes unstable. One solution for this problem is to do more simulations at this sea state. However, the wave period of this thesis is mainly from 4s to 15s, therefore such inaccurate values at this region is not of importance.

By comparison the mean values in Figure 5.21 and 5.22 are more convincing. The mean values of extreme lift wire tension become large between $Tp = 4s$ and $Tp = 9s$, which means there is an obvious resonant of the lift wire tension during this period. Combined with the result of eigenvalue analysis, the tripod roll and pitch motions and vessel heave motion dominate in this period, it is possible that the relative position between tripod and vessel changes dramatically in such a case.

5.3.2 Response of the Coupled System Motion

Generally, the large lift wire tensions should appear with extreme sea states(at the top right corner in Figure 5.20), but the result is not so ideal, thus the response of the coupled system

motion should be observed. Since the head sea is the only direction in consideration, the roll and pitch motions of the vessel and the heave and pitch motions of the tripod are more significant than others.

The following figures show contours of vessel rotational(roll and pitch) motions.

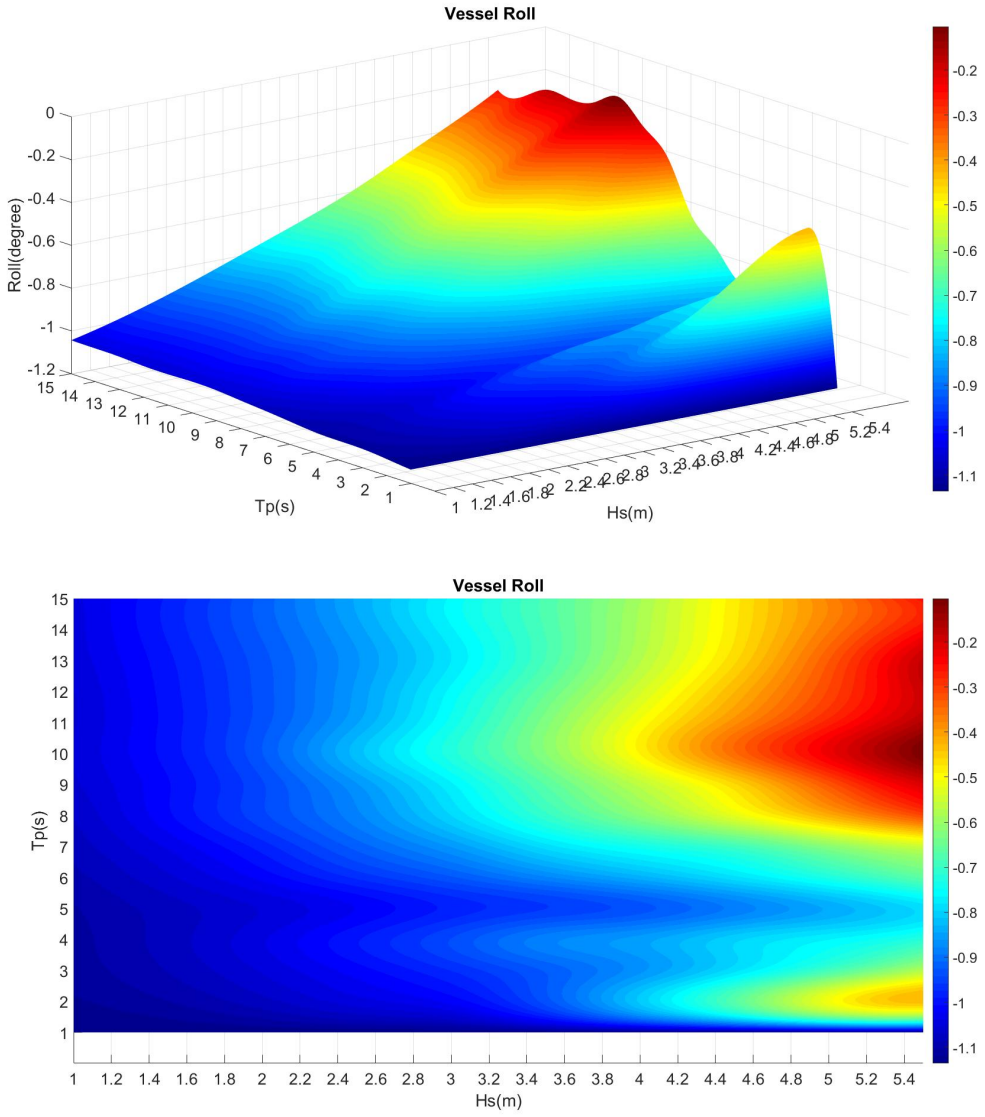

Figure 5.26: Hs-Tp contour of extreme vessel roll motion during lowering

From Figure 5.26 to 5.31, it can be found that the vessel rotational motions become significant with the sea state getting worse, such a trend is relatively ideal, especially for the vessel pitch motion. Besides, at worse sea states, the vessel rotational motions keep unstable with a high mean value.

Since the lift wire tension depends on the length elongation of lift wire, the tripod motions should be observed as well. However, during the lowering process of the tripod foundation, the

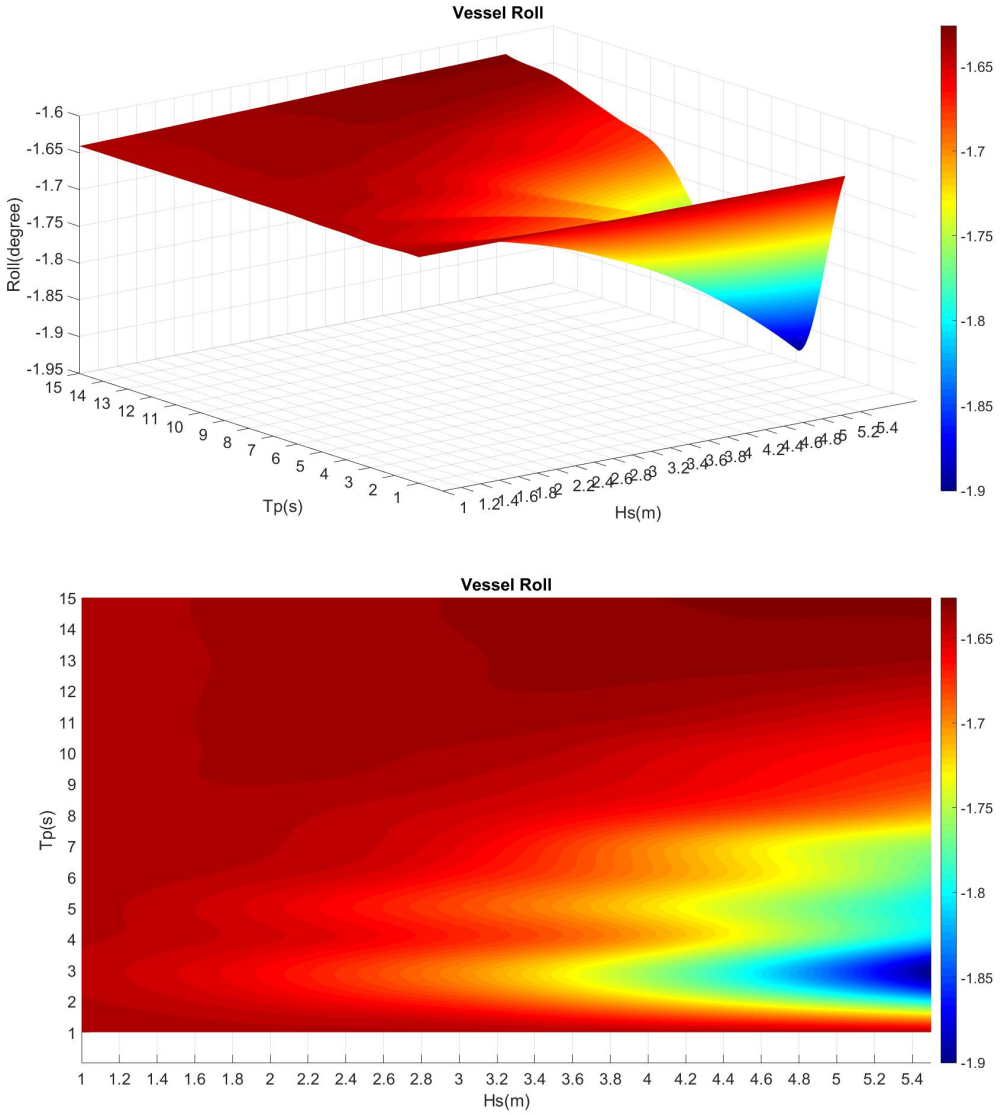

Figure 5.27: Hs-Tp contour of mean vessel roll motion

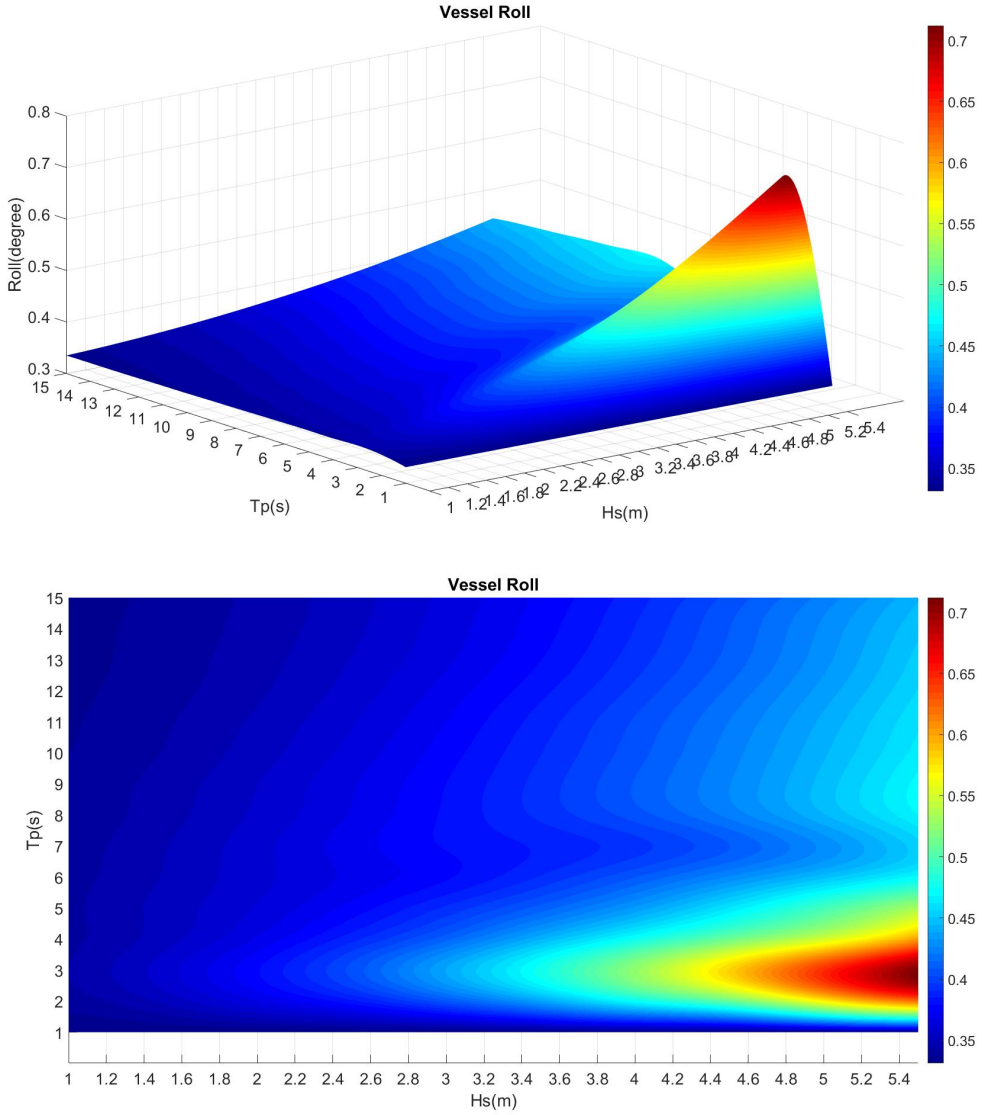

Figure 5.28: Hs-Tp contour of vessel roll motion STD

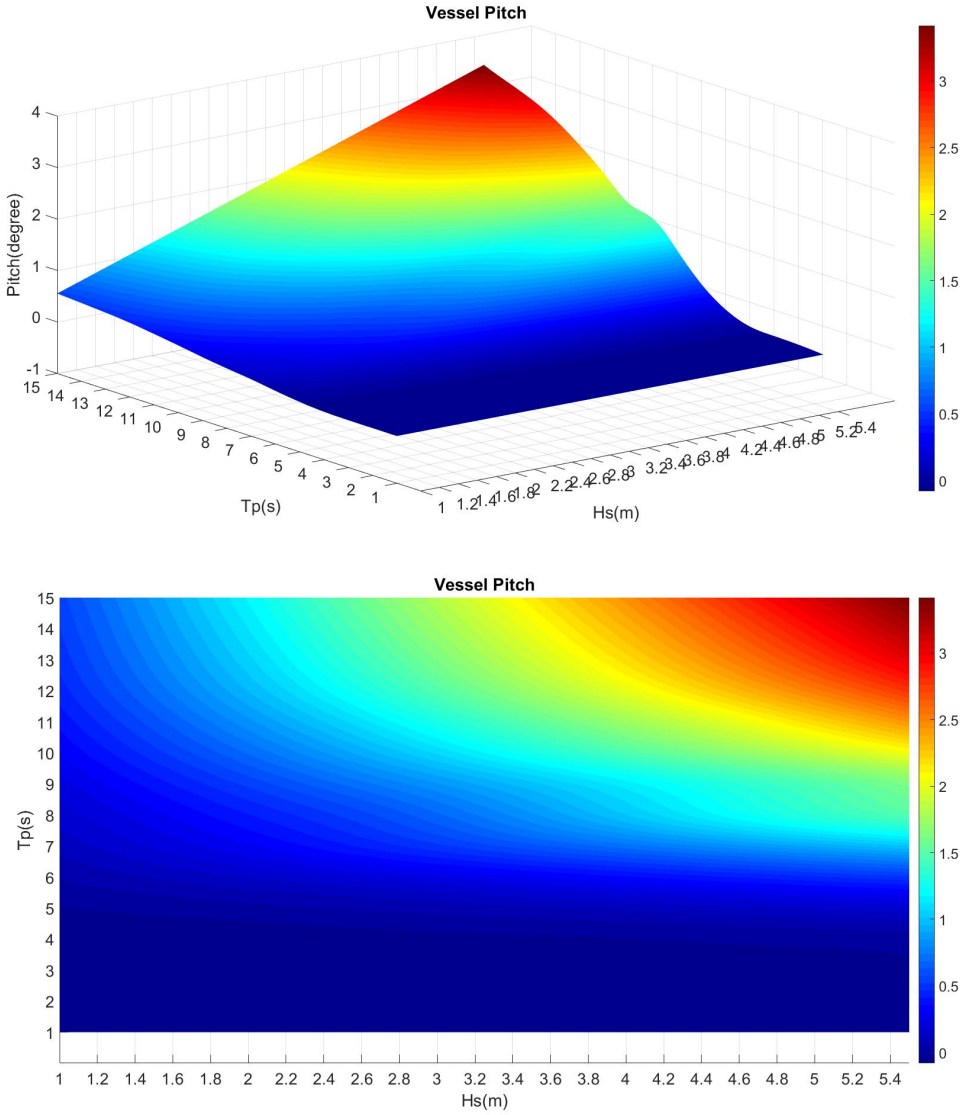

Figure 5.29: Hs-Tp contour of extreme vessel pitch motion during lowering

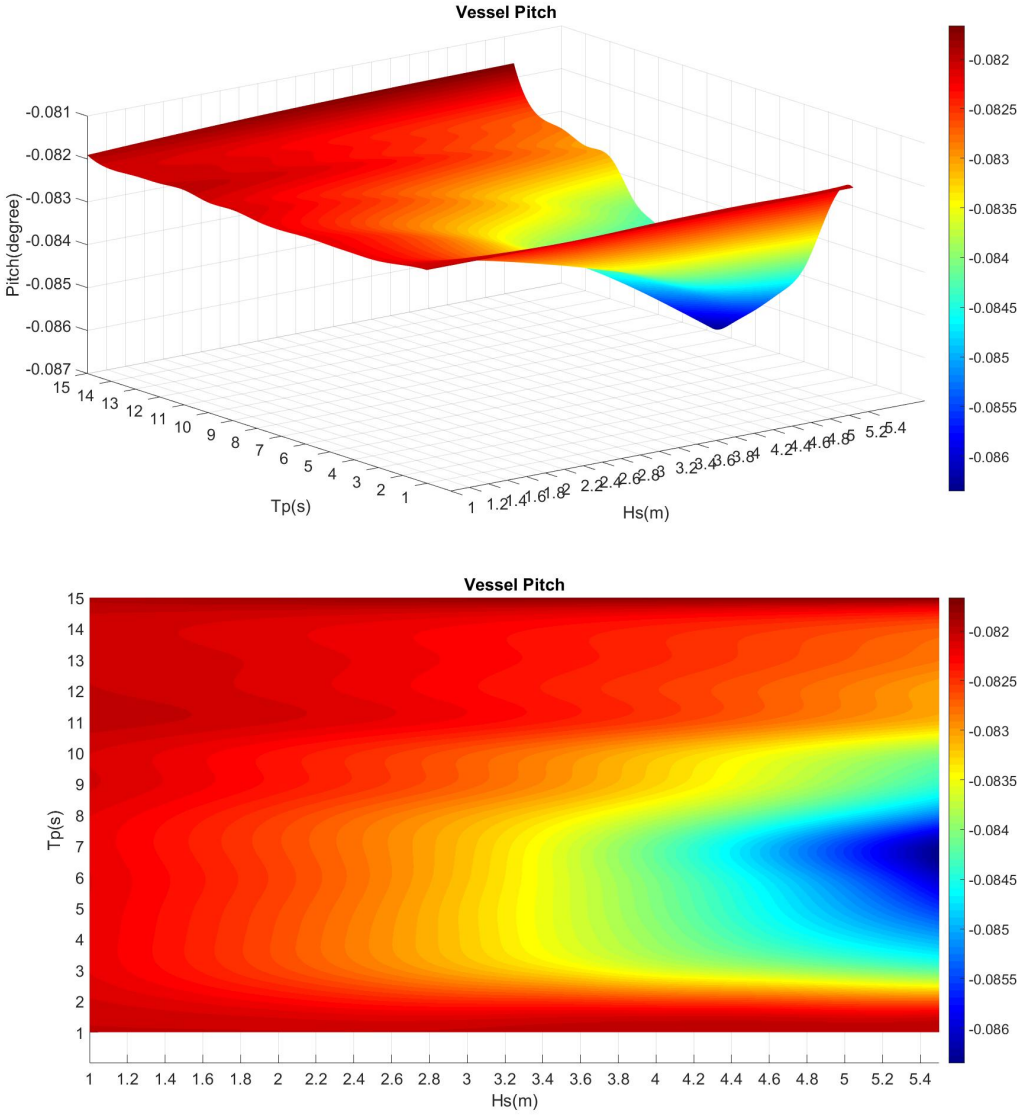

Figure 5.30: Hs-Tp contour of mean vessel pitch motion

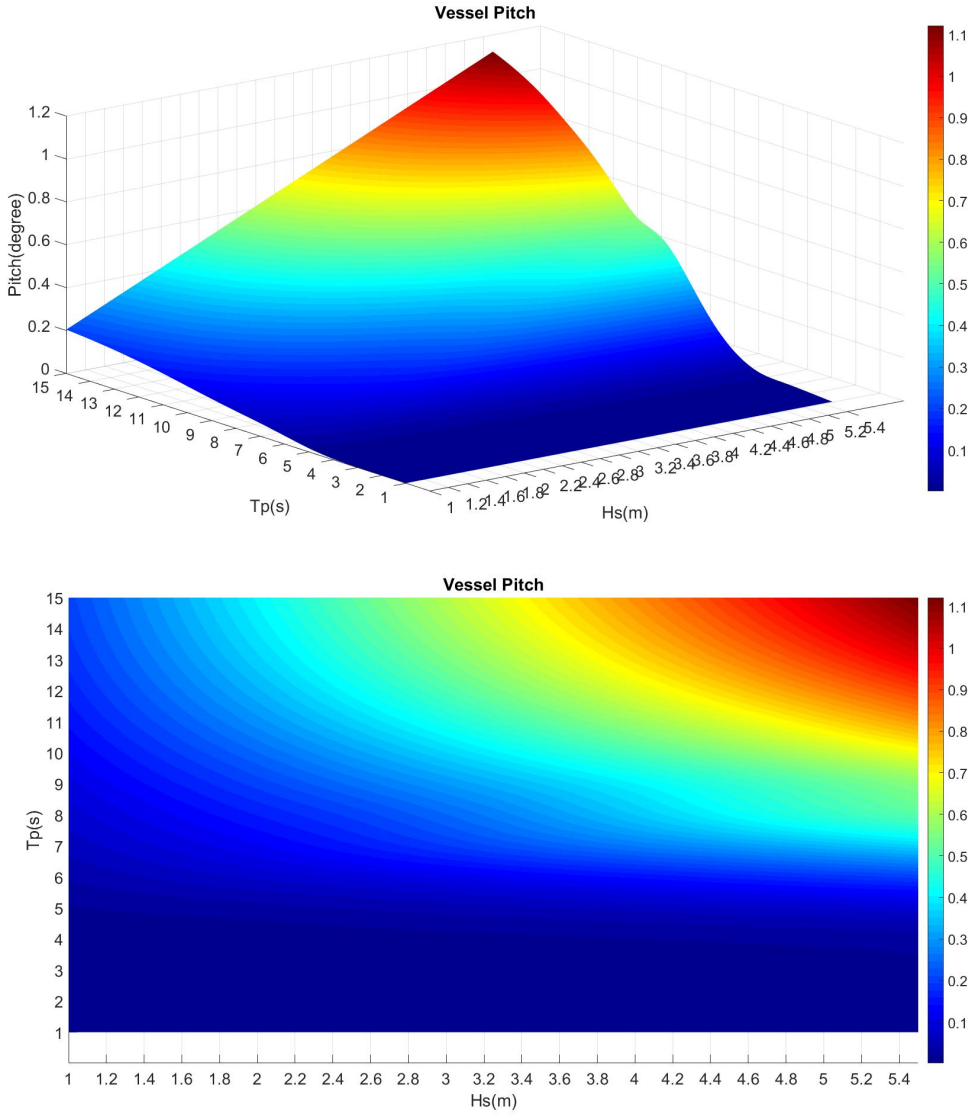

Figure 5.31: Hs-Tp contour of vessel pitch motion STD

position varies with the lift wire length. Thus, the tripod heave motion should be considered as the relative vertical position of tripod which is obtained from the vertical position of the tripod GoC excluding the the tripod draft. Then , the contours of the statistical characters can be shown as below.

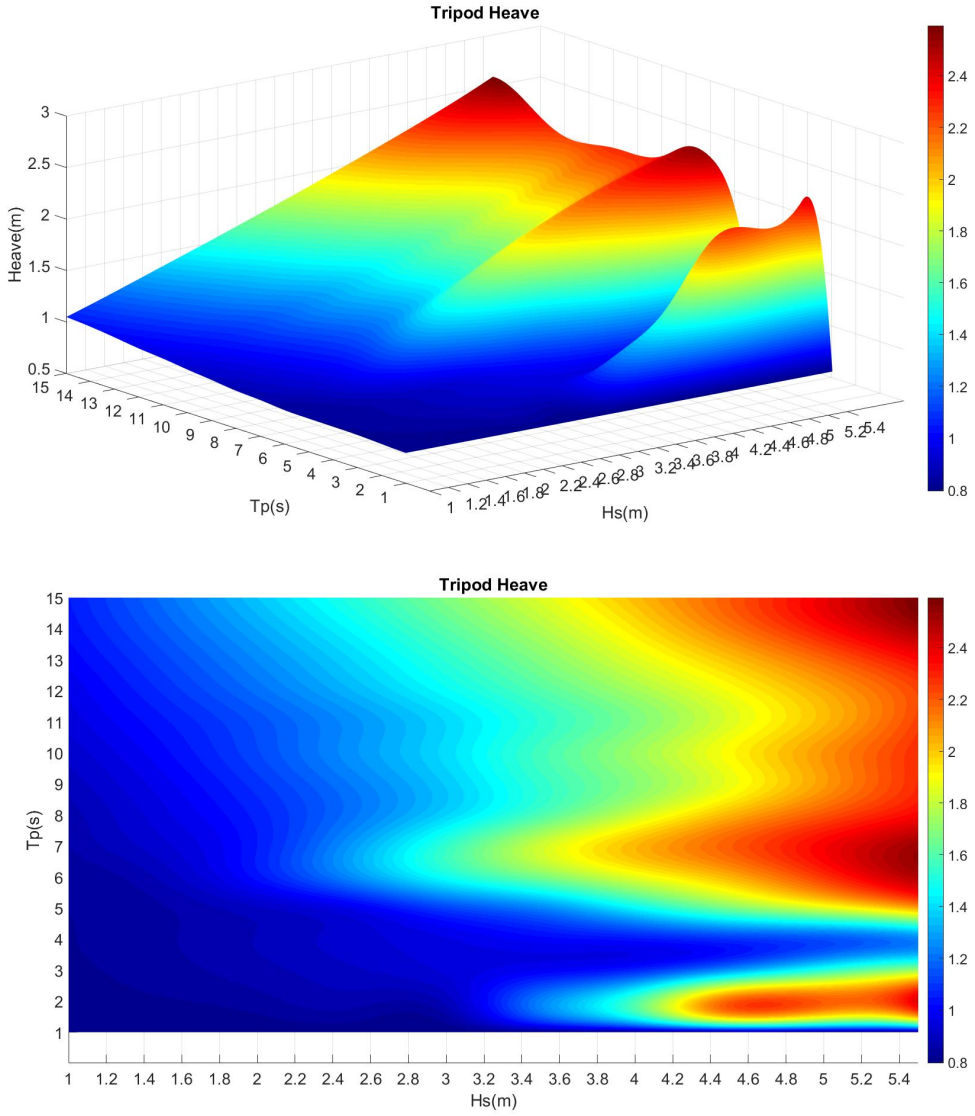

Figure 5.32: Hs-Tp contour of extreme tripod heave motion during lowering

Generally, there is not a clear trend for the tripod heave motion. In Figure 5.32, there are three red peaks. The first peak corresponding to $Tp = 15s$ is due to the bad sea state, combined with the Figure 5.34, the oscillation of the tripod heave motion in this region is very notable, which is similar as the vessel rotational motions. The second red peak is between $Tp = 5s$ and $Tp = 9s$. Although the heave motion is also obvious, different from the first peak, the tripod heave motion keeps stable at a very high mean value. Actually, the second peak area is

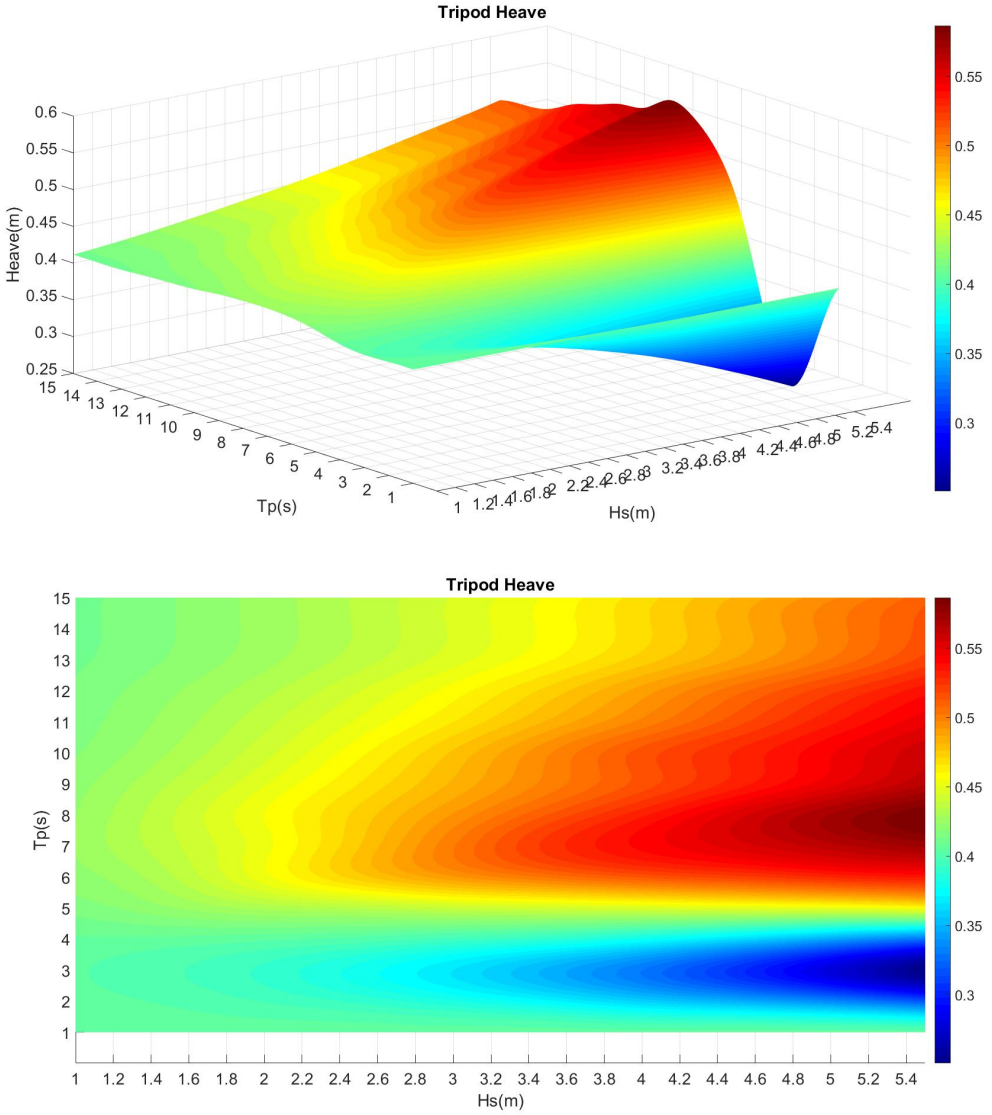

Figure 5.33: Hs-Tp contour of mean tripod heave motion

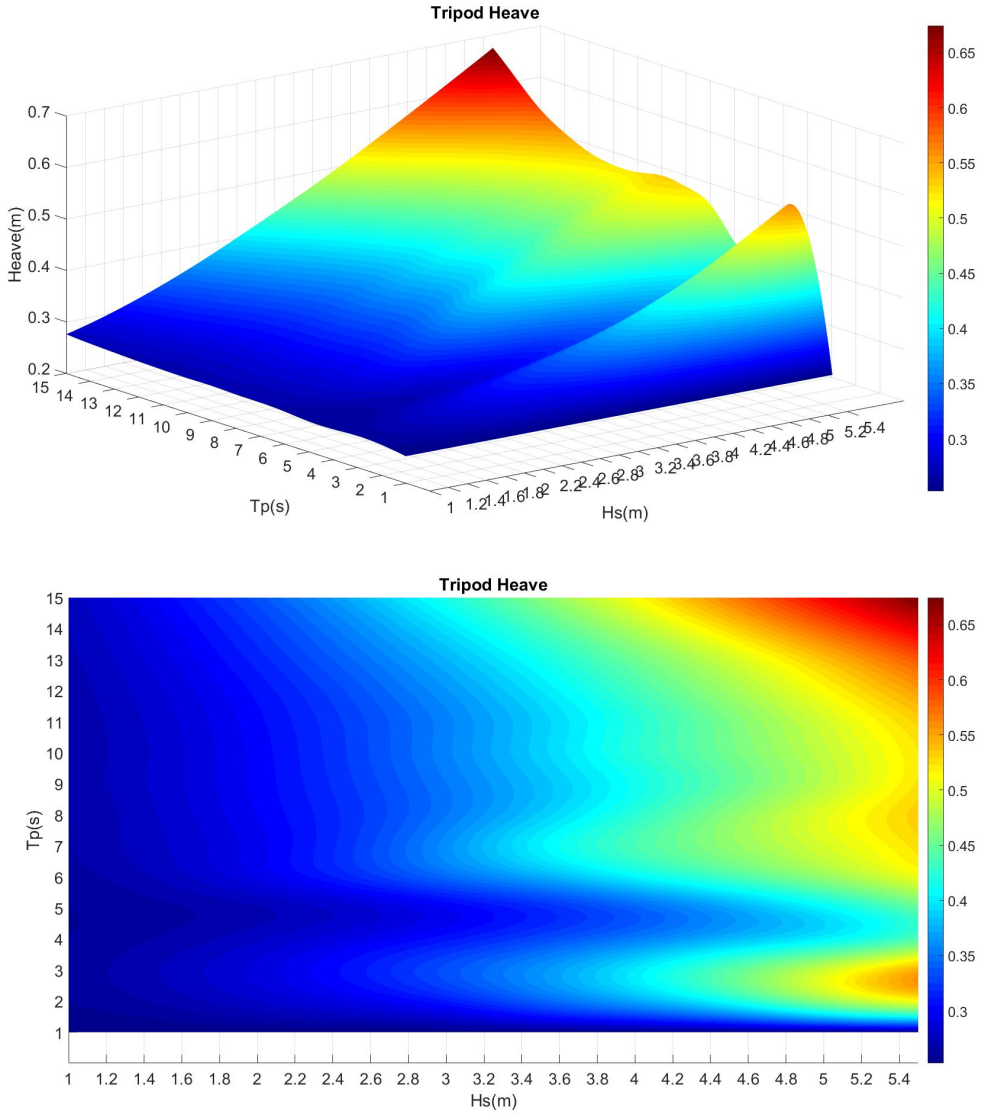

Figure 5.34: Hs-Tp contour of tripod heave motion STD

corresponded to the range of the tripod's eigenperiods. In this range, the dominating modes are the tripod roll and pitch motions instead of the tripod heave motion, however, when the tripod roll motions dominate, there is also a notable heave motion accompanying(which can be seen in the results of eigenvalue analysis). For the last peak, the reason is similar as the result of the lift wire tension talked about before, therefore, this peak region can be neglected.

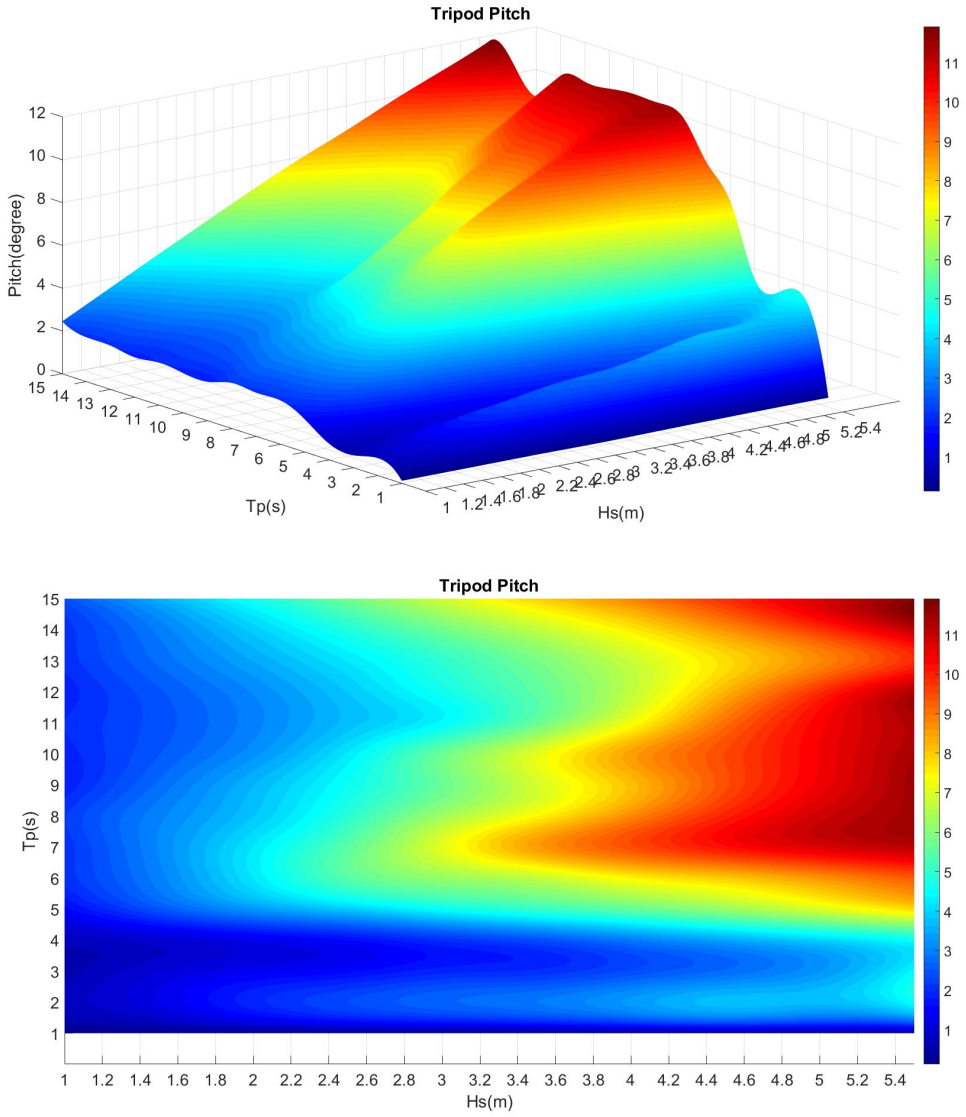

Figure 5.35: Hs-Tp contour of extreme tripod pitch motion during lowering

For the pitch motion of the tripod, the variation is similar as the tripod heave motion. The peak in Figure 5.36 proves that the tripod pitch dominates in the period corresponding to eigenvalues of the coupled system.

Combined with the contours of the vessel rotational motions, the main problem appears at the first peak region. Although there is an obvious heave motion for both tripod and vessel,

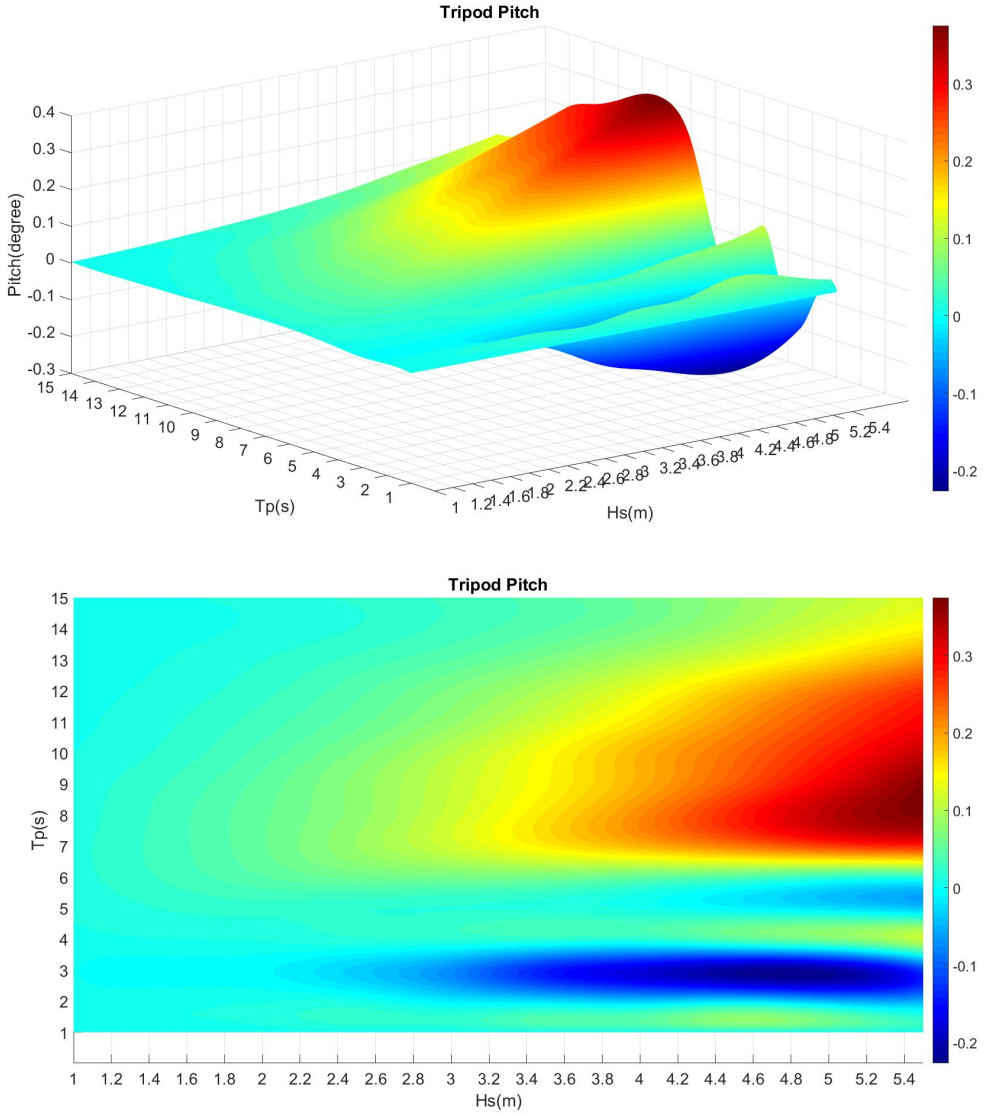

Figure 5.36: Hs-Tp contour of mean tripod pitch motion

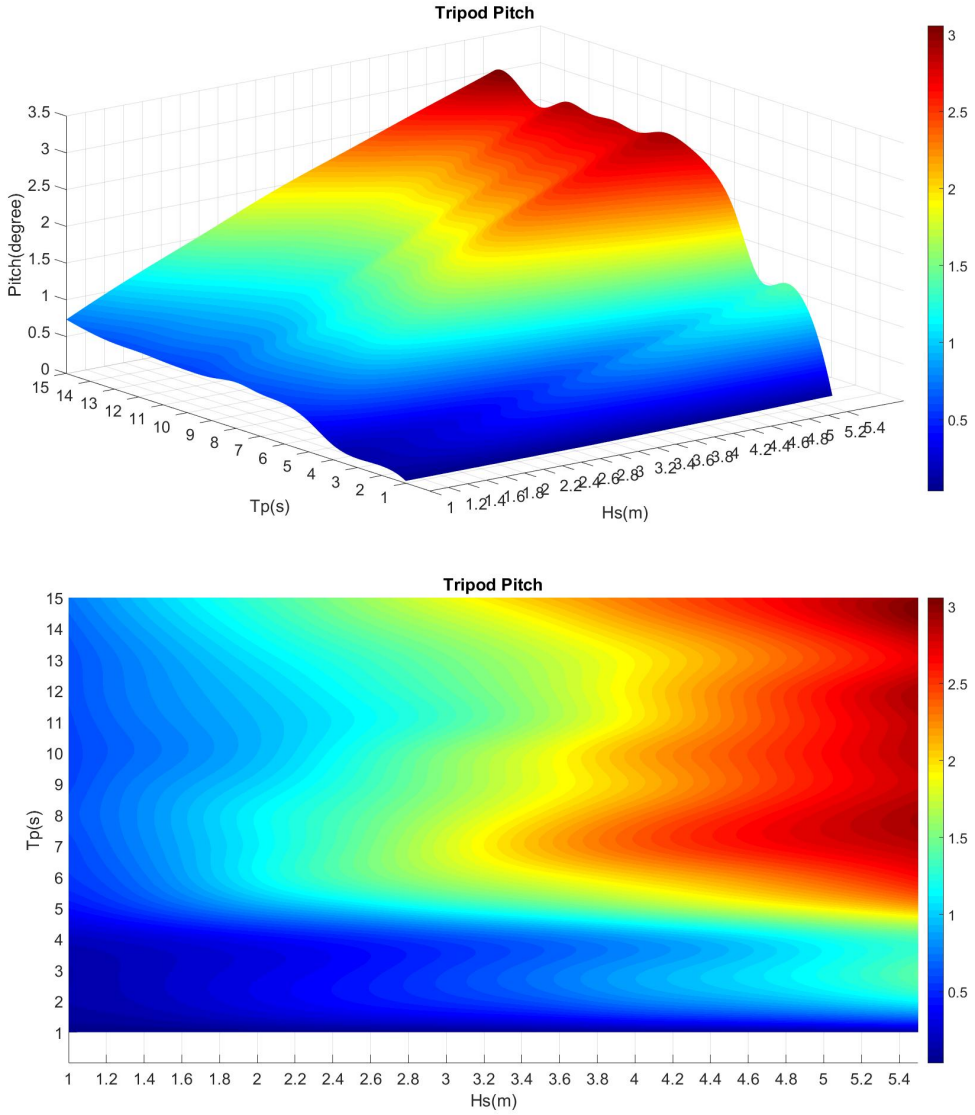

Figure 5.37: Hs-Tp contour of tripod pitch motion STD

such an effect reflecting in the lift wire tension is not clear. The possible reason for this phenomenon may be the motions of tripod and vessel become synchronized in such a long wave condition, which will not leads to a notable elongation of lift wire, thus, the response of the lift wire tension is limited. In order to prove such an assumption, more results are required, so the contours for the pitch motion of tripod and vessel were obtained as well. Since the limitation of the space, these contours are not listed one by one(can be seen in Appendix B). By analysis the results of the pitch motion are similar as the heave motion.

5.4 Influences of Different Winch Speed

As previously mentioned, the winch speed is important for the lowering operation. In order to study the influences of the winch speed, more cases should be taken into consideration. To make sure the randomness of sea states, each condition is corresponded to 20 wave seeds as well.

Table 5.7: Winch Speeds

Condition	1	2	3	4	5	6
Winch Speed(m/s)	0.02	0.05	0.075	0.1	0.2	0.5
Stop time(s)	2400	960	640	480	240	96
Simulation Length(s)	3200	2000	1500	1200	1000	800

5.4.1 Response of the Lift Wire Tension

Firstly the time series of the lift wire tension is observed. It should be mentioned that the instantaneous value in the time series is the mean value of 20 realizations. The following figure shows the changing process for condition 1,3 and 5.

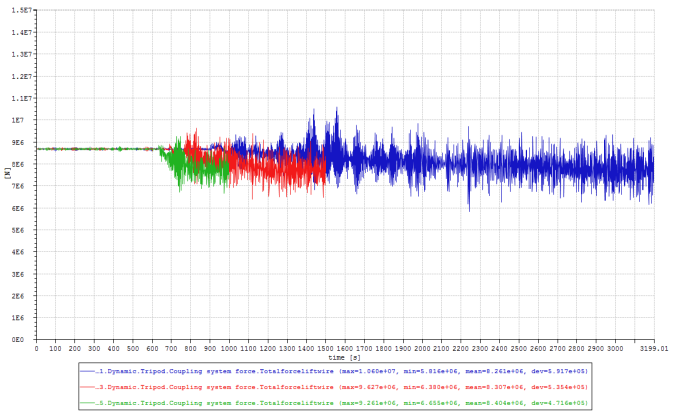

Figure 5.38: Time Series of Lift Wire Tension for Condition 1,3 and 5

From the figure, it is obvious that tension decreases with the increasing winch speed. By further studying all the data, such a trend is more clear.

Table 5.8: Liftwire Tension for Different Winch Speeds

Winch	**Lift Wire Tension(N)**			
Speed(m/s)	**Max**	**Min**	**Mean**	**STD**
0,02	1,0852E+07	5,7379E+06	8,2064E+06	6,2115E+05
0,05	1,0154E+07	6,3462E+06	8,2020E+06	5,4876E+05
0,075	1,0112E+07	6,4871E+06	8,2088E+06	5,5287E+05
0,1	9,5519E+06	6,6886E+06	8,1916E+06	4,6498E+05
0,2	9,5674E+06	6,7071E+06	8,1880E+06	5,1421E+05
0,5	8,8270E+06	7,1501E+06	8,1770E+06	4,0936E+05

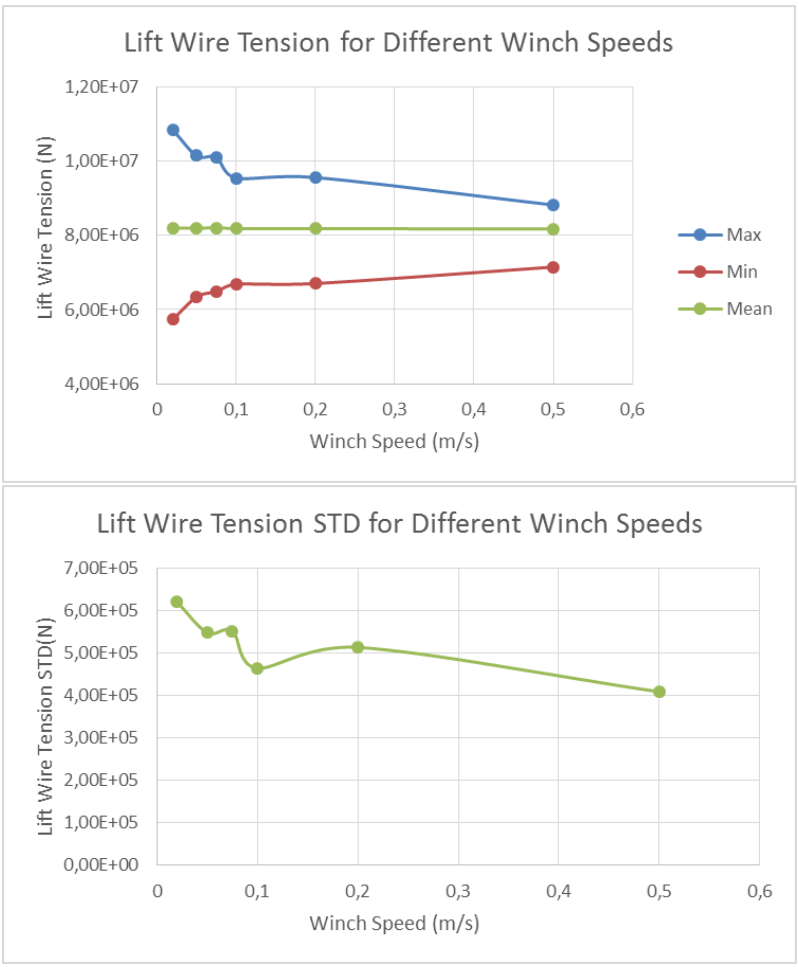

Figure 5.39: The statistical characters varying with different winch speeds

With the increasing winch speed, not only the lift wire tension shows a decreasing trend, but the oscillation of tension decreases obviously. If just based on the result so far, it is better to increase the winch speed during the process of installation. However, in the time domain simulation, the effects of slamming and breaking waves are neglected. Since these problems

are highly related to the lowering velocity of tripod foundation. With a larger lowering velocity, the water entry(slamming) force increases substantially, and the force is possible to lead to a damage to structures. Therefore, the winch speed should be increased carefully, especially when object hits the water surface. According to the result above, an appropriate method is to adjust the winch speed with different lift phases. It is better to slow down the winch speed when the tripod goes into water; After the lower part crossing the splash zone, the lowering velocity can be increased since this can decrease the effect of wave elevation to lift wire tension. But this is just a rough suggestion to the installation operation, more details need to be study further.

5.4.2 Response of the Tripod Yaw Motion

Besides the liftwire tension, winch speed also has a certain influence on the motion of tripod, especially for yaw motion. By comparing with different conditions, some interesting

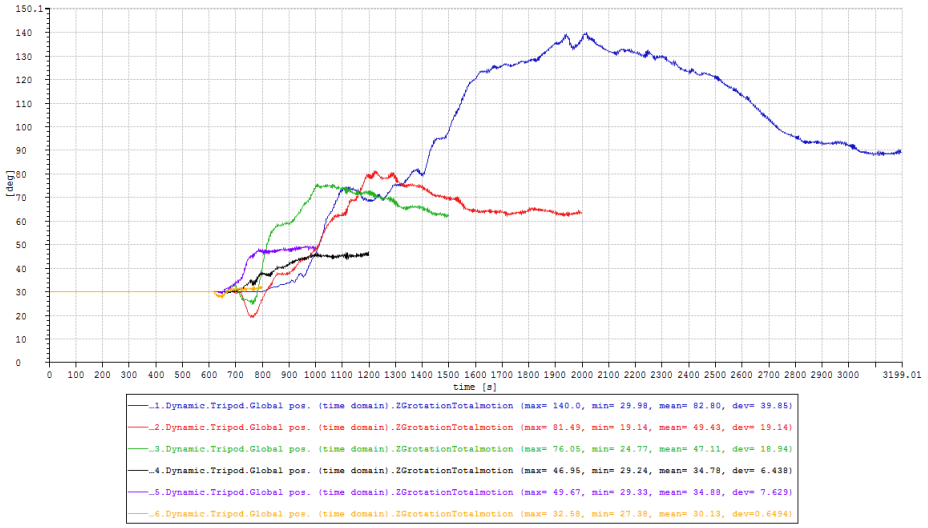

Figure 5.40: Time Series of Tripod Rotation about Z-axis for Different Winch Speeds

points can be observed:

- With increasing winch speed, the amplitude of tripod rotation about z-axis gets decreased dramatically.
- When the tripod reaches a certain water depth, there is a turning point where the trend of rotation gets slow down and even reversed. From the changing processes above, with the increasing winch speed the turning point gets not so obvious. For low winch speed, after the turning point the trend is reversed. But for high winch speed, the trend just gets slow down. Based on the data, the tripod position corresponding to the turning point

can be found. From the table below, the increasing winch speed also makes the position corresponding to the turning point lower, from 28m to 40m.

Table 5.9: Turning Point

Winch Speed(m/s)	Turning Time(s)	Descent Height(m)
0.02	2000	28
0.05	1200	30
0.075	1000	30
0.1	980	38
0.2	780	36
0.5	680	40

- At the end of simulation, the changing processes become stabilized at a certain value. And the increasing winch speed speeds up the trend to be stable, which means higher winch speed is helpful to stabilize the tripod rotation about z-axis.

From the three points obtained above, it can be better to perform the installation operation at a higher winch speed, since this decreases the time of tripod foundation crossing the splash zone, which decreases the effect from wave uncertainty indirectly.

Chapter 6

Weather Window Analysis

Based on the modelling and analysis of marine operations, the related operational limits can be defined. These operational limits can be described by environmental conditions(sea state, wind, current, temperature etc) before executing the operation. In this thesis, the lift wire tension is the main operational limit for the weather window analysis. For simplicity, the lift wire tension is only dependent on the significant wave height and the spectral peak period.

After defining the operational limits, the corresponding acceptable environmental conditions can also be obtained from the results of time-domain simulations. Then introducing the hindcast data to establish the weather window for the lowering of the tripod foundation.

6.1 Assessment for Operational Limits

For non-transitional operations, the critical events that may jeopardize the operation and the corresponding parameters to describe these events(limiting parameters) are unknown. Therefore, it is necessary to introduce a methodology to firstly identify the critical events and corresponding limiting parameters and then establish the operational limits based on relevant safety criteria.

6.1.1 Methodology

The following figure shows the main steps to assess operational limits.

1. **Identification of potentially critical events.** The preliminary selection of activities that may cause critical events is required. In the thesis work,the tripod lowering process is the focus point for the whole installation operation of the tripod foundation.

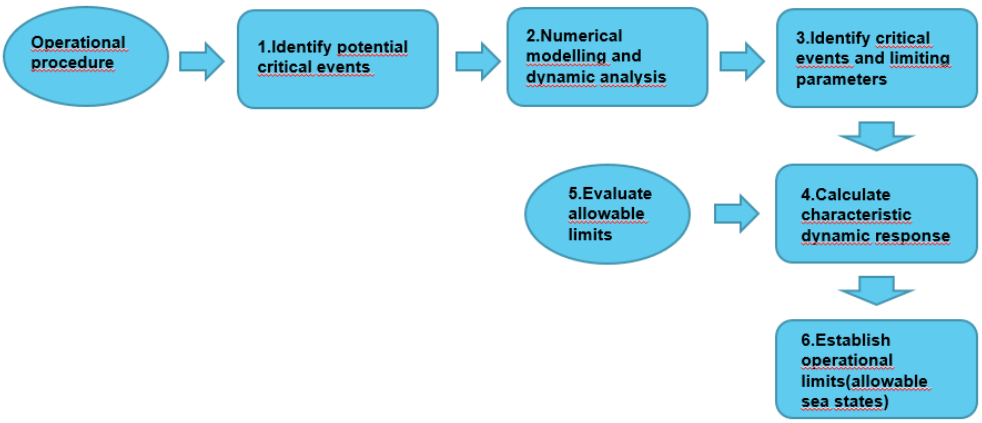

Figure 6.1: General methodology to establish the operational limits(Li et al. (2016))

2. **Numerical modelling of operational activities.** In order to simulate these activities and evaluate the corresponding dynamic responses, it is essential to establish the numerical models. For the tripod lowering operation, the numerical models have already been built in **Chapter 4**. Based on a quantitative assessment of the dynamic responses under reasonable environmental conditions, which parameters may reach high levels to limit the operation can be observed.

3. **Identification of critical events and limiting parameters.** By performing dynamic analysis for the operation process, which dynamic responses leading to failure events are defined. In this case, the lift wire breakage was defined as the critical event, which requires the tension in the lifting wires(limiting parameter) should be lower than the maximum working load of the wire.

4. **Calculation of characteristic dynamic response.** For the tripod lowering operation, the calculation of the characteristic loads should follow the practical requirements, for example the duration of the installation.

5. **Evaluation of the acceptable limits for the limiting parameters.** According to the safety criteria, it is necessary to identify the acceptable limits. These acceptable limits are selected to avoid failure in the marine operations because of large structural loads and the exceedance of installation requirements. The acceptable limits in this case are given explicitly with the lift wire tension limits of 11MN, 10.5MN, 10MN, 9.5MN and 9MN.

6. **Assessment of the operational limits.** After the acceptable limits, S_{allow} for all possible

sea states are obtained, in comparison with the characteristic dynamic responses, S, then the acceptable sea states can be defined by complying with $S < S_{allow}$.

Until now, the first steps have been done, in the following part, the last two steps will be discussed further.

6.1.2 Identification of Critical Sea States

Although the lift wire breakage values as the operational limits are already known, the sea states corresponding to the lift wire breakage are still uncertain. Therefore, before defining the acceptable sea states, these critical sea states should be identified firstly.

The following procedure is then proposed to find these critical sea states(see Figure6.2). It should be mentioned that this method is based on the assumption that a larger significant wave height can cause a larger lift wire tension when the spectral peak period is unchanged. From Figure 5.19 and 5.20, the changing trend of the lift wire tension corresponds to such an assumption.

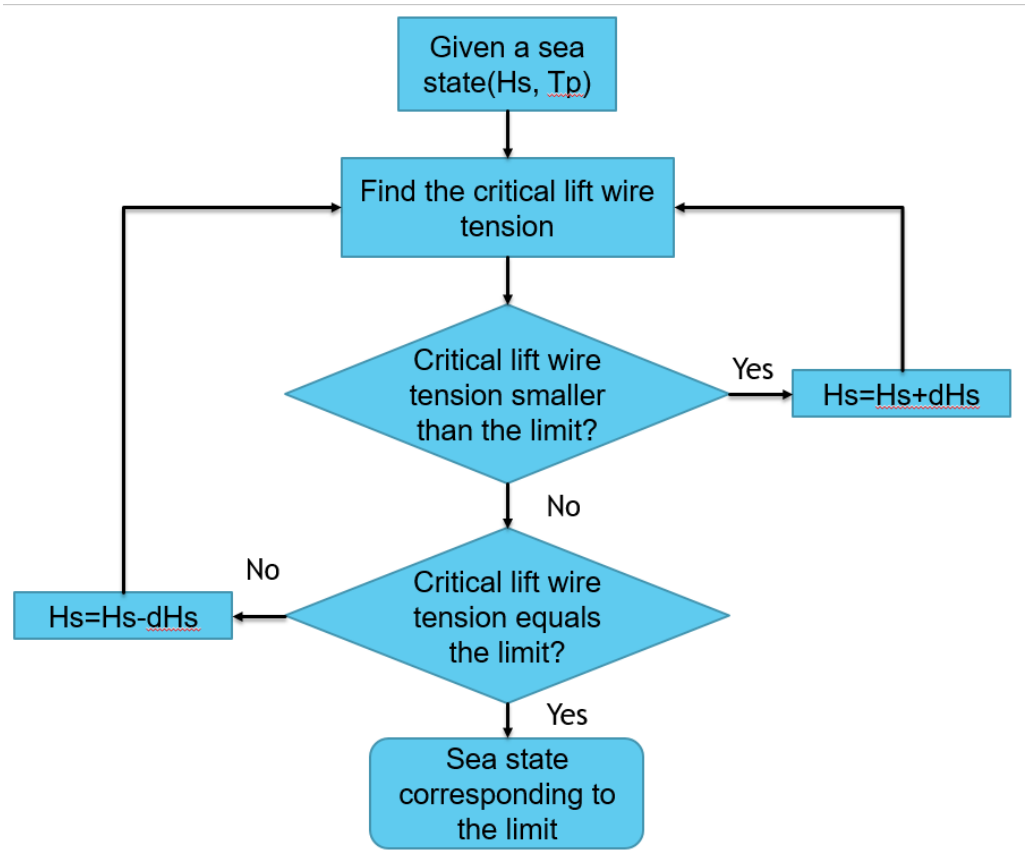

Figure 6.2: Methodology to find the critical sea states for the tripod lowering process

- For a given sea state, the first step is to calculate the "critical lift wire tension" in the dynamic simulations. In this case, the maximum lift wire tension during the lowering process is considered as the "critical lift wire tension".
- Then, in comparison with the given lift wire tension limit, if the critical lift wire tension is within the limit, which means the given sea state is acceptable, thus, the significant wave height should be increased.
- On the other hand, if out of range, it is necessary to judge whether the tension equals the limit or not. If the tension does not equal the given limit, which means the tension is larger, therefore, decrease the critical lift wire tension by reducing the significant wave height.
- Finally, the sea states corresponding to the given lift wire tension limit can be obtained. However, it is difficult to make sure the critical lift wire tension equals the limit perfectly, so an accepted range should be introduced, say 5%.

Table 6.1: Critical sea states for different lift wire tension limits

Tension Limit	**11MN**	**10.5MN**	**10MN**	**9.5MN**	**9MN**
Tp(s)			**Hs(m)**		
2	3.10	3.06	3.03	2.77	1.41
3	3.13	2.91	2.62	2.08	1.15
4	3.20	2.85	2.50	2.00	1.25
5	2.79	2.31	1.81	1.38	1.00
6	2.52	2.21	1.90	1.56	1.06
7	2.62	2.38	2.10	1.63	1.11
8	2.93	2.47	2.12	1.72	1.22
9	3.16	2.80	2.37	1.87	1.23
10	3.33	2.92	2.53	2.08	1.52
11	3.84	3.38	2.86	2.36	1.70
12	4.26	3.75	3.29	2.73	1.80
13	5.01	4.41	3.79	3.08	2.08
14	5.50	4.95	4.29	3.25	2.25
15			4.64	3.70	2.52

From the table above, all the critical sea states have already been obtained. After finding these critical sea states, under the given lift wire tension limit, a general functional relation between the significant wave height and the spectral peak period can be assessed. The results are shown in the following figure.

These fit lines in Figure 6.3 are U-shaped. Combined with Figure 5.20, if the axises are switched as in Figure 6.3, those contour lines are almost U-shaped, which proves the rationality

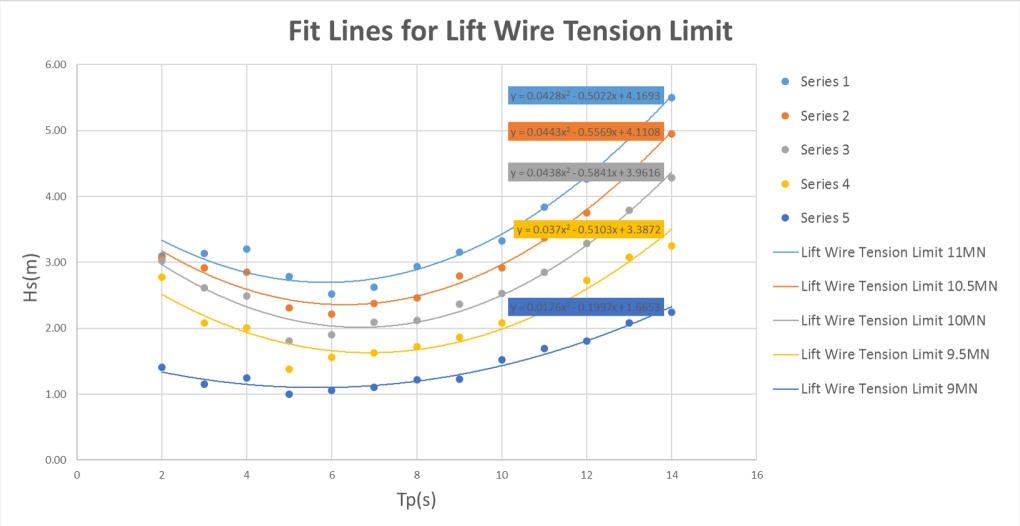

Figure 6.3: Fit Lines for Lift Wire Tension Limits

of the assessment.

6.1.3 Acceptable Sea States

Actually, the Acceptable sea states can be easily defined after Figure 6.3 established. The area below the fit line corresponds to the acceptable sea states, on the contrary, the upper area are unacceptable. In order to see the acceptable sea states more clearly, the hindcast data for between May and September from 2001 to 2010 is included in the following figure.

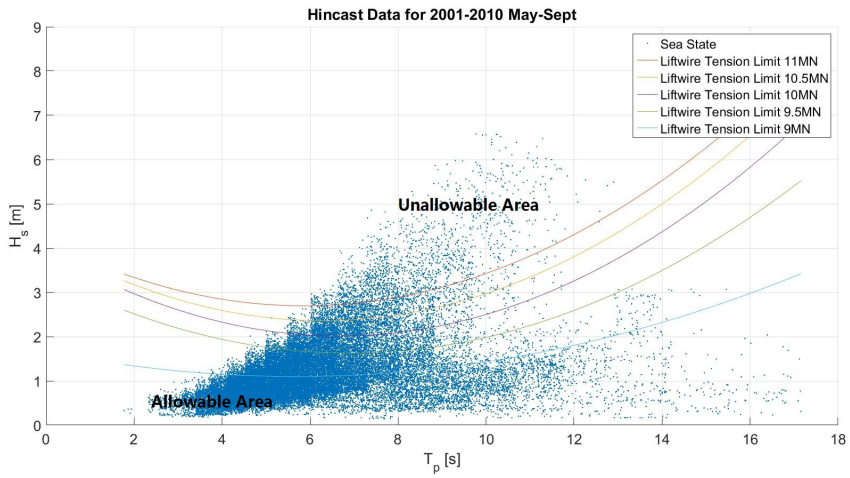

Figure 6.4: Acceptable sea states between May and September from 2001 to 2010

Then the acceptable probability can be calculated based on the acceptable sea states. The results can be seen as below.

From the trend of the curve in Figure 6.5, the lower lift wire tension limit has an obvious

Table 6.2: Acceptable probability for different lift wire tension limits

Lift Wire Tension Limit(MN)	Acceptable Probability
11.0	95.7 %
10.5	92.4 %
10.0	87.4 %
9.5	79.0 %
9.0	55.4 %

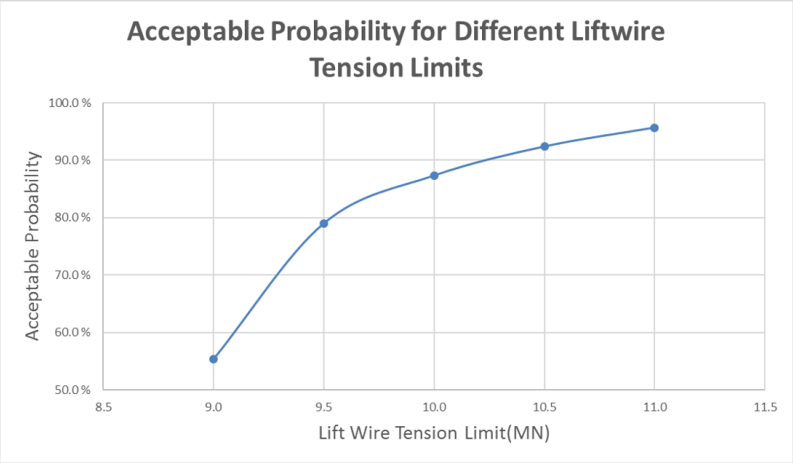

Figure 6.5: Acceptable Probability for Different Lift Wire Tension Limits

impact on the acceptable probability, which shows with lower lift wire tension limits the decreasing trend of the acceptable probability will be accelerated.. Therefore, the operator should choose a lift wire with reasonable strength to resist the lift wire breakage in most sea states.

6.2 Weather Window for the Tripod Lowering

For the tripod lowering operation which has a limited duration and which is to be executed during a certain season of the year, this operation will be started only when it can be guaranteed that acceptable weather conditions will persist until the operation is finalised. Since the tripod lowering operation is not to be planned for extreme weather conditions, the operator needs to establish estimates on the expected duration of the operations.

In order to get the weather window for the tripod lowering process, the time series of the significant wave height, Hs between May and September from 2001 and 2010 are generated from the hindcast data. Based on the functional relation between the significant wave height, Hs and the spectral peak period, Tp with the given lift wire tension limit, the time series of the significant wave height corresponding to the lift wire tension limit can also be illustrated as follow.

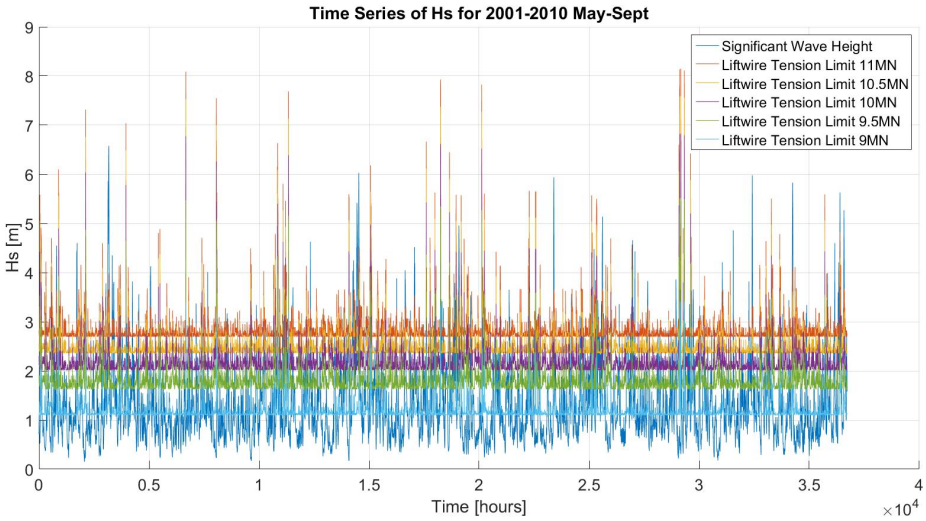

Figure 6.6: Time series of Hs between May and September from 2001 and 2010

However, since there are too much data during such a long period, the results of the weather window are not so clear. Generally, the trend in Figure 6.5 can still be seen.

In order to explain the results easily, the hindcast data for 2010 June will be discussed only in the following part. Similar as before, the acceptable probability for 2010 June is also obtained.

Table 6.3: Acceptable probability of 2010 June for different lift wire tension limits

Lift Wire Tension Limit(MN)	Acceptable Probability
11.0	93.6 %
10.5	91.4 %
10.0	88.9 %
9.5	85.0 %
9.0	70.3 %

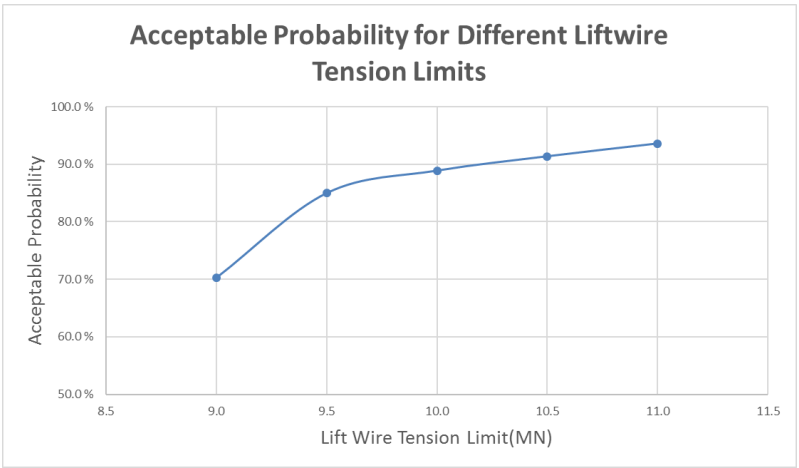

Figure 6.7: Acceptable Probability of 2010 June for Different Lift Wire Tension Limits

Combined with Figure 6.5, one can find that the sea states of 2010 June are more calm generally. There are no very high requirements for the lift wire breakage if the tripod lowering operation takes place in 2010 June.

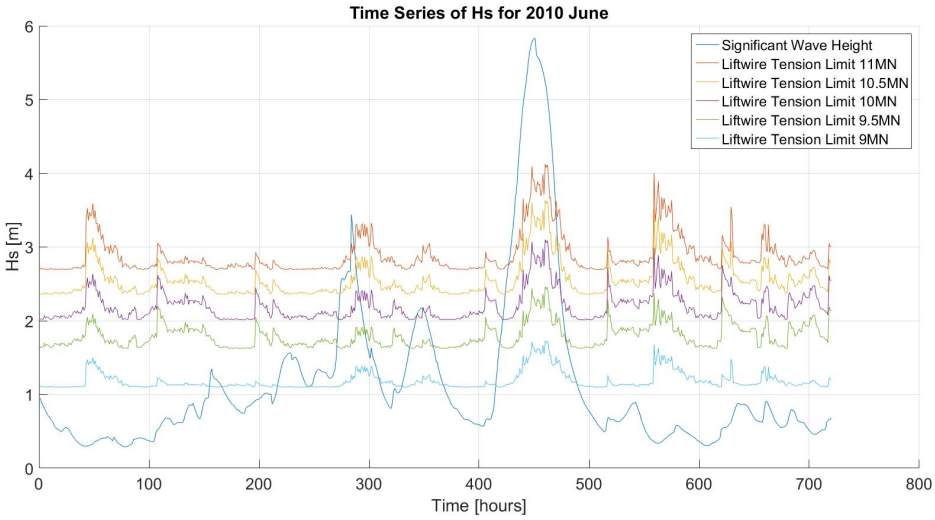

Figure 6.8: Time series of Hs in 2010 June

In Figure 6.8, when the significant wave height larger than the operational limit, the corresponding period is not of being able to work. For the condition with larger lift wire tension limit, most of time in 2010 June are good to do the tripod lowering operation.

The detailed time periods are listed in the following tables. From these tables, most acceptable working periods last more than 5 hours, which means there is enough time for operators to complete the installation operation successfully.

Table 6.4: Acceptable working time in 2010 June with the lift wire tension limit 11MN

Tension Limit 11MN	
Period(hours)	**Exact Time**
1-283	6/1/0:00-6/12/18:00
288-426	6/12/23:00-6/18/18:00
472-720	6/20/15:00-6/30/23:00

Table 6.5: Acceptable working time in 2010 June with the lift wire tension limit 10.5MN

Tension Limit 10.5MN	
Period(hours)	**Exact Time**
1-273	6/1/0:00-6/12/8:00
291-423	6/13/2:00-6/18/14:00
475-720	6/20/18:00-6/30/23:00

Table 6.6: Acceptable working time in 2010 June with the lift wire tension limit 10MN

Tension Limit 10MN	
Period(hours)	**Exact Time**
1-272	6/1/0:00-6/12/7:00
295-342	6/13/6:00-6/15/5:00
353-421	6/15/16:00-6/18/12:00
477-720	6/20/20:00-6/30/23:00

Table 6.7: Acceptable working time in 2010 June with the lift wire tension limit 9.5MN

Tension Limit 9.5MN	
Period(hours)	**Exact Time**
1-270	6/1/0:00-6/12/5:00
299-337	6/13/10:00-6/15/0:00
359-419	6/15/22:00-6/18/10:00
481-720	6/21/0:00-6/30/23:00

Table 6.8: Acceptable working time in 2010 June with the lift wire tension limit 9MN

Tension Limit 9MN	
Period(hours)	**Exact Time**
1-155	6/1/0:00-6/7/10:00
167-216	6/7/20:00-6/9/23:00
245-246	6/11/4:00-6/11/5:00
311-329	6/13/22:00-6/14/16:00
369-415	6/16/8:00-6/18/6:00
490-720	6/21/9:00-6/30/23:00

Chapter 7

Conclusions and Recommendations for Future Work

The installation of the tripod foundation in particular the lowering process was examined in this thesis. First of all, the environmental conditions for the given installation site were introduced. Then, numerical models were established based on the related numerical methods. In order to study the tripod lowering process further, the dynamic analysis was performed. According to the the results from dynamic analysis, the operational limits in terms of acceptable sea states were assessed. Finally, the weather window for the tripod lowering operation was given. In the final chapter, the conclusions and recommendations for future work are discussed.

7.1 Conclusions

Based on the thesis work of each chapter, the main conclusions can be seen as follow:

- According to the long-term wave data of the site no. 15, most sea states between May and September from 2001 to 2010 are available to execute the installation operations. Based on the one-hour hindcast data, the cumulative distributions of the significant wave height can be decided. Considering $Hs = 2.5m$ as the operational limit, 81.8% of the waves are within the limit. However, May to September, the percent increases to 92.8%, which gives a high recommendation to perform the installation in summer time. Further on, based on the scatter diagram , several typical sea states were defined in order to execute 3-hour stationary simulations for the coupled vessel-tripod system.

- By checking the applicability of the Morison formula for tripod members with different wave conditions, the slender element is recommended to be used for establish the numerical model for the tripod foundation. Then the quadratic drag coefficient was selected as $C_q = 1.0$, and inertia and added mass coefficients were used for tripod hollow members, $C_M = C_A = 2$.

- According the eigenvalue analysis for the coupled system, it can be found that there is a big difference between only vessel and the coupled system. The natural periods of tripod heave, tripod pitch and vessel heave are not affected by the changing of the tripod drafts. However, in the range of wave period, the natural period of tripod roll motion gets increased with increasing of tripod draft, due to changes in the restoring forces and significant contributions from the added mass. Combined with the spectrum analysis, at different positions, the tripod rotational motions are basically caused by the incident wave. Further on, such an influence focuses on conditions with wire length from 125m to 145m, which corresponds to the main part of the tripod crossing the splash zone. The effect from different tripod's drafts is studied further in the statistical analysis, which shows the response of the lift wire tension is also obvious when the tripod crossing the splash zone.

- In the time-domain simulations, the 20 wave seeds are recommended to be used based on the ensemble average analysis. According the dynamic response of the lift wire tension, the contour result is not ideal, the dangerous condition does not correspond to the worst sea state. However, combined with the analysis of the coupled system motions, it shows that the reason such an phenomenon is mainly caused by the tripod motions. Additionally, the influence of different winch speed is also considered, and the results show a relative high winch speed is better for stabilizing the tripod lowering process.

- A systematic methodology to obtain the operational limits is proposed and the allowable sea states for the lowering process are assessed by using the method. The critical event for the tripod lowering operation is defined as the lift wire breakage. Based on these allowable sea states, the acceptable probabilities for different lift wire tension limits can be seen in Figure 6.5, which shows with lower lift wire tension limits the decreasing trend of the acceptable probability will be accelerated. From the weather window analysis, the recommended operational time period for 2010 June is given, which shows that the tripod lowering operation is workable for most sea states even with a relatively low lift

wire tension limit in this period.

7.2 Recommendations for Future Work

Since several conclusions in the thesis are based on ideal physical models and basic assumptions, therefore, in order to enhance the reliability of these conclusions, some future work is recommended.

- **Refinement for the numerical model of the coupled system.** First of all, when modelling the connection between tripod and crane tip, only lift wire is considered instead of a more complex combination of lift wire and hook. Secondly, the ballast water should be adjustable during the tripod lowering process in order to stabilize the vessel roll motion. Then, actually, the Morsion coefficients should be different for different tripod members and different submergence of tripod, but they are simplified to perform calculation easily. Generally, there are so many places inaccurate compared with physical model, however, it is hard to reproduce such an accurate model in such a short time for this thesis work.

- **Further studies for dynamic results.** Although the results of time-domain simulations have been analyzed, the responses of the lift wire tension are more dependent on the tripod motions, the lift wire tension should be related to the elongation of the lift wire directly. Therefore, corresponding to the sea states which can lead to obvious responses, the detailed relative motions between vessel and tripod should be noted.

- **More operational limits are required.** In the thesis work, only lift wire breakage is considered, however, during the tripod lowering process, more elements should be considered, such as vessel motion limit, wind speed, current velocity ,etc.

- **Reliability-based methodology for assessment of operational limits.** When assessing the operational limits, a probabilistic approach should be applied to take into account the uncertainties in numerical models,environmental conditions, etc. Future work can be devoted to evaluate the uncertainties ans propose reliability-based methodology to assess the operational limits.

Bibliography

Archer, C. L., Colle, B. A., Monache, L., Dvorak, M. J., Lundquist, J., Bailey, B. H., Beaucage, P., Churchfield, M. J., Fitch, A. C., Kosovic, B., et al. (2014). Meteorology for coastal/offshore wind energy in the united states: recommendations and research needs for the next 10 years. *Bulletin of the American Meteorological Society*.

Clough, R. W. and Penzien, J. (1993). Dynamics of structures. 1993. *Copyright of Applied Mechanics & Materials is the property of Trans Tech Publications, Ltd and its content may not be copied or emailed to multiple sites or posted to a listserV without the copyright holder's express written permission. However, users may print, download, or email articles for indiVidual use*, page 38.

Faltinsen, O. (1993). *Sea loads on ships and offshore structures*, volume 1. Cambridge university press.

Gudmestad, O. T. and Skjerpe, P. (2012). Marine operations. *University of Stavanger, Norway*.

Jonkman, J. and Musial, W. (2010). Iea wind task 23 subtask 2 final technical report. *Golden, Colorado, USA: National Renewable Energy Laboratory.(to be published)*.

Jonkman, J. M., Butterfield, S., Musial, W., and Scott, G. (2009). *Definition of a 5-MW reference wind turbine for offshore system development*. National Renewable Energy Laboratory Golden, CO.

Li, L., Acero, W. G., Gao, Z., and Moan, T. (2016). Assessment of allowable sea states during installation of offshore wind turbine monopiles with shallow penetration in the seabed. *Journal of Offshore Mechanics and Arctic Engineering*, 138(4):041902.

Li, L., Gao, Z., and Moan, T. (2015). Joint distribution of environmental condition at five european offshore sites for design of combined wind and wave energy devices. *Journal of Offshore Mechanics and Arctic Engineering*, 137(3):031901.

Li, L., Gao, Z., Moan, T., and Ormberg, H. (2014). Analysis of lifting operation of a monopile for an offshore wind turbine considering vessel shielding effects. *Marine Structures*, 39:287–314.

Nielsen, F. G. (2007). Lecture notes in marine operations. *Department of Marine Structures, Norwegian University of Science and Technology, Trondheim, Norway*.

Ormberg, H. (2009). Simo theory manual.

Park, K.-P., Cha, J.-H., and Lee, K.-Y. (2011). Dynamic factor analysis considering elastic boom effects in heavy lifting operations. *Ocean Engineering*, 38(10):1100–1113.

Peire, K., Nonneman, H., and Bosschem, E. (2009). Gravity base foundations for the thornton bank offshore wind farm. *Terra et Aqua*, 115:19–29.

Reinholdtsen, S. and Falkenberg, E. (2001). Simo—theory/user manual. *MT51 F93-0184, MARINTEK*.

Twidell, J. and Gaudiosi, G. (2009). *Offshore wind power*, volume 425. Multi-Science Publishing Company.

Veritas, D. N. (2010a). Dnv-rp-c205. *Environmental Conditions and Environmental Loads*.

Veritas, D. N. (2010b). Wadam user manual. *Det Norske Veritas*.

Wind, G. L. (2005). Guideline for the certification of offshore wind turbines. *Germanischer Lloyd Industrial Services GmbH*.

Appendix A

Layout of the Heavy Lift Vessel

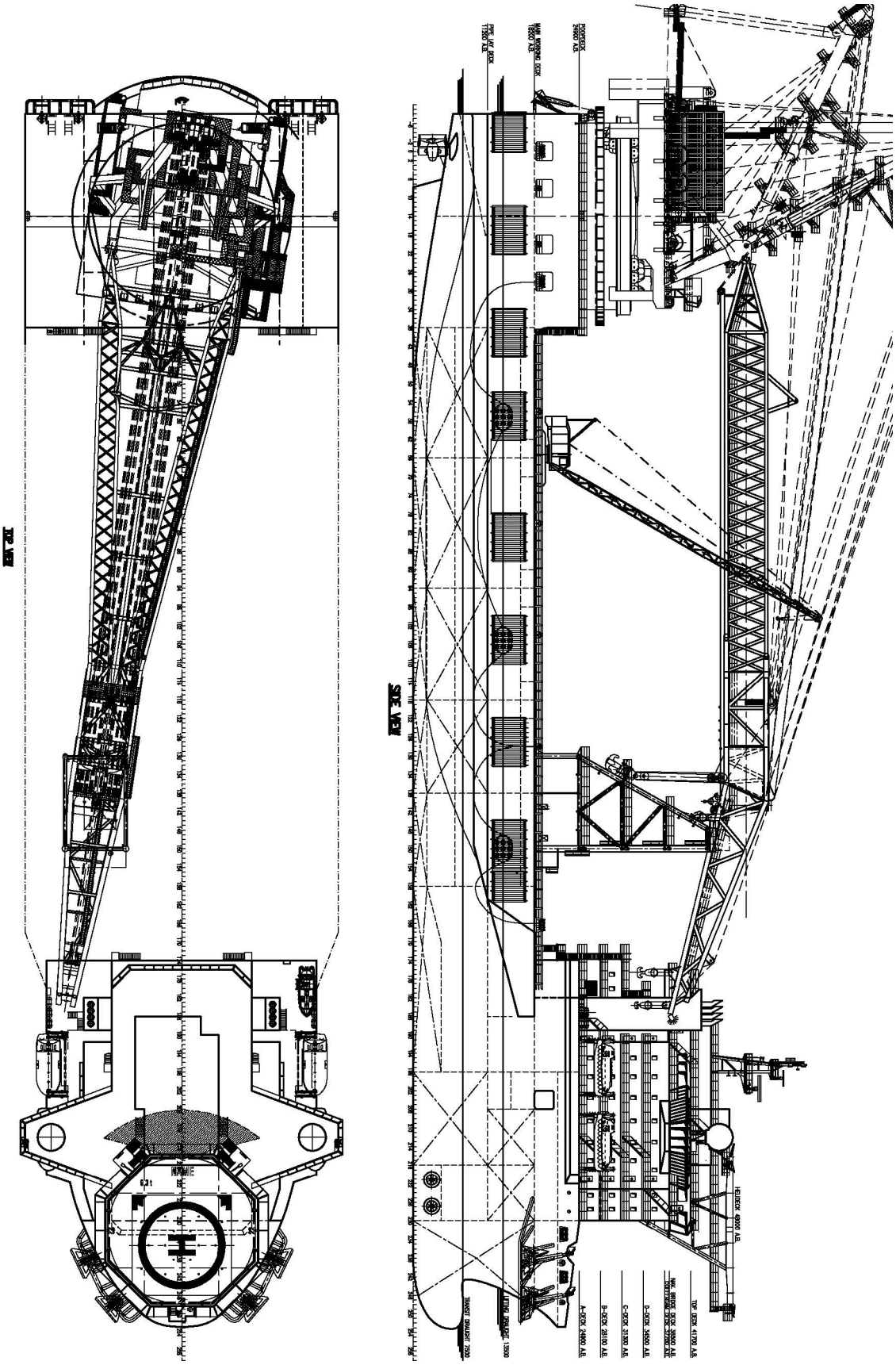

Figure A.1: Layout of HLV

Appendix B

Time Series of Lift Wire Tension for Different Lift Wire Lengths

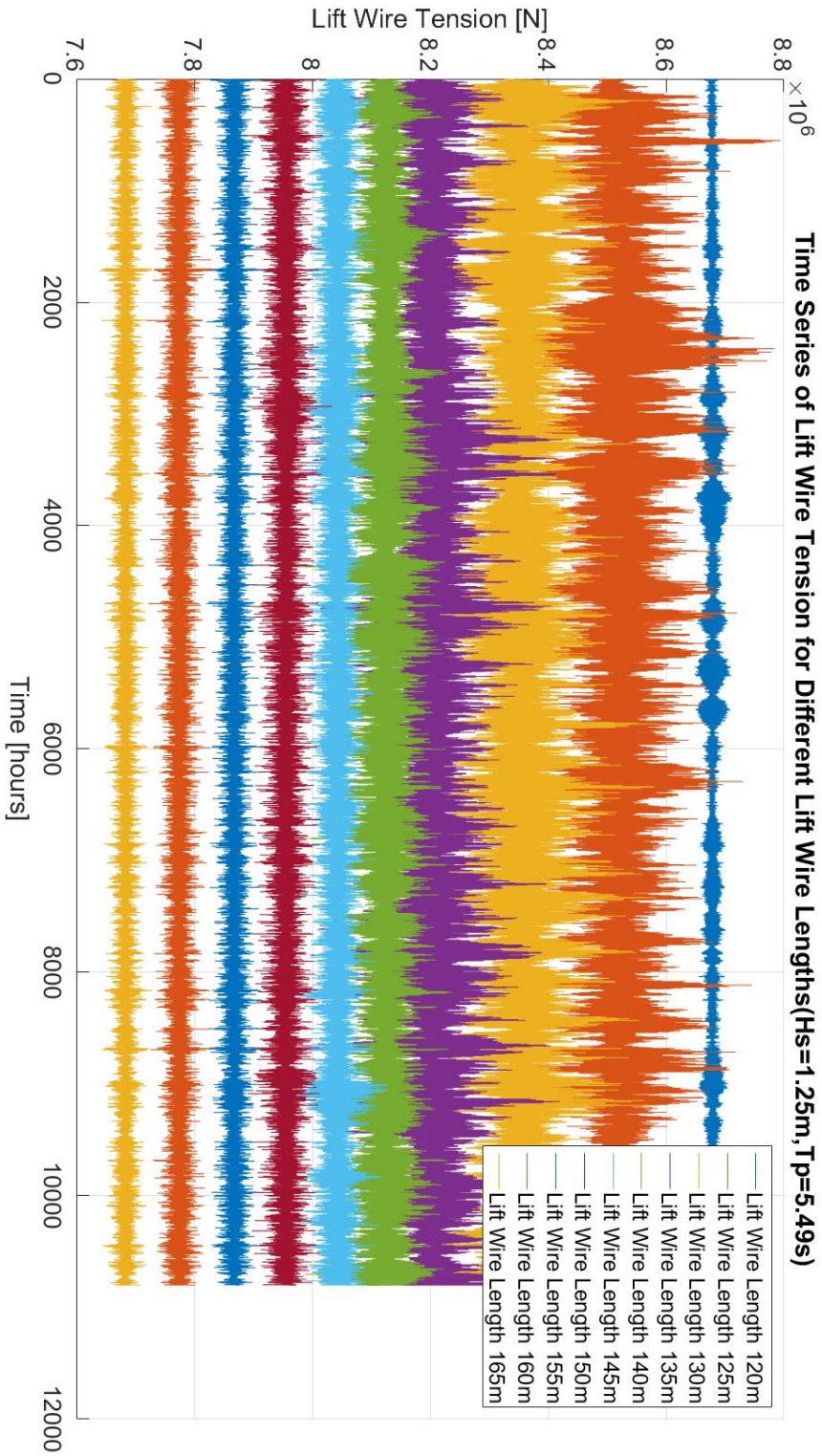

Figure B.1: Time Series of Lift Wire Tension for Different Lift Wire Lengths(Hs=1.25m,Tp=5.49s)

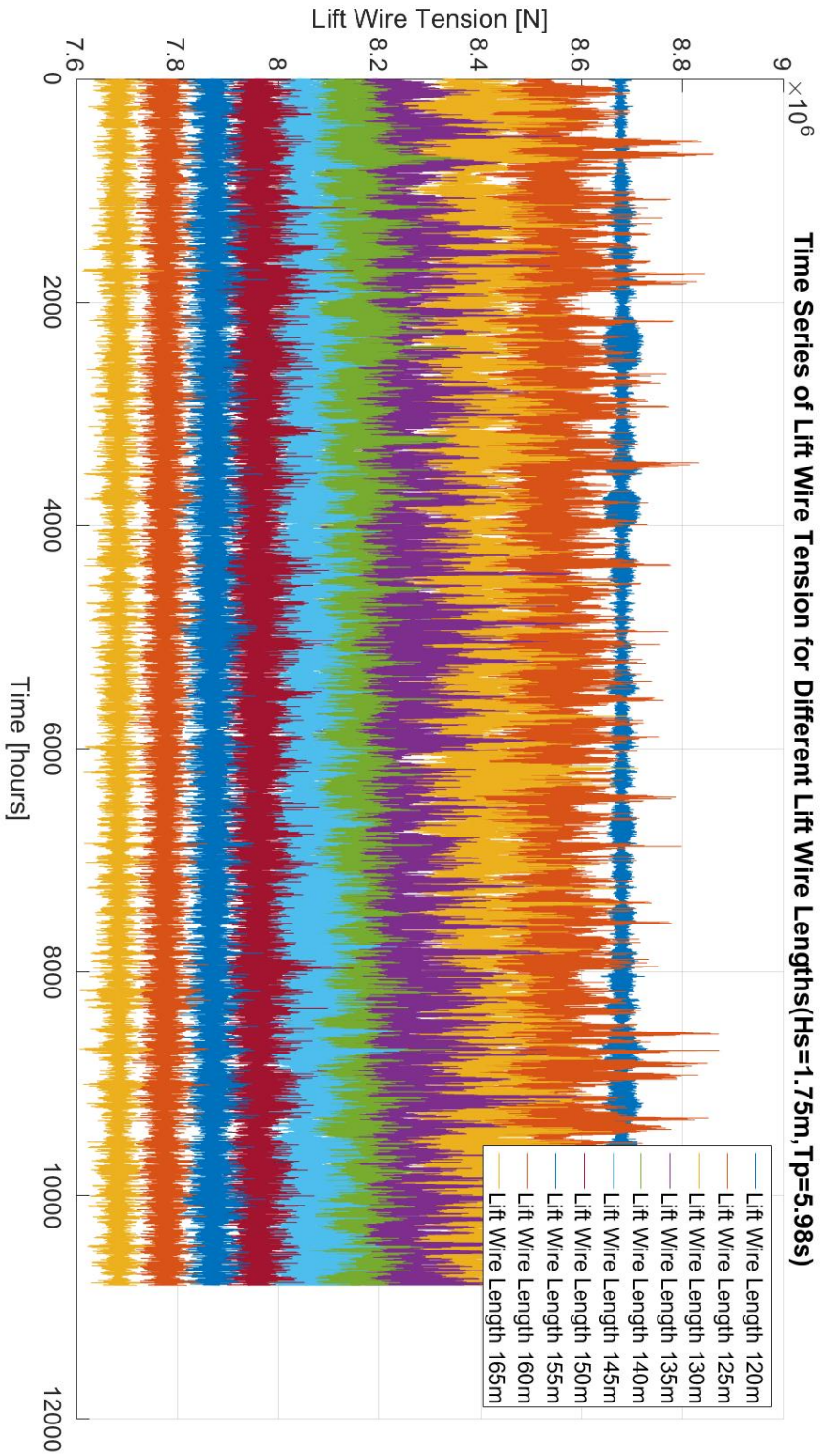

Figure B.2: Time Series of Lift Wire Tension for Different Lift Wire Lengths(Hs=1.75m,Tp=5.98s)

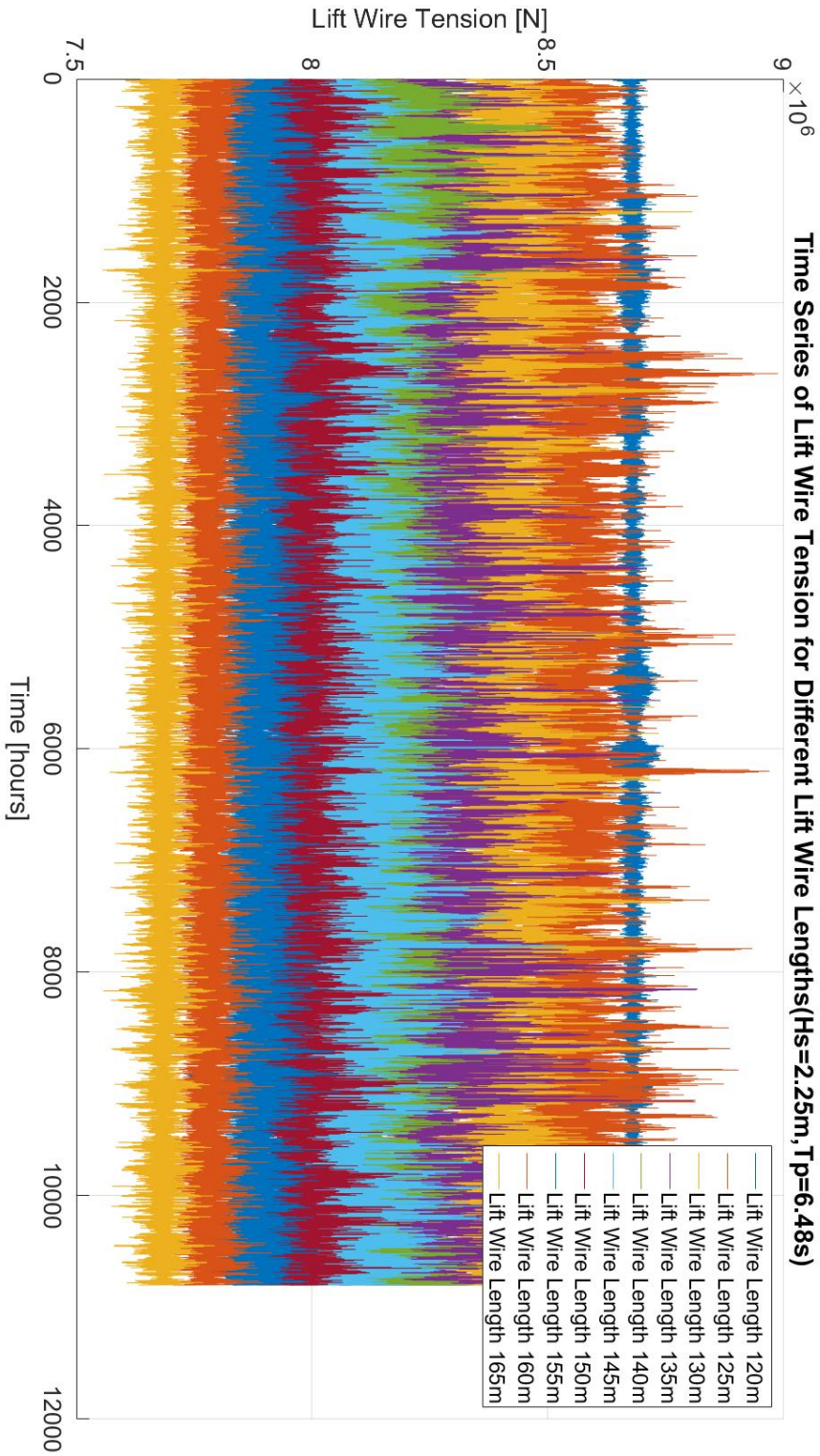

Figure B.3: Time Series of Lift Wire Tension for Different Lift Wire Lengths(Hs=2.25m,Tp=6.48s)